

ON THE SPATIAL DISTRIBUTION OF DIAPYCNAL MIXING IN THE ABYSSAL
OCEAN: AN EMPIRICAL STUDY

A DISSERTATION SUBMITTED TO
THE GRADUATE DIVISION OF THE UNIVERSITY OF HAWAI'I IN PARTIAL
FULFILLMENT OF THE REQUIREMENTS FOR THE DEGREE OF

DOCTOR OF PHILOSOPHY

IN

OCEANOGRAPHY

DECEMBER 2009

By
Thomas Decloedt

Dissertation Committee:

Douglas S. Luther, Chairperson
Mark Merrifield
Eric Firing
Axel Timmermann
John Learned

We certify that we have read this dissertation and that, in our opinion, it is satisfactory in scope and quality as a dissertation for the degree of Doctor in Philosophy in Oceanography.

DISSERTATION COMMITTEE

Chairperson

DEDICATION

To my family: Claire & Toon, Nicholas, Celine & Jurgen and of course Lotte & Nils.

ACKNOWLEDGEMENTS

I feel very fortunate to have had Douglas Luther as my advisor these past few years. Doug's continuous support and generosity have tremendously eased going through the ups and downs that is life as a graduate student. Doug has also introduced me to some distinctly American pleasures, such as yearly thanksgiving dinners with his family and the thrill of driving a Mustang 5.0. I am indebted to John Toole who gave me access to the HRP data (twice) and much advice as well as to J. Klymak , T. Sanford, J. Moum, A. Naveira Garabato and R. Lumpkin who kindly and unhesitatingly shared their data. I thank G. Carter, C. Chavanne, E. Firing , M. Merrifield, A. Timmermann for helpful comments. Many thanks to A. Timmermann and T. Friedrich for making the effort to implement the RDM in an OGCM, the next logical step after developing a parameterization. I would also like to thank J. Learned for his willingness to serve for the nth time as external committee member for a physical oceanography graduate student. A special thanks to Nancy Koike for all her help guiding me and numerous other graduate students through the intricacies of UH forms, deadlines and rules.

I have made a number of friends during my time as a graduate student at UH that have made my time here special and enjoyable. Cameron & Lianne McNaughton, EZ and Jacob have made 1331, 9th Avenue a cherished spot for barbecues and getting demolished at Boggle. Mitch Pinkerton's incredibly varied number of skills and desire to use them all for organizing parties have led to numerous unforgettable nights and events. Many thanks to Matthieu Dubarry for helping me setting up a thesis template, numerous science discussions over a few Belgian ales, and luring me to the Nevada desert at a critical time of my dissertation. I thank Jerome Aucan, Cedric & Marion Chavanne, Pierre & Tania Dutrieux, Francois & Eman Ascani, Adrian Glover

Andreas Andersson and Yves Plancherel for showing me the ropes when I arrived in Hawaii. Special thanks to Team Schneeby (Kolja Rotzoll, Fabian Schloesser, Volker Roeber, Jonathan Weiss, Tad) for all the dawn patrols and windsurf sessions. I feel fortunate to have had many stimulating discussions with Francois Ascani, Cedric Chavanne, KJ Stein, Cameron McNaughton, Mitch Pinkerton, Jerome Aucan, Matthieu Dubarry, Laurie Menviel, Ole Peters, Guy Spyropoulos and many others over the past few years.

ABSTRACT

The picture emerging from observations of turbulence in the abyssal ocean is one of weak diapycnal mixing in the interior and bottom-intensified mixing, by orders of magnitude, over rough topography. Numerical simulations indicate that the large-scale ocean circulation is sensitive to the spatial distribution of diapycnal mixing in the abyssal ocean. In addition, spatially varying mixing may largely control the structure of the abyssal stratification. Consequently, insofar as the complex processes generating abyssal turbulence cannot be directly simulated in OGCM's, mixing parameterizations with realistic spatial distributions in the abyssal ocean are desirable. While spatially varying mixing parameterizations based on internal tide dissipation have been proposed in the past decade, the external tide likely provides no more than half of the mechanical energy available for mixing in the abyssal ocean. A plethora of complex flow-topography interactions deriving their energy from various sources can be expected to contribute to the observed bottom-intensification of diapycnal mixing.

A simple empirical model for the spatial distribution of the abyssal ocean's diapycnal diffusivity K_ρ is introduced based on microstructure observations of turbulence. The Roughness Diffusivity Model (RDM) is dependent upon the observation that observed bottom-intensified mixing amplitudes actually stratify according to a simple metric of topographic roughness. The functional vertical dependence of the RDM is founded on a heuristic recipe developed by K. Polzin (2004, 2009) containing an inverse square law decay with height above bottom. In developing the RDM, both the scale height and maximum boundary diffusivity are assumed to be functions of topographic roughness. The empirical functions were determined from iterated nonlinear regressions on the microstructure data. Armed with these functions, the mean vertical

diffusivity profiles at the locations of the microstructure data can be reproduced to within a factor of two at all heights above bottom. This is a superior comparison with the microstructure data than achieved by $K\rho$ models that use an exponential decay with constant scale height in the vertical.

Basin-averaged diffusivities predicted by the RDM increase from $\sim 3 \times 10^{-5} \text{ m}^2/\text{s}$ at 1 km depth to $\sim 1.5 \times 10^{-4} \text{ m}^2/\text{s}$ at 4 km and are shown to be consistent with inverse model results by Lumpkin and Speer (2007) and Ganachaud (2003), supporting the contention that strong localized mixing plays a major role in maintaining the observed abyssal stratification against deep and bottom water formation. Ocean volumes containing known passages of deep flow (e.g., Romanche Fracture Zone, Samoan Passage) are regions where the RDM underestimates diffusivities compared to inverse model results, suggesting that these passages require a separate parameterization. The power required to sustain the stratification in the abyssal ocean (defined as 40S-48N, 1-4 km depth) is shown to be sensitive to the spatial distribution of $K\rho$. The power consumption in this domain, given the parameterized bottom-intensified and horizontally heterogeneous diffusivity structure in the RDM, is estimated as approximately 0.37 TW, considerably less than the canonical value of ~ 2 TW estimated under the assumption of a uniform diffusivity of $\sim 10^{-4} \text{ m}^2/\text{s}$ in the abyssal ocean.

TABLE OF CONTENTS

CHAPTER ONE 1

1. INTRODUCTION..... 1

1.1. Overview and dissertation outline.....1

1.2. Small-scale turbulent diapycnal mixing.....6

1.3. Diapycnal mixing, the abyssal stratification and circulation.....8

1.4. Diapycnal mixing and the MOC16

1.5. Dynamical significance of spatially varying diapycnal mixing17

1.6. Spatially varying mixing parameterizations: The current state of affairs21

1.7. Spatially varying mixing: a multi-component process24

CHAPTER TWO..... 30

2. THE ROUGHNESS DIFFUSIVITY MODEL (RDM) 30

2.1. Rationale of the RDM30

2.2. Observations of turbulent diapycnal mixing in the abyssal ocean31

 2.2.1. Diapycnal mixing inferred from microstructure data.....32

 2.2.2. Diapycnal mixing inferred from fine-scale parameterizations.....42

 2.2.3. Diapycnal mixing inferred from inverse models.....46

2.3. A metric for topographic roughness.....50

2.4. Construction of the RDM56

2.5. Comparison of the SL02 tidal parameterization to the microstructure data.....69

2.6. General comments about the spatial distribution predicted by the RDM.....75

2.7. Comparison of the RDM to inverse model results83

 2.7.1. Comparison of RDM to Lumpkin and Speer, 200783

 Global comparison84

 2.7.2. Comparison of RDM to Ganachaud, 200391

 Indian ocean.....91

 Atlantic Ocean.....101

 Pacific Ocean.....119

CHAPTER THREE 127

3. SOME INFERENCES ABOUT DIAPYCNAL MIXING BASED ON THE RDM	127
3.1. Vertical structure of diapycnal mixing	128
3.2. Horizontal distribution of diapycnal mixing	129
3.3. Missing diapycnal Mixing ?	130
3.4. Power consumed by spatially varying diapycnal mixing	130
3.5. Conclusions	137
REFERENCES	139

Chapter one

1. INTRODUCTION

1.1. Overview and dissertation outline

The global ocean circulation and tracer distributions exhibit structure on a vast range of space and time scales. The largest spatial scales, $O(10^7 \text{ m})$, are chiefly limited by the size of the ocean basins whereas the smallest scales of motion and scalar gradients depend on a combination of molecular properties of seawater and the ambient turbulence. For typical deep ocean values of the turbulent kinetic energy (TKE) dissipation rate $\epsilon \sim 10^{-9} \text{ Wkg}^{-1}$ (about one hairdryer per km^3 of ocean), the smallest scales are $O(10^{-1} \text{ m})$. The spatial scales thus span some nine orders of magnitude. Scalar and velocity structures on scales of a few centimeters evolve on time scales of seconds to minutes whereas climate studies seek to understand ocean variability with periods of decades to millenia (Toole, 1998). Time scales thus span some ten or more orders of magnitude. Given these space and time-scales ranges, summarized in Figure 1, it is obvious that no global-scale Ocean General Circulation Model (OGCM) can resolve all scales of motion simultaneously over long times. Current OGCMs and climate models generally truncate the horizontal resolution at tens of kilometers to degrees and the vertical resolution at tens-to-hundreds of meters. Smaller scale motions (subgrid-scale or SGS) are not resolved and must be parameterized, that is, represented in terms of explicitly resolved variables or prescribed by certain empirically or theoretically-based rules. Today, parameterization of the effects of small scale and high frequency processes is one of the more pressing tasks in oceanography.

Small-scale turbulent diapycnal¹ mixing in the abyssal ocean (depth > 1 km), the subject of this thesis, is one such SGS process. The aim of this thesis is the development of an empirical model of the spatial variability of diapycnal mixing in the abyssal ocean. This brings us to a fundamental problem in oceanography. How does one adequately sample the roughly $1.3 \times 10^9 \text{ km}^3$ of water, opaque to electromagnetic radiation, that make up the global ocean? The sampling problem is especially severe for the abyssal ocean. Satellite altimetry does not reveal much information about the abyssal circulation or water properties. Instruments must be physically placed at the desired locations and therefore oceanographic research vessels necessary for deployment remain the major observational tool. Data collection is thus limited in both space and time. The study of turbulence in the abyssal ocean is further complicated by the fact that highly specialized instruments, capable of measuring velocity fluctuations and temperature gradients on dissipation scales, are required for reliable estimates of the TKE dissipation rate. Few of these instruments exist, they are costly and difficult to operate and were unable to sample at depths greater than about $\sim 1 \text{ km}$ until the mid 1990s. As a result, the total number of existing microstructure profiles extending into the abyssal ocean is less than a thousand at the time of writing.

It is therefore not surprising that theories of the Meridional Overturning Circulation (MOC)

¹ Diapycnal mixing refers to mixing across surfaces of equal density (isopycnals). Strictly speaking, we are here concerned with dianeutral mixing, i.e., mixing across surfaces along which water parcels can be exchanged locally without requiring work. Because of the nonlinearity of the equation of state, isopycnal surfaces do not generally coincide with neutral surfaces. Nevertheless, in the context of ocean mixing, people usually use the terms “vertical” or “diapycnal” to mean dianeutral. We will here follow convention and use the term diapycnal mixing. Given the small isopycnal slopes in the abyssal ocean, these terms are nearly equivalent (De Szoeke and Bennet, 1993).

and the abyssal circulation have generally assumed uniform mixing and upwelling in the abyssal ocean (e.g., Wyrki, 1961; Bryan, 1987; Munk and Wunsch, 1998; Gnanadesikan, 1999; Webb and Sugimoto, 2001). The assumption of spatially uniform mixing and upwelling in the abyssal ocean is inadequate in view of recent direct (microstructure observations) and indirect (fine-scale parameterizations applied to hydrographic data) observations however. It is now generally accepted that diapycnal mixing is mostly weak, $O(10^{-5} \text{ m}^2\text{s}^{-1})$, in the abyssal ocean interior (e.g., Gregg, 1987; Kunze and Sanford, 1996) and bottom-intensified by orders of magnitude in regions of rough topography (e.g., Gregg and Sanford, 1980; Toole et al., 1997; Polzin et al., 1997; Klymak et al., 2006; Aouine et al., 2006; Levine and Boyd, 2006b). Recent numerical studies (e.g., Hasumi and Sugimoto, 1999, Simmons et al., 2004, Saenko and Merryfield, 2005) demonstrate that both the magnitude and spatial distribution of diapycnal mixing have a bearing on the abyssal circulation and stratification as well as on the MOC. In turn, these have a bearing on the ability of the ocean to store and transport heat and greenhouse gases. The cliché statement that small-scale turbulent mixing processes influence climate dynamics is based on this reasoning. This particular cliché does retain much of its validity (Ferrari and Wunsch, 2009) and it is now recognized that mixing parameterizations capturing the observed spatial heterogeneity are sorely needed.

A number of preliminary parameterizations of spatially varying diapycnal mixing have been proposed the past few years, mostly focused on the spatial variability resulting from the interaction of the barotropic tides with topography. Rough energy budgets indicate that the mechanical energy of tidal origin represents no more than half of the mechanical energy

available for mixing in the abyssal ocean however. A plethora of complex flow-topography interactions deriving their energy from various sources contribute to diapycnal mixing and these may be of equal importance to the spatial distribution of mixing. The goal of the empirical approach adopted here is to model the diapycnal mixing resulting from a broad range of mixing processes, not just tidal mixing. The remainder of chapter 1 is devoted to providing the necessary background and concepts for this work. Chapter 2 describes the data sets that were examined and details the construction of a simple model, or parameterization if you will, for the mean spatial distribution of K_p . The model, dubbed the Roughness Diffusivity Model (RDM), is a function only of topographic roughness and height above bottom. In contrast to other published efforts, no assumption is made about the source of mechanical energy sustaining the mixing. In the final chapter, some implications of the RDM are examined. Given the scarcity of data on which to base and validate any model of diapycnal mixing, all results must be considered with a healthy dose of skepticism. The RDM is however a step forward from the assumption of a constant diapycnal diffusivity. It also differs conceptually from other work. It is hoped that some of the results discussed here may provide some fresh ideas towards the development of more realistic diapycnal mixing parameterizations for use in OGCMs and climate models.

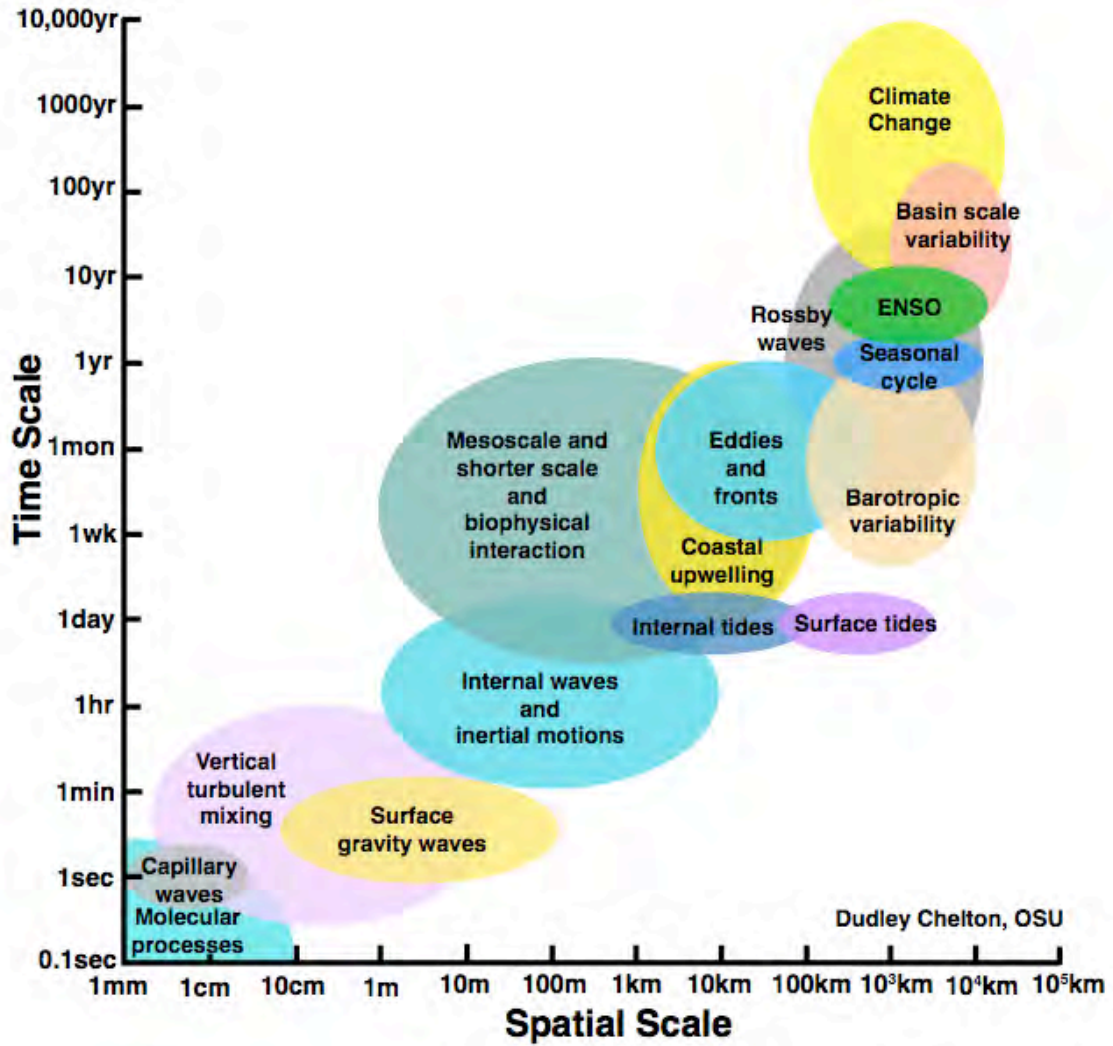


Figure 1: Approximate time and space scales spanning from micro to climate-scales. Figure from Chelton, 2001².

1.2. *Small-scale turbulent diapycnal mixing*

Basic to the discussion in this thesis is the distinction between mixing and stirring. Stirring refers to the straining of property distributions by fine-scale, $O(10\text{m})$, or larger scale flows resulting in ever-larger root-mean-square (rms) property gradients. Mixing refers to the irreversible destruction of these rms gradients through the action of molecular diffusion and viscosity. In a turbulent fluid, the smallest scales at which scalar and velocity gradients exist are about the Batchelor scale $L_b \sim 2\pi(\kappa^2\nu/\varepsilon)^{1/4}$ and the Kolmogoroff scale $L_k \sim 2\pi(\nu^3/\varepsilon)^{1/4}$ respectively. Observations indicate that 90 % of the mixing occurs between 1.5 and 70 times these length scales (Lueck, 2005). For a typical deep ocean value of the turbulent kinetic energy dissipation rate $\varepsilon \sim 10^{-9}$ W/kg and given the values of molecular viscosity $\nu \sim O(10^{-6} \text{ m}^2\text{s}^{-1})$, diffusivity of heat $\kappa_T \sim O(10^{-7} \text{ m}^2\text{s}^{-1})$ and salt $\kappa_S \sim O(10^{-9} \text{ m}^2\text{s}^{-1})$ in seawater, these scales are on the order of millimeters to centimeters (e.g., Toole, 1998). The molecular diffusivities and viscosity are so small as to have negligible effects on the large-scale velocities and density structure of the abyssal ocean. However, small-scale three-dimensional turbulence acts to transfer energy down to dissipative scales and drastically enhances scalar property gradients at diffusive scales by stirring. The result is an effective diffusion of properties at rates orders of magnitude greater than the molecular rates that would occur in laminar flow with the same average distribution of flow and scalar properties. It is this turbulent enhancement that makes diapycnal mixing a significant process in the abyssal ocean (Gnanadesikan and Hallberg, 2002).

We are here concerned with the turbulent diapycnal diffusion of density, commonly

represented by a Fickian or eddy diffusion coefficient³ K_ρ . Note that the concept of an eddy diffusion coefficient itself is a parameterization of turbulent mixing. The idea was hinted at in the late nineteenth century in papers by Boussinesq and Lord Kelvin (see Frisch, 1996 for a detailed historical perspective) and appears clearly in the work by G. I. Taylor (Taylor, 1915). The effect of turbulent motion remains too difficult to model in detail. Appealing to an analogy between turbulent eddies and molecular diffusion, with the small-scale eddies playing the role of molecules and the correlation length or integral scale that of the mean free path, the turbulent flux of a quantity is treated as being proportional to an empirically determined eddy diffusion coefficient and the mean gradient of that quantity. Adopting the eddy diffusivity assumption, the turbulent diapycnal flux of density ρ is given as

$$\langle w'\rho' \rangle = -K_\rho \frac{\partial \bar{\rho}}{\partial z} \quad (1)$$

where w is the diapycnal velocity, the primes denote turbulent fluctuations and the averaging operator $\langle \rangle$ is generally taken to be over time. The concept of an eddy diffusivity has perhaps become the most frequently used tool in modeling turbulent flow yet is a limited concept, described by some theoreticians as a pedagogical device at best (Frisch, 1996). The trouble is that there is often no clear separation of scales in turbulence such that the analogy between the mean free path and the correlation length is hard to justify.

³ Note that the eddy diffusivities for heat, salt and density are generally assumed to be equal, i.e., $K_\rho = K_T = K_S$. Munk and Wunsch, 1998 argue this is a natural assumption since otherwise observed distributions of temperature and salt would be sharply different. Direct observations (e.g., Nash and Moum, 1999) indicate this is not the case however and numerical experiments allowing for $K_T \neq K_S$ indicate that major features of steady state model solutions, including the magnitude and direction of the meridional overturning circulation, are sensitive to the ratio K_S/K_T (Gargett and Holloway, 1992).

1.3. Diapycnal mixing, the abyssal stratification and circulation

Two now classic papers remain central to our view of the diapycnal mixing and its relation to the abyssal circulation and stratification: Stommel et al., 1958 and Munk, 1966. Stommel and coworkers developed a model for the stationary, geostrophic abyssal circulation driven by slow, widespread upwelling out of the abyss in response to isolated sources of deep and bottom waters at high latitudes. Due to a lack of data to decide otherwise, spatially uniform upwelling in the abyss or, equivalently, a single value for the diapycnal diffusion rate was assumed. The Stommel-Arons model consists of weak, poleward interior flow resulting from vortex stretching and is closed by a series of deep western boundary currents that link to the regions of deep water formation to balance the mass budget. An idealized sketch of the Stommel-Arons abyssal circulation is shown below.

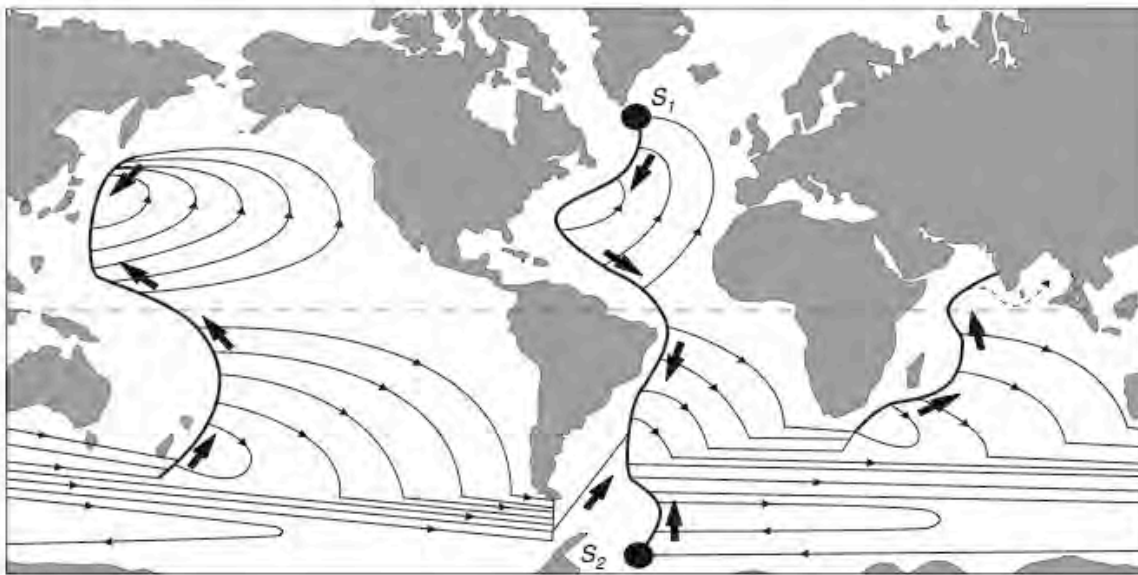


Figure 2: An idealized sketch of the abyssal circulation due to point sources of deep and bottom water formation (black circles) and uniform upwelling (mixing) elsewhere. After Stommel (1958). Figure from Stewart, 2008.

In parallel, Wyrтки, 1961 and Munk, 1966 argued that diapycnal mixing plays a crucial role in maintaining the observed abyssal stratification. A distinguishing feature of the ocean is its nearly universal stable density stratification, even in the abyssal ocean (see Figure 3). A first glimpse of the ocean’s deep density structure dates back to 1751 when Henry Ellis, captain of the British slavetrader *Earl of Halifax*, observed that deep water, even in the tropics and sub-tropics, is all cold using a “bucket sea gauge”. Ellis did not realize the significance of his finding but did put it to good use: “*By its means, we supplied our cold bath and cooled our wines, which is vastly agreeable in this burning climate.*” (Warren, 1981). As hypothesized by Count Rumford in 1797, it is now understood that the densest waters found in the open ocean are formed at high latitudes by air-sea interaction. In a few narrow, sporadic regions at high latitudes, near-surface fluid occasionally becomes sufficiently dense to sink to great depths. It is estimated that roughly 25-30 Sv (1 Sv= $10^6 \text{ m}^3\text{s}^{-1}$) reach the bottom 1000 m of the global ocean (Wunsch and Ferrari, 2004). For comparison, the Amazon River has a flow of about 0.15 Sv. The abyssal ocean does not simply fill up with fluid at the temperature and density of the waters formed at high latitudes however. Robinson and Stommel, 1959 proposed that the abyssal density stratification is maintained against the continual influx of deep and bottom waters by a 1-D balance between diapycnal upwelling of cold, dense water and downward, turbulent diapycnal mixing of heat, i.e.,

$$w \frac{\partial \rho}{\partial z} = K_{\rho} \frac{\partial^2 \rho}{\partial z^2} \quad (2)$$

Wyrтки, 1961 estimated the required numerical value of K_{ρ} based on a reasonable guess for the upwelling rate of $O(10^{-7} \text{ ms}^{-1})$, equivalent to the global deep and bottom water formation

rate of some 30 Sv upwelling through the thermocline, and the observed temperature profile down to 1000 m of depth at Carnegie Station. Wyrтки concluded a diffusivity of $O(10^{-4} \text{ m}^2\text{s}^{-1})$ was needed. Munk (1966) considered the distributions of salinity, temperature and ^{14}C in the central Pacific between 1 and 4 km of depth. Based on the advection-diffusion balance, coupled with a decay term for ^{14}C , he was able to estimate w and K_p independently. Consistent with Wyrтки's estimate, Munk concluded that an average diapycnal diffusivity of $O(10^{-4} \text{ m}^2\text{s}^{-1})$ below 1 km of depth is consistent with the observed property distributions. The diapycnal diffusivity value of $K_p \sim 10^{-4} \text{ m}^2\text{s}^{-1}$ has become a benchmark in physical oceanography, sometimes jokingly referred to as 1 Munk.

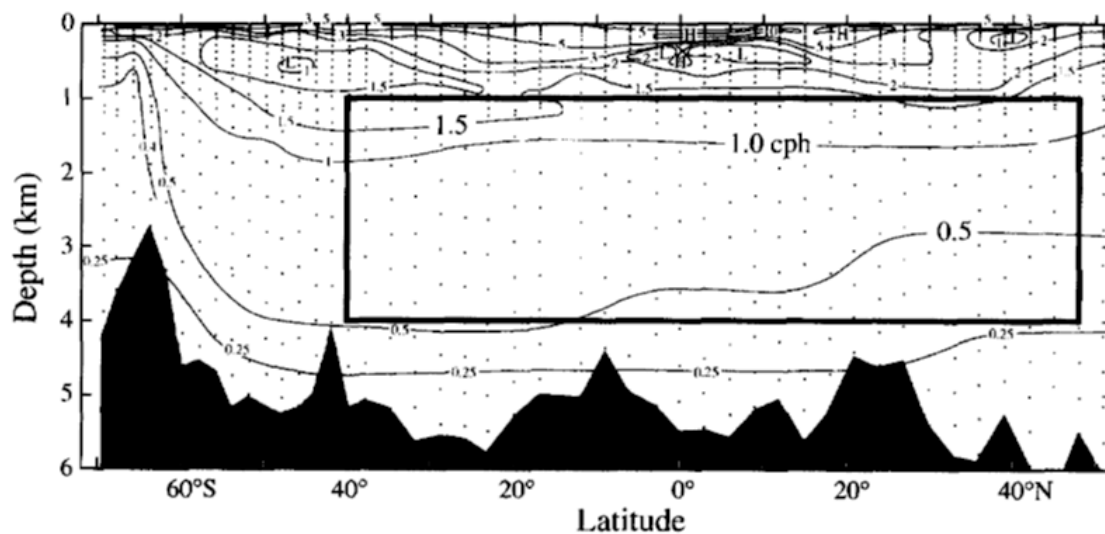


Figure 3: Contours of buoyancy frequency as a function of latitude and depth in the Central Pacific at 170° W . Contours are relatively uniform within the “abyssal ocean”, defined by Munk and Wunsch (1998) as extending from 40°S to 48°N between 1 and 4 km of depth. This definition is chosen such that isopycnals in the abyssal ocean only outcrop in the regions deep water formation. Figure from Munk and Wunsch (1998)

Indirect diffusivity estimates based on heat budgets for semi-enclosed basins or channels (Hogg et al., 1982; Saunders, 1987; Roemmich et al., 1996; Morris et al., 2001) return averaged values of $O(10^{-4} \text{ m}^2\text{s}^{-1})$ as predicted. More recently, the high quality hydrographic data collected in the context of the World Ocean Circulation Experiment (WOCE) has made inversions possible on basin-scales (e.g., Macdonald and Wunsch, 1996; Ganachaud and Wunsch, 2000; Lumpkin and Speer, 2003; Ganachaud, 2003; Lumpkin and Speer, 2007). These inversions also return average diffusivities of $O(10^{-4} \text{ m}^2\text{s}^{-1})$ or greater below the thermocline, consistent with the work of Wyrтки and Munk.

It was therefore an unpleasant surprise when microstructure-based estimates of diapycnal mixing rates at thermocline depths consistently returned values of $O(10^{-5} \text{ m}^2\text{s}^{-1})$, an order of magnitude less than expected from indirect estimates (e.g., Gregg and Sanford, 1980; Gregg, 1987; Ledwell et al., 1993; Kunze and Sanford, 1996) and dynamical ideas. At first, the validity of diapycnal mixing estimates inferred from microstructure data were questioned. Issues related to undersampling and intermittency of turbulence were cited as reasons for the microstructure estimates being biased low (Gibson, 1982) and the theoretical framework linking mixing to temperature microstructure variance was called into question (Davis, 1994). The microstructure results were vindicated by the tracer release studies by Jim Ledwell and colleagues in the North Atlantic (Ledwell et al., 1993; Ledwell et al., 1998). After 30 months of evolution, the tracer cloud described by Ledwell et al., 1998 covered $O(1000 \text{ km}^2)$ and the spread of the tracer gave diffusivities of $O(10^{-5} \text{ m}^2\text{s}^{-1})$ consistent with and restoring confidence in the microstructure estimates.

Given the discrepancy between the canonical $K_p \sim 10^{-4} \text{ m}^2\text{s}^{-1}$ and the weak observed diffusivities in the ocean interior, different points of views regarding the role of diapycnal mixing in maintaining the abyssal stratification developed. One view, already suggested by Munk (1966), is that the ocean mixes primarily at its boundaries. The advection-diffusion balance (2) is then assumed to apply to spatially averaged properties of an abyssal ocean where diapycnal mixing is weak in the interior but much enhanced near the boundaries. The mixed products, but not the turbulence, are then assumed to be advected into the ocean interior along isopycnals (e.g., Armi, 1978; Munk and Wunsch, 1998). The latter assumption has led to some heated debates (e.g., Garrett, 1979) but is now generally accepted. By the mid-nineties, full-depth, deep microstructure profiles became technologically feasible for the first time. These direct measurements, and a number of recent indirect estimates, are much in line with the boundary mixing hypothesis, suggesting weak, $O(10^{-5} \text{ m}^2\text{s}^{-1})$, mixing over most of the ocean interior and bottom-intensified mixing in regions of rough topography. Turbulent diapycnal mixing rates 10-1000 greater than interior values have been observed in regions of rough topography such as seamounts (e.g., Lueck and Mudge, 1997; Toole et al., 1997; Carter et al., 2006), ridges (e.g., Althaus et al., 2003; Ledwell et al., 2000; Finnigan et al., 2002; Klymak et al., 2006; Auran et al., 2006; Lee et al., 2006) and canyons (Carter and Gregg, 2002; Thurnherr, 2006; St Laurent and Thurnherr, 2007). Intense mixing has also been observed where abyssal waters flow through bathymetric constrictions (e.g., Saunders, 1987; Roemmich et al., 1996; Polzin et al., 1996; Ferron et al., 1998; MacKinnon et al., 2008). Somewhat frustratingly, attempts to reconcile observations of bottom-intensified mixing to the large average diffusivities called for by Munk (1966) and indirect estimates

(heat budgets, inverse models) have generally fallen short (e.g., Toole et al., 1997; Kunze and Sanford, 1996; Kunze et al., 2006a). The apparent incompatibility between direct observations of bottom enhanced mixing and indirect estimates spawned the concept of “missing mixing” or “dark mixing”. The attempts to extrapolate observations of localized mixing to entire basins or globally were very crude however, representing observations of enhanced mixing near topography either as a step-function (e.g., Toole et al., 1997) or, at best, exponential decay (e.g., Kunze et al., 2006a). One finding of the work presented here and in Decloedt and Luther, 2009, is that use of a more realistic vertical structure function to represent the observations yields basin-averaged diffusivities roughly consistent with diffusivities derived from inverse models. That is, a more careful extrapolation of the observations of bottom-intensified mixing supports Munk’s (1966) contention that strong, localized mixing plays a major role in maintaining the abyssal stratification.

An alternative view is that the ocean mixes primarily at near-surface outcrops of neutral surfaces, that is, primarily in the Southern Ocean. This view has been explored by a number of authors (Toggweiler and Samuels, 1995; Doos and Coward, 1997; Toggweiler and Samuels, 1998; Toggweiler and Key, 2001; Webb and Sugimoto, 2001). The premise is that upwelling results predominantly from wind-driven upwelling in the Southern Ocean where isopycnals outcrop. The strong Westerlies result in northward Ekman flow, forcing deep water to the surface where the dense-to-light conversion occurs via mixing and buoyancy exchange with the atmosphere. In contrast to the majority of the ocean, where wind-driven upwelling is confined to the upper ocean, the upwelling in the Southern Ocean comes from deep waters. The reason is a peculiar dynamic constraint on the rotating Earth

called the “Drake Passage Effect” (Toggweiler and Samuels, 1995). Due to the lack of topographic barriers at the latitude band of the Drake Passage, no zonal pressure gradient and thus no geostrophic meridional flow outside frictional boundary layers can be maintained there. This means that the surface waters pushed northwards via the Ekman transport induced by the Westerlies can only be returned to the south at depths greater than ~ 2500 m, below which topographic features exist to support meridional flow. In this view, there is only need for minimal diapycnal mixing in the abyssal ocean to balance the deep and bottom water formation rate.

Figure 4 is a cartoon summarizing both extremes. In the real ocean, both wind-driven upwelling and enhanced boundary mixing likely contribute to the abyssal circulation. A quantitative knowledge of their respective contributions is still lacking. Based on inversion of WOCE hydrographic data, the case for wind-driven upwelling only can quite safely be ruled out however, since the observed geostrophically balanced flow requires strong abyssal mixing given the observed property distributions (Ganachaud and Wunsch, 2000).

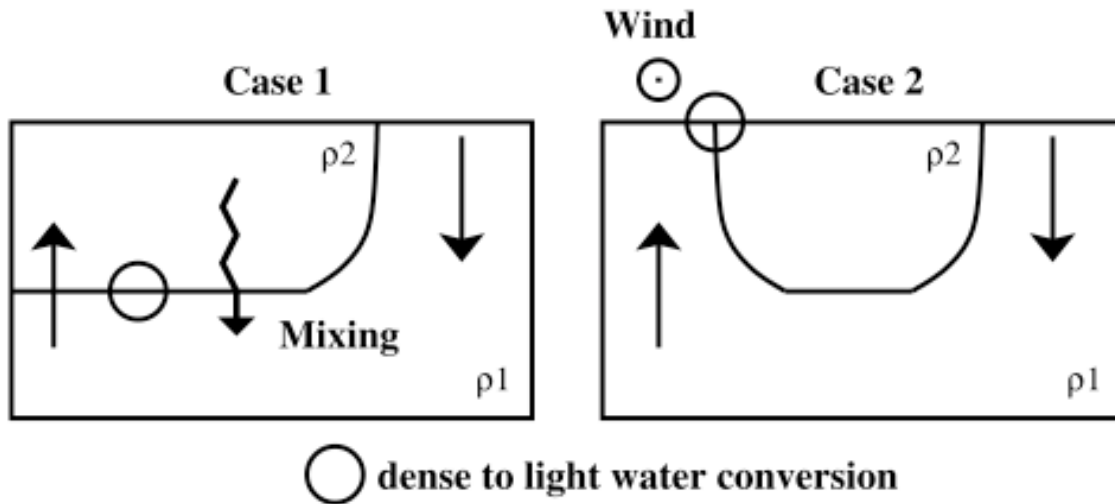


Figure 4: Sketch of two extreme cases: only diapycnal mixing (case 1) and only wind-driven upwelling (case 2). The sketches represent highly simplified meridional sections with North Atlantic Deep Water (NADW) formation at the right (northern) end. The curved line represents the thermocline separating dense from light waters. The open circles indicate regions of dense-to-light conversion of water masses. In the wind-driven case, the Southern Ocean westerlies are represented by the vector coming out of the page. Straight arrows indicate volume transport and the zigzag arrow stands for downward heat flux due to diapycnal mixing. Figure from Kuhlbrodt et al., 2007.

1.4. *Diapycnal mixing and the MOC*

The importance of diapycnal mixing with respect to the climatically important MOC is very much intertwined with the previous discussion regarding the maintenance of the abyssal stratification against the influx of deep and bottom water. It is now generally accepted that deep and bottom water formation is a prerequisite for the existence of the overturning circulation but does not drive it in the sense of providing the energy required to close the circulation (e.g., Wunsch and Ferrari, 2004; Kuhlbrodt et al., 2007). Instead, it is argued that the processes allowing for the upwelling and conversion of deep water “drive” the MOC, or form its closing limb. That is, strong abyssal mixing or wind-driven upwelling and mixing at near-surface outcrops in the Southern Ocean. Determining the relative importance of abyssal mixing to wind-driven upwelling in the Southern Ocean in driving the MOC is of great relevance to climate studies. Clearly, determining the relative importance of the tides versus the wind (or other sources) in supplying the mechanical energy required for diapycnal mixing in the abyssal ocean is a related question of importance.

The above argument is often rationalized using Sandstrom’s postulate that no overturning circulation can occur for a stratified fluid both heated and cooled at the surface (approximately the case for the ocean) without some external mechanical driving process (Sandstrom, 1908; Sandstrom, 1916; Kuhlbrodt, 2008 for an English translation). That is, no work can be extracted from a stratified fluid both heated and cooled at the surface and thus no overturning circulation can occur. As an aside, note that Sandstrom’s postulate, while intuitively appealing, does not take the Earth’s rotation into account and is therefore of

dubious relevance in the real ocean. Without rotation, meridional pressure gradients created by the density gradient drive a down-gradient flow balanced by friction in steady state, resulting in a 2-dimensional overturning circulation. Allowing for rotation, meridional pressure gradients are largely balanced by the Coriolis force and meridional transports are driven by zonal pressure gradients, resulting in a 3-dimensional circulation considerably more complex than suggested by Sandstrom's postulate (F. Schloesser, 2009, personal communication).

1.5. *Dynamical significance of spatially varying diapycnal mixing*

Dynamically, vertical gradients of the diapycnal diffusivity dictate the strength of diapycnal upwelling via the buoyancy equation (St Laurent, 1999):

$$w \approx -N^{-2} \partial_z J_b = N^{-2} \partial_z (K_\rho N^2) \quad (3)$$

where N is the buoyancy frequency and $J_b = -K_\rho N^2$ the buoyancy flux. In turn, the vertical gradient of upwelling influences the geostrophic vorticity balance. For a neutral density layer of thickness h , the steady-state geostrophic vorticity balance can be written as:

$$\beta v = \frac{f}{h} \vec{u} \cdot \nabla h + \frac{f}{h} (w(z_u) - w(z_b)) \quad (4)$$

where f is the coriolis frequency, β the planetary vorticity gradient, \vec{u} the flow along neutral density surfaces and $z_{u,b}$ denote the upper and bottom bounding neutral density surfaces.

From substitution of (3) into (4), it follows that the geostrophic vorticity balance is influenced by the vertical structure of the diapycnal diffusivity. St Laurent et al., 2001 present observational evidence for deep flow driven by buoyancy forcing provided by small-scale turbulent mixing in the abyssal Brazil Basin. That is, large-scale flow is influenced by turbulent motion on centimeter scales! In the abyssal ocean, far removed from the wind-driven Ekman layer, buoyancy forcing provided by turbulent diapycnal mixing may be the dominant forcing of abyssal flow (St Laurent et al., 2001).

Another noteworthy consequence of spatially varying K_ρ follows from (3). Expanding the right-hand side yields:

$$w = \partial_z K_\rho + \frac{K_\rho}{N^2} \partial_z N^2 \quad (5)$$

For a diffusivity increasing towards the bottom as observed, the first term on the right-hand side of (5) produces downwelling that opposes the upwelling generally implied by the second term (e.g., Talley et al., 2003; Simmons et al., 2004b; Saenko and Merryfield, 2005). The downwelling implied by (5) for bottom-intensified mixing is wildly at odds with the concept of ~ 30 Sv of deep and bottom water upwelling via diapycnal mixing across the thermocline, at least at first sight. This issue, usually unceremoniously swept under the rug, is discussed by Toole, 1998; St Laurent et al., 2001 and Polzin, 2009 in the context of the Brazil Basin Tracer Release Experiment (BBTRE). In light of flow entering the Brazil Basin through the

Vema Channel, mass balance conservation of bottom waters requires upwelling. This balance is suspected to be achieved by strong “upward” flow across isopycnal within the many canyons on the Mid-Atlantic Ridge. This conjecture is supported by the estimates of flow in canyons by Thurnherr et al., 2005 and prompted Polzin (2009) to liken the Mid-Atlantic Ridge to a lung, inhaling deep water on its flanks and exhaling at the canyon heads.

Considering the above discussion, global and basin-scale circulation patterns computed with spatially heterogeneous diapycnal mixing can be expected to differ from those obtained with uniform mixing. Early numerical studies of the sensitivity of the circulation to spatially localized mixing (e.g., Samelson, 1998; Hasumi and Sugimoto, 1999) confirmed that this is indeed the case. A growing number of studies now illustrate consequences of non-uniform mixing on the ocean circulation. Non-uniform mixing significantly alters the abyssal circulation from the classical Stommel-Arons pattern (e.g., Huang and Jin, 2002; Katsman, 2006). Katsman (2006) extended the classical Stommel-Arons theory for the stationary abyssal circulation by introducing bathymetry in the form of a mid-ocean ridge with strongly enhanced upwelling in the vicinity of the ridge. It was found that locally enhanced upwelling over the ridge drives a β -plume circulation modified by topographic stretching. Figure 5 compares the case of uniform upwelling over a flat bottom (Stommel-Arons) to non-uniform upwelling over topography mimicking a ridge. Spatially varying mixing also improves the representation of water masses (e.g., Simmons et al., 2004b; Koch-Larrouy et al., 2007) in OGCMs, has a bearing on the simulated deep ocean stratification (Saenko, 2006) and results in a stronger and deeper simulated Antarctic Circumpolar Current (e.g., Saenko and Merryfield, 2005; Jayne, 2009). Additionally, non-uniform mixing was found to affect the

poleward heat transport (Simmons et al., 2004b) although later studies (Saenko and Merryfield, 2005; Jayne, 2009) indicate that the poleward heat transport is more affected by the value of diapycnal mixing in the upper ocean and thermocline than in the abyssal ocean. Clearly, the observed bottom-enhancement of mixing in regions of rough topography must be included in mixing parameterizations to improve confidence in ocean circulation simulations.

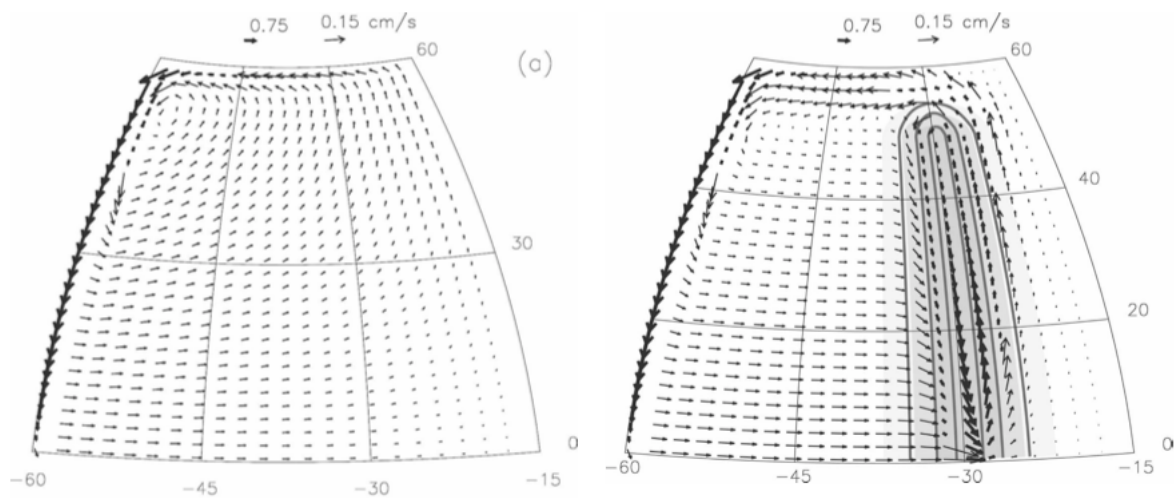


Figure 5: On the left, the stationary abyssal circulation forced by uniform upwelling over a flat bottom (Stommel-Arons). The downwelling source is in the top left corner. On the right, the stationary abyssal circulation forced by non-uniform upwelling over topography mimicking a mid-ocean ridge. Upwelling over the ridge is two orders of magnitude greater over the ridge than that applied over flat areas of the domain. Figure from Katsman (2006).

1.6. Spatially varying mixing parameterizations: The current state of affairs

Traditionally, OGCMs employ constant, ad hoc diapycnal diffusivities used as a tuning parameter or a diffusivity profile varying only in the vertical (e.g., Bryan and Lewis, 1979). Mixing parameterizations based on local energy arguments have also been implemented in OGCMs (e.g., Large et al., 1994) where diapycnal mixing is related to the Richardson number and a background diffusivity. Short of running at unrealistically high resolutions supporting the internal wave field, these Richardson number schemes effectively result in spatially uniform mixing in the abyssal ocean.

The work by Hasumi and Suginohara, 1999 is the first attempt to incorporate bottom-intensified mixing in regions of rough topography into an OGCM. They used the standard deviation of ETOPO5 bathymetry divided by the average ocean depth for each grid box as an index of topographic roughness and assigned a bottom-intensified diffusivity profile everywhere this index exceeded a critical value. The enhanced profile decreased exponentially with height above bottom and was roughly consistent with values presented by Kantha and Tierney, 1997. The scheme was necessarily crude and arbitrary but the resulting simulation results illustrated well the sensitivity of the global ocean circulation on the spatial distribution of diapycnal mixing.

St. Laurent and co-authors (St Laurent, 1999; Jayne and St Laurent, 2001; St Laurent et al., 2002), SL02 hereafter, propose a parameterization for the tidal component of bottom-intensified mixing. Internal tides are generated by barotropic tidal flow over rough

topographic features, with energy going into a wide range of vertical modes or scales. The lowest modes typically radiate away and can travel thousands of kilometers before being dissipated whereas the higher modes have small group velocities, small vertical scales and more shear and are therefore prone to being dissipated locally. The SL02 parameterization seeks to characterize diapycnal mixing resulting from the local dissipation of high modes near internal tide generation sites in terms of an internal tide drag term added to the Laplace tidal equations. The turbulent kinetic energy dissipation rate is estimated as the product of 3 terms: 1) $E(x,y) \cong 1/2\rho N_b \kappa h^2 \langle u_{bt}^2 \rangle$, the rate of energy conversion from barotropic to baroclinic tide as a function of topographic roughness, bottom stratification N_b and the time mean square barotropic tidal velocity $\langle u_{bt}^2 \rangle$; 2) q , the fraction of this energy dissipated locally; and, 3) $F(z) = [e^{-(H+z)/\zeta}] / [\zeta(1 - e^{-H/\zeta})]$, an assumed exponential vertical structure function for the TKE dissipation rate. Using the Osborn (1980) relation between the diapycnal diffusivity and the TKE dissipation rate,

$$K_\rho = \frac{\Gamma \varepsilon}{N^2} \quad (6)$$

where $\Gamma \approx 0.2$ is the mixing efficiency, the spatial distribution of the diapycnal diffusivity is given by

$$K_\rho(x,y,z) = \frac{q\Gamma E(x,y)F(z)}{\rho N^2} + K_0 \quad (7)$$

$K_0=10^{-5} \text{ m}^2\text{s}^{-1}$ is the background diffusivity. The vertical decay scale $\zeta = 500 \text{ m}$ and choice of $q=0.3\pm 0.1$ are motivated by the Brazil Basin microstructure data. The topographic roughness is characterized by a topographic wavenumber κ and amplitude scale h where the latter is estimated from Smith and Sandwell, 1997 bathymetry. The wavenumber κ is tuned to minimize the difference between modeled and observed barotropic tides in a least-squared sense (Jayne and St Laurent, 2001). The SL02 tidal parameterization yields a spatially varying diapycnal mixing distribution on a global scale and has been widely implemented in OGCM studies (e.g., Simmons et al., 2004b; Saenko and Merryfield, 2005; Koch-Larrouy et al., 2007; Jayne, 2009). As cautioned by Jayne and St. Laurent (2001), the SL02 parameterization remains a preliminary formulation and has not been validated extensively against observations. A number of details of the SL02 certainly need refinement. For instance, the parameters q and ζ , the fraction of internal tide energy dissipated locally and the vertical decay scale respectively, are specified as constants although it is likely these are functions of space and perhaps even time.

A heuristic recipe towards a dynamical parameterization of the TKE dissipation has been laid out by K. Polzin (Polzin, 1992; Polzin, 1999; Polzin, 2004a; Polzin, 2004b; Polzin, 2009). Polzin interpreted the observed bottom-intensified TKE dissipation profile in the Brazil Basin as the interplay between bottom-generated internal waves propagating upwards and the nonlinear transfer of energy within the internal wave field by wave-wave interactions towards smaller-scale, subsequently breaking internal waves. Idealized analytical solutions for the vertical structure of the TKE dissipation rate decay with height above bottom h as $\varepsilon = \varepsilon_0(1 + h/h_0)^{-2}$ where the maximum dissipation at the bottom ε_0 and decay scale height h_0

are to be determined from models of internal wave generation and scattering. In principle, the recipe can be altered to account for different sources (i.e., not just tidal internal waves). The philosophy laid out in Polzin (2009) is however that the energetics of the finescale internal wavefield is dominated by tidal frequencies and that this is a local process. This last assumption goes against the current nonlocal paradigm, where it is assumed that a large fraction of the internal tide energy radiates away from the generation sites and is dissipated elsewhere, possibly thousands of kilometers away (e.g., Jayne and St Laurent, 2001; St Laurent and Nash, 2003). Polzin (2009) describes his decision to only include tides in the recipe as “throwing caution to the wind”. Developing a parameterization is an iterative process however and other sources of energy can be included in the future.

1.7. Spatially varying mixing: a multi-component process

The spatial heterogeneity of diapycnal mixing is due to a plethora of complex flow-topography interactions deriving their energy from various sources. Tidally driven dissipation as parameterized by SL02 and Polzin (2009) may not be the dominant component. Little progress has been made in parameterizing other components of topography-catalyzed mixing although these are likely to have a comparable impact on the spatial distribution of mixing. For instance, abyssal mixing can also be sustained by instability of internal lee waves associated with near-bottom mesoscale currents (e.g., Polzin and Firing, 1997; Marshall and Naveira Garabato, 2007), or by the interaction of remotely generated internal waves (e.g., near-inertial internal waves, low mode internal tides radiating away from distant generation sites) with topography through for instance reflection from a critical slope (e.g., Eriksen, 1998; Legg, 2003; Nash et al., 2004; Aujan and Merrifield,

2008) or scattering off rough topography (Muller and Xu, 1992). A recent numerical study (Saenko, 2008) demonstrates that wind-driven abyssal flow can have magnitudes rivaling that of barotropic tidal flow over vast areas on seasonal time scales, thus potentially contributing significantly to abyssal mixing. Other processes contributing to topography-catalyzed mixing not yet parameterized include (but are not limited to) boundary layer turbulence (e.g., Armi, 1978; Ivey, 1987), hydraulic flow through constricted passages (e.g., Ferron et al., 1998; Thurnherr et al., 2005) and episodic overflow events at deep sills (e.g., Lukas et al., 2001). As is clear from this list, the tides are not the sole source of energy available for mixing the abyssal ocean; the wind is generally held to be a source of equal importance (e.g., Munk and Wunsch, 1998; Wunsch and Ferrari, 2004).

Another interesting source of turbulence is biomixing. Again, this concept was first introduced by Munk (1966). Munk considered the turbulence engendered by the sinking of fecal pellets. This was however more of a joke (M. Gregg, personal communication). More recently, a number of papers have put the concept of biomixing on more solid ground. The turbulent dissipation produced by swimming of schools of animals, be they Antarctic krill, northern anchovy, bluefin tuna or jellyfish, turns out to be several orders of magnitude greater than background values of the TKE dissipation rate (e.g., Huntley and Zhou, 2004; Dewar et al., 2006; Kunze et al., 2006b; Visser, 2007; Gregg and Horne, 2009; Katija and Dabiri, 2009). It may very well be that biomixing is important in determining the coastal stratification in certain areas of the global ocean such as Saanich inlet. The domain of interest here is the abyssal ocean. There is little evidence that biomixing plays any role at such depth.

Figure 6 is a rough sketch of energy flow from sources to dissipation near topography suggesting that tidal mixing likely accounts for no more than half of the diapycnal mixing occurring in the abyssal ocean. This is consistent with the rough energy budgets presented in Munk and Wunsch, 1998 and Wunsch and Ferrari, 2004. The role of tidal mixing may therefore have been overemphasized the past decade, as for instance suggested by Toole, 2007 and Ferrari and Wunsch, 2009. This serves as the motivation for the development of the RDM in the following chapter.

For completeness, the buoyancy work done by geothermal heating should be taken into consideration. The buoyancy work done by geothermal heating is generally considered unimportant (e.g., Wunsch and Ferrari, 2004) compared to the buoyancy flux resulting from bottom-intensified turbulence. A scaling argument to justify this assumption was discussed by St. Laurent, 1999. The geothermal heat flux, F_{bot} , has values varying from 50 mWm^{-2} across abyssal plains to 250 mWm^{-2} near the axis of Mid-Ocean Ridge systems (e.g., Wei and Sandwell, 2006). The associated buoyancy flux is given by

$$J_{bot} = \frac{g\alpha F_{bot}}{\rho c_p} \quad (8)$$

where $c_p \sim 4000 \text{ J Kg}^{-1} \text{ }^\circ\text{C}^{-1}$ is the specific heat capacity of seawater, g is the acceleration due to gravity and $\alpha \sim 1.7 \times 10^{-7} \text{ K}^{-1}$ is the thermal expansion coefficient. Taking F_{bot} as 100 mWm^{-2} , the buoyancy flux resulting from geothermal heating is $O(10^{-11}) \text{ W kg}^{-1}$. This is to

be compared to the buoyancy flux resulting from turbulence $\Gamma\varepsilon \approx 0.2\varepsilon$. For observed values of bottom-intensified turbulence $\varepsilon \sim 10^{-9} \text{ W kg}^{-1}$, the buoyancy flux resulting from diapycnal mixing exceeds those by geothermal heat fluxes by at least an order of magnitude. Nonetheless, a number of papers demonstrate the potential dynamical importance of geothermal heating with respect to the abyssal circulation (e.g., Adcroft et al., 2001). Furthermore, geothermal heating has a complex spatial distribution, see Figure 1. As for diapycnal mixing, it is likely that the localized nature of geothermal heating is of dynamical importance and certainly requires further investigation.

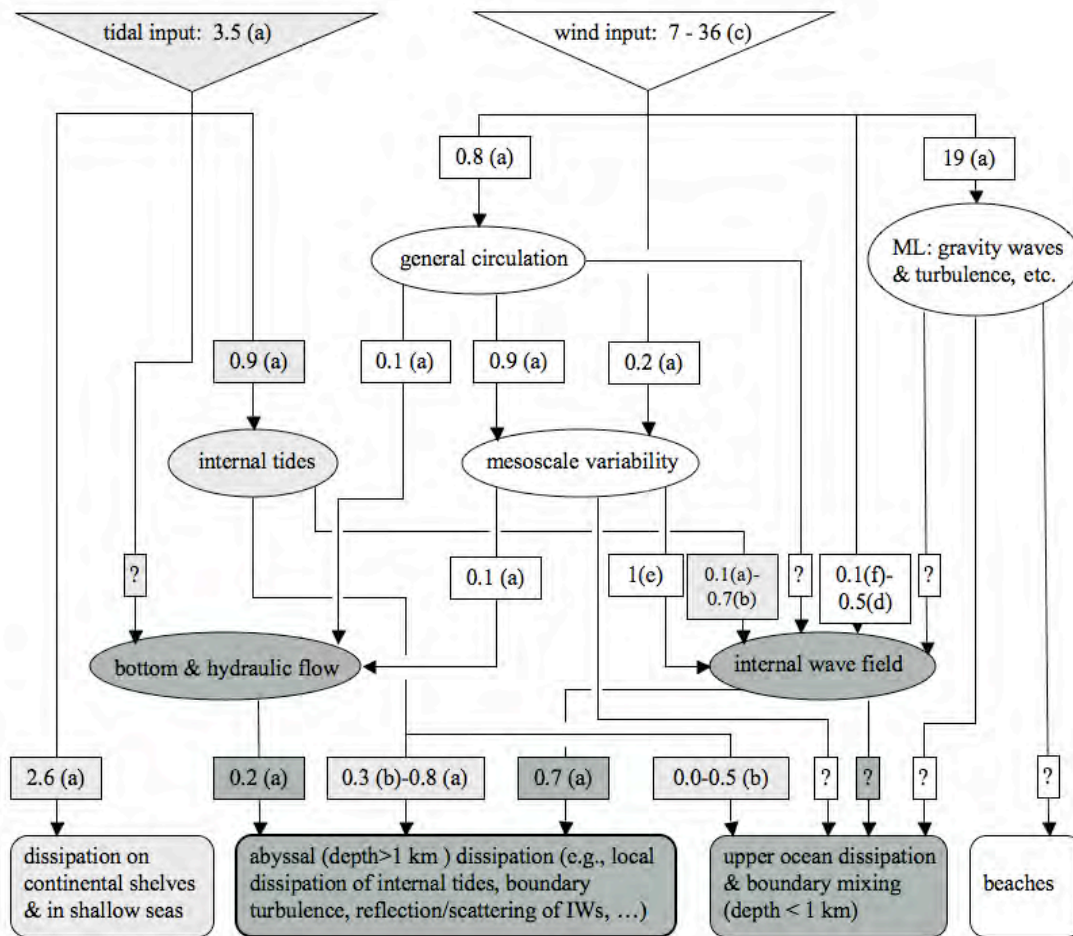


Figure 6: Speculative energy paths from principal sources (top row) to dissipation (an update of Fig. 5 of Wunsch and Ferrari, 2004)). Fluxes are in TW (10^{12} W) with uncertainties of at least factors of 2 and possibly as large as 10. Colors are indicative of the dominant source of energy flux, white corresponding to wind work, light gray to tidal work and the dark gray to a combination of both. Letters indicate references: (a) Wunsch and Ferrari, 2004) (b) Jayne and St Laurent, 2001), (c) Lueck and Reid, 1984), (d) Alford, 2003) and (e) Williams et al., 2008). The astronomically-determined tidal energy dissipation rate is 3.7 TW, of which 0.2 TW drives the solid Earth tides, leaving 3.5 TW to be dissipated in the ocean. 2.6 TW is dissipated in the shallow seas and 0.9 TW is thought to be converted to internal tides. The wind stress causes inertial oscillations in the surface mixed layer with a flux of 0.5 TW into near-inertial internal waves. Surface gravity wave generation, langmuir cells and mixed-layer turbulence by wind stress may take 19 TW, an unknown fraction of which goes into the internal wave field through resonant interaction and forcing at the base of the mixed layer. Roughly 1 TW of the wind work goes into the general circulation, which may leak energy to the internal wave field (e.g., through lee wave generation over rough topography) or directly produce near-bottom turbulent mixing catalyzed by rough topography. Barotropic and

baroclinic instabilities of the general circulation lead to mesoscale eddies which in turn can lose energy to the internal wave field through loss of balance and through near-bottom topography-catalyzed turbulence. Possible energy paths from eddies and mixing to the general circulation (e.g., Wunsch and Ferrari, 2004) and the $O(1 \text{ TW})$ estimate of biomechanical mixing (e.g., Dewar, 2006) are not shown.

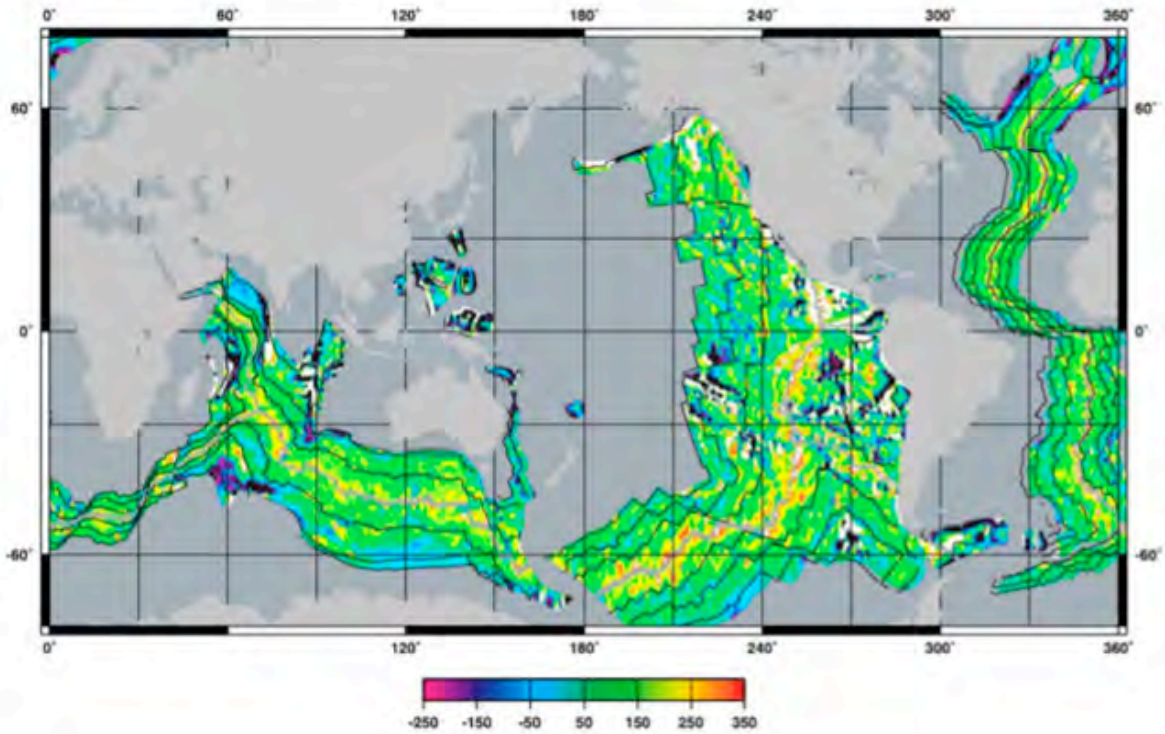


Figure 7: A global map of geothermal heat flow in mWm^{-2} . Figure from Wei and Sandwell, 2006.

Chapter Two

2. The Roughness Diffusivity Model (RDM)

2.1. *Rationale of the RDM*

As discussed in the previous chapter, a large number of processes contribute to topography-catalyzed mixing in the abyssal ocean. To date, efforts towards spatially varying mixing parameterizations have focused mostly on one physical process related to tidally driven mixing, the local dissipation at sites of internal tide generation (e.g., SL02, Polzin (2009)). Rough energy budgets suggest that the mechanical energy extracted from the barotropic tides likely represents no more than half of the mechanical energy available for diapycnal mixing in the abyss however. Furthermore, it appears that a dominant fraction of the internal tide energy radiates away in the form of low modes rather than resulting in local dissipation although Polzin (2004b, 2009) argues otherwise. It is thus likely that processes other than local dissipation at internal tide generation sites significantly influence the spatial distribution of diapycnal mixing. The premise of the RDM developed here is that topography-catalyzed diapycnal mixing resulting from a broad range of processes can be approximated as depending mainly on topographic roughness. Conceptually, this is akin to assuming that the abyssal ocean is replete with background currents of tidal and lower frequencies, and that there are numerous processes modifying these currents and the ambient internal wave field itself near topography leading to an energized internal wave field and enhanced mixing. Supposing that the decay to background internal wave conditions is not prohibitively

dependent on the process energizing the near- boundary internal wave field, a relation between the spatial distribution of diapycnal mixing and topographic roughness can be expected. Such a dependence is here sought empirically, using as much quality data as possible.

2.2. Observations of turbulent diapycnal mixing in the abyssal ocean

The first measurements of oceanic turbulence were made during the summer of 1950 by a small group of young researchers at the Pacific Naval Laboratory in British Columbia, Canada. The group was directed by R. Stewart who had only just completed his Ph. D. at Cambridge where he studied turbulence in G. I. Taylor's group under the supervision of G. Batchelor and A. Townsend. The Canadian Defense Research Board funded his group to see if the turbulent wake of submarines could be detected for a useful distance behind submarines. Initial (published) attempts to detect the wake of submarines were a complete failure (Stewart and Grant, 1999). Prompted by Batchelor who had just discovered the work by A. N. Kolmogorov and W. Heisenberg⁴, the group towed a mine-sweeping paravane instrumented with anemometers and thermometers through Discovery Passage, a coastal tidal channel where turbulence is intense ($Re = \frac{ul}{\nu} \approx 10^8$). This experiment verified Kolmogorov's famous prediction of a $k^{-5/3}$ slope in the inertial subrange at high Reynolds numbers

⁴ Werner Heisenberg's (1923) doctoral thesis was on turbulent flow. Being prohibited from working on nuclear physics by the allied forces after the war, he briefly returned to turbulence and developed a theory for the energy transfer from larger to smaller scales, (Heisenberg, 1948), similar to the 1941 paper by A.N. Kolomogorov which remained unknown in the west until after the war.

(Kolmogorov, 1941). The initial military failure was thus a great scientific success and started the field of ocean microstructure measurements (Lueck et al., 2002).

Since then, a wide variety of instruments and techniques have been developed to infer oceanic turbulence. A number of datasets were gathered for the study here. These consist of diapycnal mixing inferred from direct microstructure measurements as well as diapycnal mixing inferred from standard hydrographic data using i) theoretical ideas of energy transfer within the internal wave field (fine-scale parameterizations), and ii) inverse geostrophic box models. These datasets and techniques are discussed in more detail below.

2.2.1. Diapycnal mixing inferred from microstructure data

Microstructure profilers are highly specialized sensors capable of measuring the turbulent velocity and temperature gradient variances down to millimeter scales. The term microstructure refers to scales smaller than 0.5 meter in the vertical (Polzin and Montgomery, 1996). The most common method to infer diapycnal diffusivities from microstructure data is the Osborn method (Osborn, 1980) based on energetic arguments. Assuming isotropy, the turbulent kinetic energy (TKE) dissipation rate is directly related to the turbulent velocity variance by $\varepsilon = 7.5\nu\langle u_z'^2 \rangle$ where ν is the molecular viscosity. Osborn, 1980 related the TKE dissipation rate ε to the diapycnal diffusivity K_ρ via a 3-term dominant balance in the turbulent kinetic energy:

$$\langle u'w' \rangle \overline{U_z} = -\frac{g}{\rho_o} \langle w'\rho' \rangle - \varepsilon \quad (9)$$

That is, the production of turbulent kinetic energy by turbulent stresses $\langle u'w' \rangle$ on the mean shear $\overline{U_z}$ is balanced in the mean by the viscous dissipation of TKE ε and/or an increase of potential energy by a turbulent diapycnal buoyancy flux $-\frac{g}{\rho_o} \langle w'\rho' \rangle$. The flux Richardson number is defined as:

$$R_f = \frac{-\frac{g}{\rho_o} \langle w'\rho' \rangle}{\langle u'w' \rangle \overline{U_z}} \quad (10)$$

and we can therefore rewrite the turbulent kinetic energy balance (9) as:

$$\frac{g}{\rho_o} \langle w'\rho' \rangle = \frac{R_f}{1-R_f} \varepsilon \quad (11)$$

Then, since $\langle w'\rho' \rangle = -K_\rho \overline{\rho_z}$ (eddy diffusivity assumption) and $N^2 = -\frac{g}{\rho_o} \overline{\rho_z}$, we obtain the

celebrated Osborn relation :

$$K_\rho = \frac{R_f}{1-R_f} \frac{\varepsilon}{N^2} = \Gamma \frac{\varepsilon}{N^2} \quad (12)$$

The Richardson flux number is generally taken to be a constant in the oceanographic context, with values between $R_f = 0.15$ (Osborn, 1980) and $R_f = 0.20$ (Oakey, 1982). Accordingly, a mixing efficiency $\Gamma = 0.20 \pm 0.05$ is generally assumed.

Microstructure profiles provide the most direct estimate of diapycnal mixing to date. The TKE dissipation rate profiles considered here were obtained from the Absolute Velocity Profiler (AVP) and the High Resolution Profiler (HRP). Both these instruments are so-called multi-scale profilers, designed to measure turbulent and non-turbulent velocity and velocity shear over vertical scales ranging from microstructure to the full depth of the ocean.

The AVP (Figure 8) is an old fine-scale profiler upgraded by T. Sanford at the Applied Physics Laboratory (APL), University of Washington with shear probes to convert it into a multi-scale profiler. The AVP is a free-fall profiler carrying a variety of sensors which determine horizontal velocity, temperature, electrical conductivity, pressure, oxygen, optical transmissivity (turbidity) and the turbulent kinetic energy dissipation rate. Horizontal velocity is measured relative to an unknown but depth-independent constant using the voltage across the body induced by seawater's motion in the Earth's magnetic field. It is made absolute by measuring the Doppler shifts of bottom-scattered acoustic echoes when the AVP is within about 400 m of the seafloor. The AVP resolves dissipation rates as small as $\epsilon \sim 3 \times 10^{-9} \text{ W kg}^{-1}$ (Lueck et al., 2002).

The HRP was developed at the Woods Hole Oceanographic Institution (WHOI) by R. Schmitt and J. Toole. The HRP is a 5.3 m long multi-scale profiler capable of reaching full ocean depth. Like the AVP, it is true free-fall profiler without a tether. The sensors consist of CTD probes, microstructure sensors (shear, temperature, conductivity) and an acoustic current meter for fine-scale velocity measurements. The HRP noise levels of the dissipation estimates are the lowest obtained with any instrument to date. The HRP resolves dissipation

rates as low as $\epsilon \sim 3 \times 10^{-11} \text{ W kg}^{-1}$ (Polzin and Montgomery, 1996). See Figure 9 for a schematic of the HRP.



Figure 8: The Absolute Velocity Profiler (AVP). Picture from <http://opd.apl.washington.edu/tools/index.html>

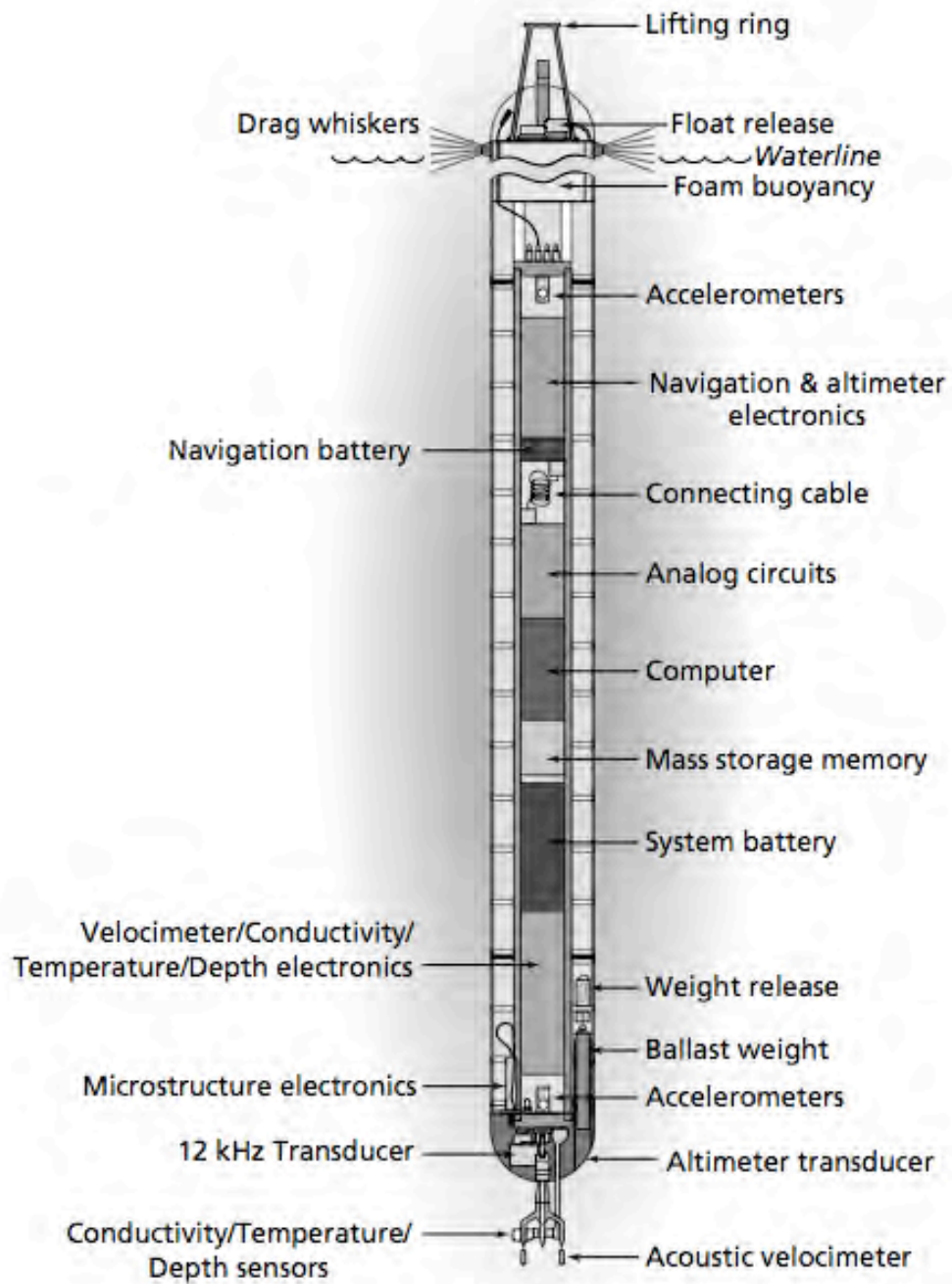


Figure 9: Schematic of the High Resolution Profiler (HRP).

TKE dissipation rate profiles inferred from microstructure data from three different oceanic regions are considered in this thesis:

- 95 profiles of the TKE dissipation rate derived from High Resolution Profiler (HRP) microstructure data collected in 1991 around the Fieberling Guyot, a seamount in the subtropical northeast Pacific Ocean ($32^{\circ} 26' N$, $127^{\circ} 46' W$), as part of the Topographic Interactions Accelerated Research Initiative. These profiles were generously provided by Dr. John Toole. For precise details of the dissipation calculation see Montgomery and Toole, 1993. Further discussion and analysis of this data can be found in Toole et al., 1997; Kunze and Toole, 1997; Eriksen, 1998. Non-tidal internal wave reflection and diurnal tide driven, vortex-trapped near-inertial internal waves atop of the seamount are thought to be responsible for most of the observed intensified mixing.
- 165 full depth profiles of the TKE dissipation rate derived from HRP deployments acquired in 1996 and 1997 during the Brazil Basin Tracer Release Experiment (BBTRE), a component of the World Ocean Circulation Experiment. These profiles were also obtained courtesy of Dr. John Toole. The collective microstructure data set spanned nearly 30 degrees in longitude from the relatively smooth western Brazil Basin to the rough fracture zones of the Mid-Atlantic Ridge. The 1996 and 1997 data sets are henceforth referred to as Brazil Basin I and Brazil Basin II, respectively. A survey of the data is given in Montgomery, 1998 and analysis in St Laurent, 1999; Polzin et al., 1997; Zhang et al., 1999; Ledwell et al., 2000; St Laurent et al., 2001; Morris et al., 2001; Polzin, 2004b; Thurnherr et al., 2005; Toole, 2007. The strong turbulence over the Mid-

Atlantic Ridge has been attributed to internal waves generated by semi-diurnal tidal flow over rough topography, shear due to near-inertial motions, and sill-related processes in ridge-flank canyons.

- 13 mean profiles of the TKE dissipation rate derived from deployments of the deep Absolute Velocity Profiler (AVP) around the Hawaiian Islands ridge at the French Frigate Shoals, Necker and Nihoa Islands, and the Kauai Channel. These profiles were obtained courtesy by Drs. Jody Klymak, Thomas Sanford and Jim Moum. Each station was occupied for approximately 20 hours, allowing 4 to 6 full depth casts to be acquired and incorporated into the mean TKE profiles. These data were collected as part of the 2000 Hawaii Ocean Mixing Experiment (HOME) field program described in Rudnick et al., 2003. Mixing around the Hawaiian ridge has been studied extensively, e.g., Finnigan et al., 2002; Merrifield and Holloway, 2002 Klymak et al., 2006; Aucan et al., 2006; Carter et al., 2006; Lee et al., 2006; Levine and Boyd, 2006a; Martin et al., 2006; Rainville and Pinkel, 2006a; Rainville and Pinkel, 2006b; Zaron and Egbert, 2006; Klymak et al., 2007; Martin and Rudnick, 2007; Aucan and Merrifield, 2008. Intensified mixing near the Hawaiian Ridge has been attributed to local dissipation of the M2 internal tide generated at the ridge, dissipation of near-inertial internal waves generated north of the ridge by winter storms and strong nonlinear interactions via Parametric Subharmonic Instability (PSI).

The AVP data were obtained preprocessed in the following way; TKE dissipation rates were computed spectrally over 5-m depth intervals, these were then depth bin averaged into 100-m

depth intervals $\langle \varepsilon \rangle$. Average diapycnal diffusivities $\langle K_\rho \rangle = \Gamma \langle \varepsilon \rangle / \overline{N^2}$ (Osborn, 1980) were computed based on $\langle \varepsilon \rangle$, the survey mean stratification $\overline{N^2}$ and a mixing efficiency $\Gamma=0.2$ (Oakey, 1982). These estimates are considered conservative minima (Lee et al., 2006).

The TKE dissipation rate estimates collected by the HRP were obtained as 0.5-m binned averages. For the purposes of this work, these were further averaged over 10-m depth bins. Integral time scale estimates using the ARMAse1 algorithm (Broersen, 2002) indicated that an averaging length of 10-m is sufficient to obtain uncorrelated estimates of ε , consistent with the findings of Gregg et al., 1993. Diapycnal diffusivities K_ρ were obtained from the Osborn (1980) scaling using the 10-m depth bin averaged TKE dissipation rates, a mixing efficiency $\Gamma=0.2$ and the local stratification profiles. The HRP profiles were obtained over a large geographical area and to varying depths. We therefore used the local stratification profiles since lateral variability in the background buoyancy frequency may incur serious errors when using a spatially mean stratification profile (e.g., Polzin, 1992). For the HRP surveys used here, as well as for the AVP study around the Hawaiian islands, the differences in the inferred K_ρ depending on whether the local profile or the survey mean stratification profile is used are minimal however. The stratification profiles were computed via the adiabatic leveling method (Bray and Fofonoff, 1981) over 10-db pressure intervals centered about each dissipation estimate. TKE dissipation rates and diapycnal diffusivities were then bin averaged over 100-m height above bottom bins $\langle \varepsilon \rangle$ and $\langle K_\rho \rangle$. In the subsequent analysis, only data deeper than 500 m of depth are included so as to avoid enhanced dissipation from

upper ocean effects. Figure 10 shows the arithmetic⁵ mean vertical profiles of the deep ocean TKE dissipation rate $\langle \varepsilon \rangle$ and inferred diapycnal diffusivity $\langle K_\rho \rangle$ for the data sets discussed above. As a function of depth (not shown), no vertical structure is apparent. As a function of height above bottom, the mean diapycnal diffusivity profiles have maxima of $O(10^{-3}) \text{ m}^2\text{s}^{-1}$ at the bottom boundary and decay with height above the bottom towards background values of $O(10^{-5}) \text{ m}^2\text{s}^{-1}$. The mixing is intensified at least up to 1 km from the bottom and thus the influence of topography-catalyzed mixing extends well into the stratified ocean interior. The mean TKE dissipation rate profiles tend to have maxima near the bottom and at thermocline depths and shallower due to the strong stratification in the upper ocean.

⁵ The mean vertical diffusivity profile was also computed using the maximum likelihood estimator described in Baker and Gibson, 1987). We found that the microstructure data is sufficiently densely sampled to allow the use of the arithmetic mean without significant bias.

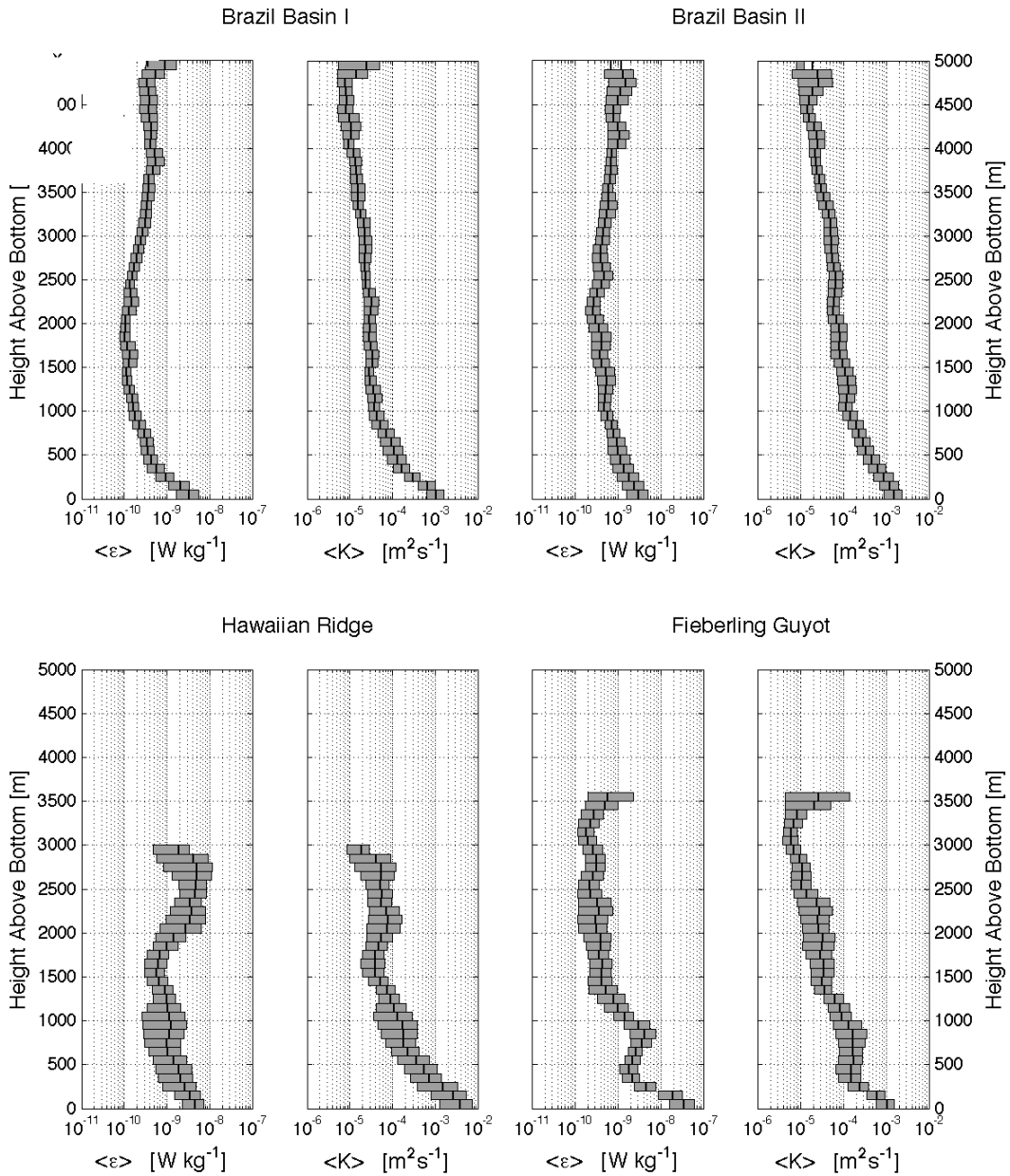


Figure 10: Mean vertical profiles of TKE dissipation rates $\langle \epsilon \rangle$ and diapycnal diffusivities $\langle K_\rho \rangle$ for each microstructure dataset smoothed over 500 m. $\langle \epsilon \rangle$ and $\langle K_\rho \rangle$ are bin averaged over 100-m height above bottom intervals. Only data from depths > 500 m are employed. The gray bins denote 95% bootstrap confidence intervals.

2.2.2. Diapycnal mixing inferred from fine-scale parameterizations

Oceanic turbulence in the ocean interior is generally associated with the breaking of internal waves. The premise of fine-scale parameterizations is that the resulting TKE dissipation rate at microscales equals the rate of energy transfer through the internal wave spectrum. The rate of energy transfer can be related to fine-scale, $O(10\text{m})$, shear- and strain variance based on nonlinear internal wave-wave interaction theory. A number of recent studies relied on fine-scale parameterizations to infer diapycnal mixing rates from hydrographic data in regions where microstructure profiles are not yet available (e.g., Garabato et al., 2003; Garabato et al., 2004; Sloyan, 2005; Kunze et al., 2006a; MacKinnon et al., 2008). The attraction of fine-scale parameterizations is that the TKE dissipation rate can be inferred from standard hydrographic and LADCP data, thus potentially increasing oceanic turbulence observations from several hundred microstructure profiles to the thousands of hydrographic profiles obtained during WOCE. Figure 11 contrasts the global coverage of the WOCE hydrographic database to the relatively few locations where the major microstructure experiments discussed earlier have been conducted.

Courtesy of Dr. Alberto Naveira-Garabato, 165 TKE dissipation rate profiles based on LADCP/CTD data in the Southern Ocean were obtained. These profiles, discussed in Garabato et al., 2004, suggest diapycnal diffusivities of $O(10^{-4} \text{ m}^2\text{s}^{-1})$ throughout most of the watercolumn in the Scotia Sea.

Courtesy of Dr. Eric Kunze, ~ 3500 TKE dissipation rate profiles inferred from WOCE LADCP /CTD profiles were obtained. These profiles, described in Kunze et al., 2006a are based on the Gregg-Henyey scaling (Gregg et al., 2003). Kunze encountered a number of surprises and difficulties however. For buoyancy frequencies $N < 5 \times 10^{-4} \text{ rad s}^{-1}$, corresponding to depths greater than ~1000 m at mid-latitudes, instrument noise was found to dominate shear variance estimated from LADCP velocity profiles. In the absence of reliable shear variance estimates in weakly stratified waters (e.g., the abyssal ocean, Southern Ocean), Kunze resorted to a strain-based parameterization with an assumed shear/strain variance ratio. Surprisingly, Kunze found the shear/strain variance ratio to be a little over twice the expected value from the Garret-Munk model (GM) (See Figure 3 of Kunze et al., 2006a). This finding implies that the internal wave field is more energetic in the near-inertial peak than the canonical GM model.

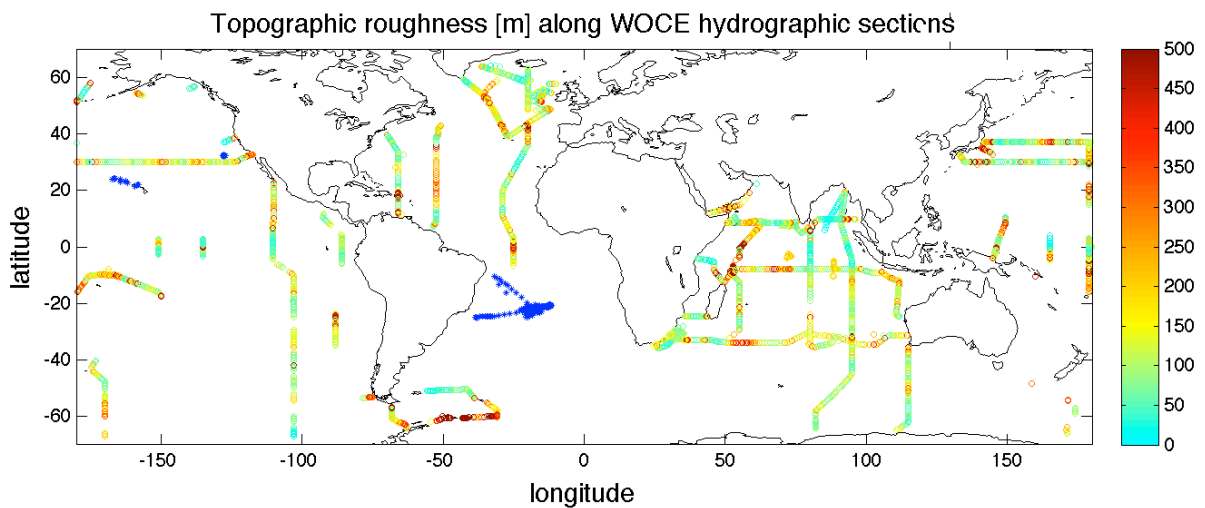


Figure 11: Topographic roughness (based on the metric of DeCloedt and Luther, 2009) at WOCE stations illustrating the global coverage. Blue stars indicate the locations of microstructure profiles extending into the abyssal ocean obtained during the Topographic Interactions Accelerated Research Initiative (TIARI), the Brazil Basin Tracer Release Experiment (BBTRE) and Hawaiian Ocean Mixing Experiment (HOME)

Importantly, this finding illustrates that much remains to be learned about fine-scale parameterizations before results can be interpreted with confidence, in particular in environments where little validation against microstructure has been attempted. The difficulties inherent in accurately estimating shear variance in weakly stratified water and the assumption of a GM type internal wave field may lead to large errors in diffusivity estimates. For instance, Kunze et al., 2006a argue that Garabato et al. (2003, 2004) overestimated mixing by an order of magnitude in the Scotia Sea because they did not recognize the impact of noise in the shear variance estimates on the stratification, whereas an assumption of a GM type internal wave field led Mauritzen et al., 2002 and Kunze, 2003 to underestimate diapycnal mixing by factors of three. Klymak et al., 2008 estimated dissipation at Kaena Ridge, Hawaii based on microconductivity probe measurements, Thorpe scale analysis, and the Gregg-Henyey parameterization. Comparing the fine-structure estimates to microstructure estimates, they note that the Gregg-Henyey parameterization results in significant underestimates of dissipation at depths greater than 400 m, with the discrepancy increasing with depth until they diverge by almost two orders of magnitude at the bottom of the measurement domain (see Figure 12). Similarly, Finnigan et al., 2002 and MacKinnon et al., 2008 note that estimates based on fine-scale parameterizations are weaker than Thorpe scale estimates by factors of three up to more than an order of magnitude in the deep ocean. Note that the inadequacy of fine-scale parameterizations as a predictor of the TKE dissipation rate in internal wave fields deviating from the GM model was previously suggested by Polzin et al., 1995.

Our own analysis of the Kunze data indicates that the diffusivities inferred in deep water (say depth >2000 m) are more correlated with the roughness of bottom topography at thermocline depths than near the actual bottom. In view of the microstructure data showing bottom-intensification in regions of rough topography, this result is suspicious. Given the already well-documented difficulties of employing fine-scale parameterizations in the abyssal ocean and our own lack of confidence in the data, the diffusivities inferred from the fine-scale parameterizations are not used in the construction or validation of the RDM. A Thorpe scale analysis of the WOCE may yield more reliable mixing estimates.

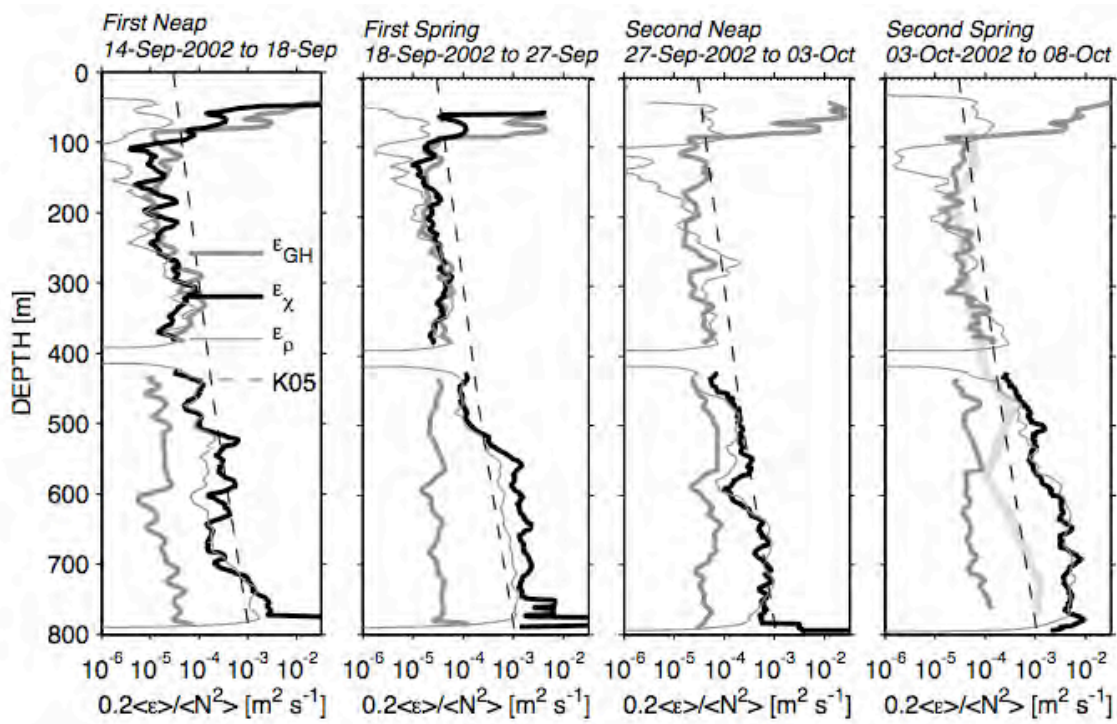


Figure 12: Average vertical profiles of the diapycnal diffusivity on the flanks of Kaena Ridge, Hawaii, for four time periods. Klymak et al., 2008 inferred the diapycnal diffusivity in three ways: from microconductivity data (thick black line); Thorpe-scale analysis (thin shaded line) and the Gregg-Henyey (2003) fine-scale parameterization (thick shaded line). The dashed line is the composite profile from microstructure measurements atop the ridge during the Hawaiian Ocean Mixing Experiment (HOME) (Klymak et al., 2006). The fine-scale parameterization underestimates by often more than an order of magnitude estimates based on microstructure data. Figure from Klymak et al., 2008.

2.2.3. Diapycnal mixing inferred from inverse models

An alternative approach to inferring diapycnal mixing is through inverse box models. Assuming the circulation is in geostrophic balance, budgets of flow into and out of volumes of the ocean whose boundaries are defined by topography, hydrographic sections and isopycnals can be balanced to yield the average diapycnal diffusivity over the volume. Lumpkin and Speer, 2007 estimated the decade-mean global ocean circulation using inverse techniques from recent WOCE hydrographic sections as well from direct current measurements. The global box model geometry is shown in Figure 13. The Lumpkin and Speer, 2007 inversions derived net diapycnal advection (in Sv) across each neutral density layer driven by interior mixing, and separately by air-sea buoyancy fluxes. The effective diffusivity estimates are based on the area-averaged diapycnal transport across layers driven by interior mixing, as determined from the inversions, and estimates of the mean area of these surfaces based on the Gouretski and Jancke, 1998 climatology. The effective diapycnal diffusivity estimates have been obtained, courtesy of Dr. Rick Lumpkin. These were derived for 45 neutral density layers for the global ocean and for the Indian, Atlantic and Pacific basins between 32°S-48°N.

Ganachaud (1999, 2003) and Ganachaud, 2000 performed a global inversion on a subset of hydrographic data from the World Ocean Circulation Experiment (WOCE) and the Java Australia Dynamic Experiment (JADE). Note that all these papers are based on A. Ganachaud's Ph. D. dissertation (Ganachaud, 1999). The famous Ganachaud and Wunsch, 2000 paper summarizes some of the most important results of Ganachaud's thesis whereas Ganachaud, 2003 is essentially a condensed version of his dissertation. The inversion yielded

estimates of the oceanic mass transports and vertical diffusivities. The analysis is based on the linear inverse box model of Ganachaud, 1999 that consistently combines the transoceanic sections. A globally consistent solution was obtained for a depth-independent adjustment to the thermal wind field, the freshwater flux divergences, the Ekman transport, and the advective and diffusive diapycnal fluxes between layers. A detailed error budget (described in Ganachaud, 2003b) permitted calculation of statistical uncertainties, taking into account both the non-resolved part of the solution and the systematic errors due to the temporal oceanic variability. Unlike the Lumpkin and Speer, 2007 inversion, no attempt was made to explicitly include buoyancy transformation due to surface air-sea interactions. The results of the Ganachaud, 2003 inversion were obtained⁶. The hydrographic sections used in the Ganachaud (1999, 2003) and Ganachaud and Wunsch , 2000 global inversion are shown in Figure 14.

Inverse models only predict the mean diffusivity over large ocean volumes. As such, they do not yield much information on the detailed spatial structure of diapycnal mixing near topography. The inverse model estimates do form a valuable dataset against which to compare averaged predictions of diapycnal diffusivity models.

⁶ available at www.ird.nc/UR65/Ganachaud/glbwoceamodel.html#vertrans

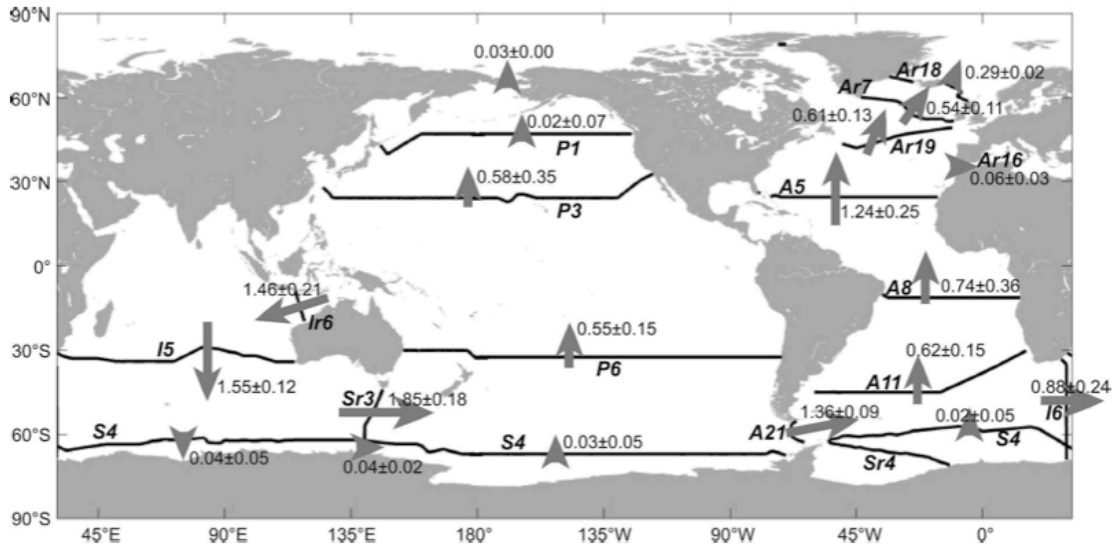


Figure 13: Global box model geometry used in Lumpkin and Speer (2007). 25 WOCE hydrographic sections form 18 boxes in which various properties are conserved and other constraints, such as the strengths of western boundary currents, are satisfied. Heat transports across the sections (arrows; units are 10^{15} W) are from the inverse model solution. Sections at a nominal latitude of 32°S separate the Atlantic, Indian, and Pacific basins from the Southern Ocean; a nearly circumpolar composite section at 62°S separates the bottom-water formation regions against Antarctica from the rest of the Southern Ocean. Figure from Lumpkin and Speer (2007).

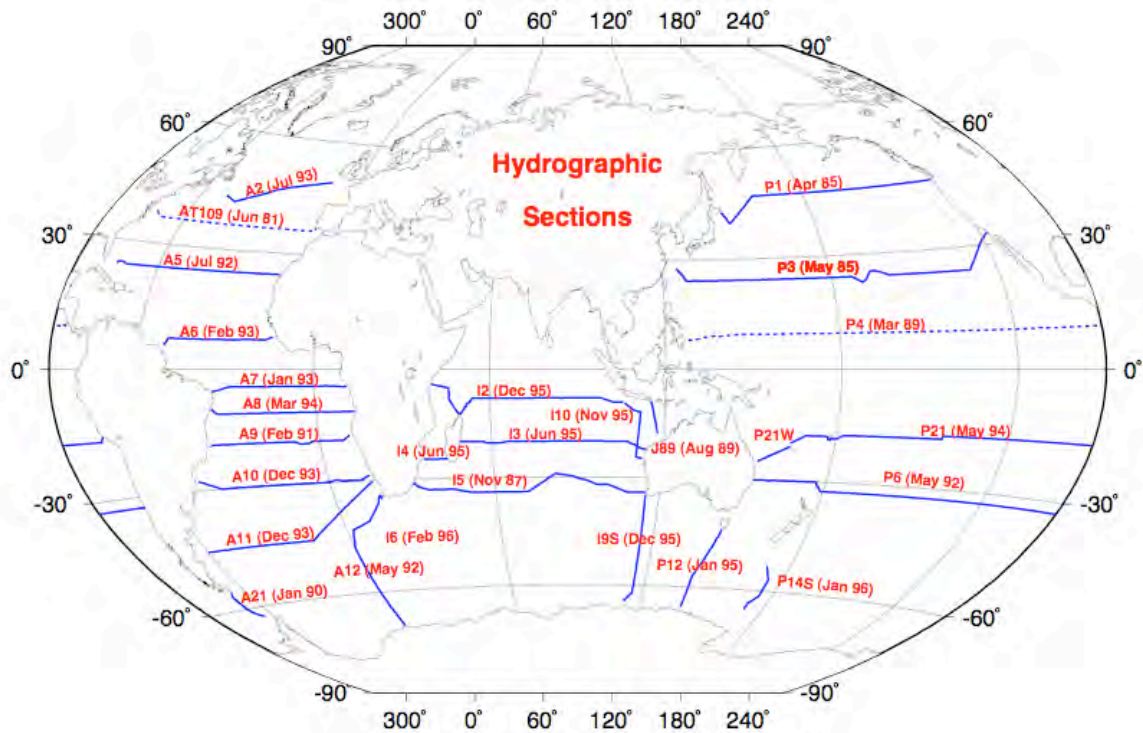


Figure 14: Select WOCE, pre-WOCE and JADE hydrographic sections covering the period 1985-1996 used in the global inversion by Ganachaud (1999, 2003).

2.3. *A metric for topographic roughness*

No global bathymetric dataset has the required resolution to adequately determine parameters such as the topographic slope, slope variance, curvature and wavenumber content needed for a realistic prediction of topography-catalyzed turbulence and its decay above the seafloor. The Smith and Sandwell, 1997 (SS97 hereafter) global seafloor topography is currently the best available global topographic data set, and although SS97 report data at 2 arc-minute-resolution, the altimeter-derived topography does not accurately resolve features with spatial wavelengths less than about 2π times the ocean depth. We here nonetheless seek a simple and conservative measure of seafloor roughness based on SS97 bathymetry in the hope that some generic features of the topography-catalyzed turbulence may be captured. For this purpose, several seafloor roughness metrics based on SS97 developed in the literature were examined, shown in Figure 15 for the seamount-rich area north of the Enewetak and Bikini Atolls.

In the SL02 tidal dissipation estimate (and in subsequent papers by these authors and coworkers), topographic roughness is characterized by (κ, h^2) , the roughness wavenumber and amplitude scale. The amplitude scale h^2 is computed as the mean square residual height difference between the SS97 bathymetry and a polynomial sloping surface fit $Z=a+bx+cy+dxy$ over 0.5 by 0.5 degree, non-overlapping cells. (The choice of 0.5 by 0.5 degree cells was motivated by the grid size of the tidal model used.) The wavenumber κ is not estimated from the topography but treated as a free parameter tuned to minimize the difference between the modeled and observed barotropic tides. In **Error! Reference source**

not found., the quantity κh^2 is plotted with $\kappa = 2\pi / 10$ km. Gille et al., 2000 computed roughness on a 0.25° latitude by 0.2° longitude grid by first applying a high-pass filter (retaining wavelengths $\lambda < 160$ km) to SS97 bathymetry, squaring the filtered bathymetry, applying a low-pass filter (retaining wavelengths $\lambda > 160$ km) and then taking the square root. Kunze et al., 2006a defined the topographic roughness as the variance of the SS97 bathymetry in $32 \text{ km} \times 32 \text{ km}$ boxes. In the present study, we opt for a root-mean-square approach in the vein of Gille et al., 2000 but at the resolution of the SS97 bathymetry since we are not tied to the grid size of a numerical model. We define the seafloor roughness r as the weighted rms height of SS97 bathymetry H (which is already a smoothed version of the true bathymetry), i.e.,

$$r = \left\langle (H - \langle H \rangle)^2 \right\rangle^{1/2} \quad (13)$$

The weighted mean of the bathymetry H is here given by $\langle H \rangle = \sum_i w_i H_i$ where the sum is carried out over all grid points contained within a circle of radius l . The weighting function is a Gaussian $w_i(s) = A \exp(-s_i^2 / 2\sigma^2)$ with standard deviation $\sigma = l/2$, s the radial distance from the center of the circle and normalization constant $A = 1 / \sum_i w_i$. The weighting function was introduced to limit the horizontal smearing of large roughness values calculated at sharp topographic features. The effect of varying the circle of influence of the weighting function is shown in **Error! Reference source not found.** While equation (13) is a subjective measure of seafloor roughness, it is also conservative in the sense that the influence of sharp topographic features remains localized and it appears to be more reflective of the underlying bathymetry than other schemes. A value of $l=30$ km was judged appropriate, because (i) acute topographic features are not spread over large areas with this

value; and, (ii) reducing l further results in the increasing importance in r of short-scale structures dependent on short-scale bottom slopes that are not reliable in the bathymetric dataset that is already a spatially smoothed representation of the seafloor topography.

A global map of the topographic roughness r and its distribution are shown in Figure 16. The roughness r reaches values as high as 1000 m but 95% of the seafloor has values between 0-400 m. The most common roughness value is about 100 m⁷. Whether a physical argument can explain these attributes is unclear. It is now recognized that topographic roughness is an important variable to diapycnal mixing and ocean circulation (e.g., Whittaker et al., 2008). A more in-depth study of what constitutes a good metric for topographic roughness is clearly desirable but beyond the scope of this thesis. A physically based metric for topographic roughness will likely depend on geological variables such as the seafloor spreading rate, sediment cover, magma driving pressure, plate thickness and more. Clearly, defining a physically-based metric will require close collaboration with geophysicists. Note that a dynamical parameterization of topographic roughness allowing for the movement of tectonic plates, etc... may be desirable for paleo-climate studies.

A statistical approach towards characterizing seafloor topography was introduced by Goff and Jordan, 1988 for the description of abyssal hills resulting from faulting and volcanism near mid-ocean ridge spreading centers (not intended to apply to larger scale features such as canyons or isolated seamounts). Interestingly enough, they find the topological character of these features to be fractal, meaning that topographic slope variance is unbounded as smaller

⁷ By coincidence, the observed near-boundary shear spectrum in the Brazil Basin peaks at vertical wavelengths ~ 100 m (Polzin, 2009).

and smaller scales are included in the slope estimate. Goff and Jordan, 1988 provide a parameteric representation of the topographic spectrum, used by Polzin (2009) to compute internal tide generation. Polzin introduces a smoothing function to avoid infinite shear and energy at high wavenumbers that would result from the fractal nature of topography. It is unclear however how relevant the Goff and Jordan's parameterization of the topographic spectrum is to ocean mixing, given that it does not describe features other than abyssal hills at mid-ocean ridge spreading centers (i.e., it does not apply to topography such as isolated seamounts, canyons, fracture zones, trenches, the continental shelf,...).

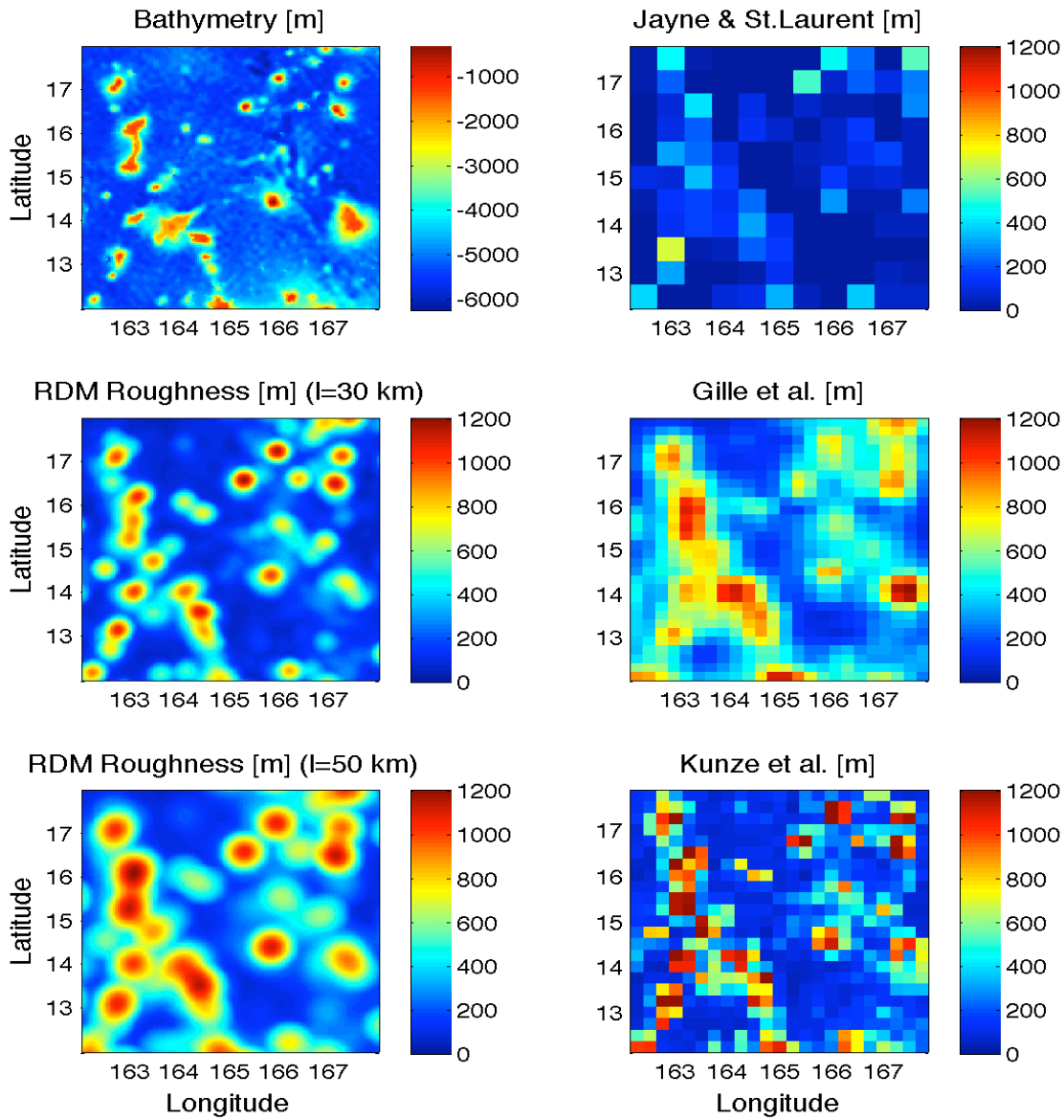


Figure 15: Topographic roughness [m] for a seamount-rich area in the West Pacific. Four different metrics are compared, equation (13) versus methods by Gille et al., 2000, Jayne and St Laurent, 2001 (κh^2 shown), and Kunze et al., 2006a. Results from (13) are shown for two different values of l , the radius of the circular area used to calculate the mean. Equation (1) with $l=30$ km, considered more conservative, is used in this study because large roughness values associated with steep seamounts are not spread over large areas

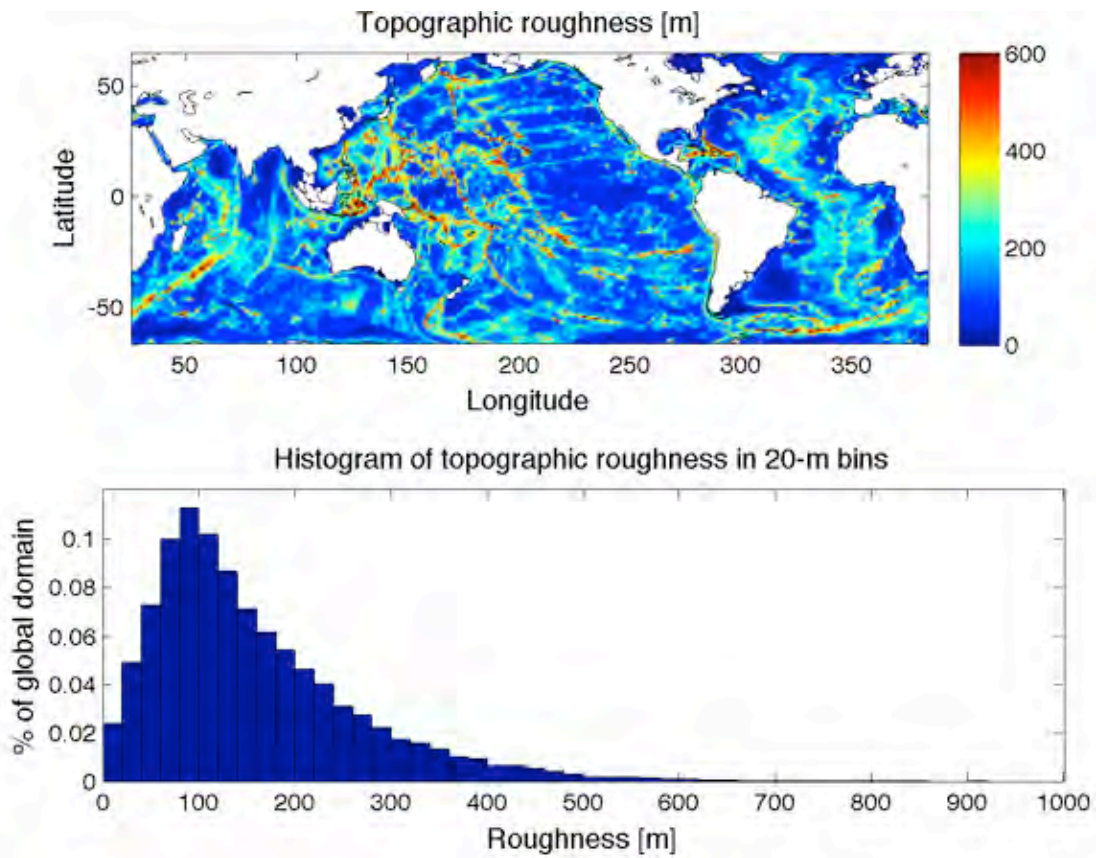


Figure 16: Global map of topographic roughness based on (13). Shown are 1x1 degree averages. The roughness distribution is shown in the lower panel. 95 % of the seafloor has roughness values less than 400 m.

2.4. Construction of the RDM

Inspection of the microstructure profiles (Figure 12) reveals that

- the mean diffusivity profiles decrease with height above bottom, unlike the mean TKE dissipation rate profiles which tend to have both near-bottom and near-surface maxima due to the strong stratification in the upper ocean
- the mean diffusivity profiles have curvature in lognormal space, unlike exponential decay
- the vertical decay structure of the mean diffusivity with height above bottom at all geographical locations is similar, in spite of the variety of mixing processes contributing to the observations.

Examining the data for a dependence on topographic roughness reveals that the mean near-boundary diffusivity tends to increase with increasing topographic roughness. This is illustrated in Figure 17, showing 95 % confidence intervals for the mean K_p profiles grouped into three intervals of increasing topographic roughness. The statistical confidence intervals were computed using the bootstrap method (Efron and Gong, 1983). For each roughness range, values⁸ of K_p were binned in 100-m height above bottom interval. These binned profiles were subsampled and averaged 100 times. The confidence intervals shown in Figure

⁸ depth-averaged over 10-m intervals for the 0.5 m HRP data such that samples are statistically independent according to run tests (Gregg et al., 1993) and integral time scale estimates. The AVP data were obtained as averages over 100-m depth intervals from HOME investigators.

17 represent the 3rd and 97th percentile of the distribution of 100 means formed by randomly sampling one half of the data in each bin.

After trial and error, the functional form adopted for the RDM is

$$K_\rho(h,r) = K_b(r)(1 + h/h_0(r))^{-2} + K_{back} \quad (14)$$

where h is height above bottom. The boundary diffusivity $K_b(r)$ and scale height $h_0(r)$ are assumed to be functions of the topographic roughness r and $K_{back} = 5.6 \times 10^{-6} \text{ m}^2\text{s}^{-1}$ is the background diffusivity. This choice of K_{back} accommodates the many observations below the traditional background diffusivity of $10^{-5} \text{ m}^2\text{s}^{-1}$ (e.g., St Laurent et al., 2002) and corresponds to the diffusivity associated with background Garrett-Munk internal wave conditions assuming a mixing efficiency $\Gamma = 0.2$ (Polzin et al., 1995). The functional dependence for the decay with height above bottom of K_ρ is identical to the idealized decay of the TKE dissipation rate proposed by Polzin (2004a, 2009); $\varepsilon = \varepsilon_0 / (1 + h/h_0)^2$. This equivalence would follow if one applied the Osborn relation with constant buoyancy frequency and mixing efficiency, not unreasonable low order approximations in the abyssal ocean. Further motivation for casting the RDM in terms of the diffusivity rather than the TKE dissipation rate comes from the buoyancy scaling implied by the internal wave-wave interaction theory proposed by Henyey et al., 1986. Polzin et al., 1995 discuss several proposed wave-wave interaction models in their examination of ocean microstructure and finestructure observations and find greatest support for the Henyey model. The Henyey model predicts that the turbulent dissipation rate associated with the energy flux through the Garrett-Munk

internal wave field goes like $\varepsilon \sim N^2$. That means that the diapycnal diffusivity is independent of the stratification (Toole, 1998). A parameterization for diapycnal diffusivity can therefore be extrapolated globally in spite of the spatial variability of the stratification.

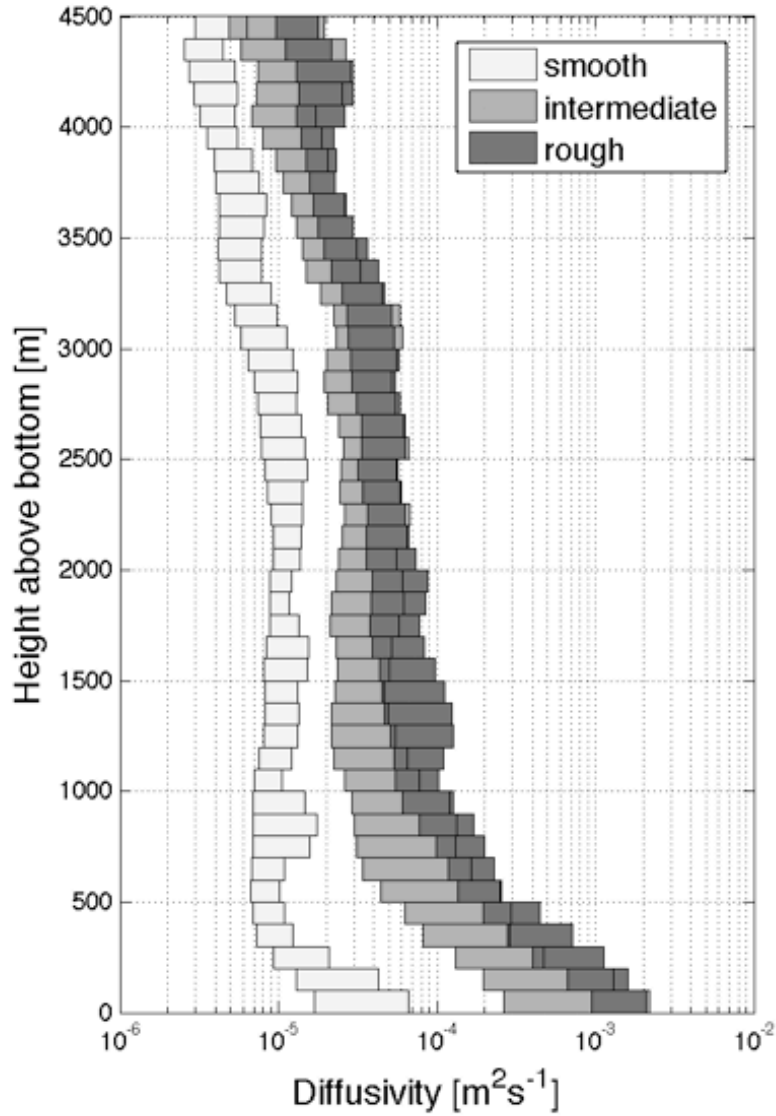


Figure 17: 95 % bootstrap confidence intervals of the mean diffusivity profiles from locations with topographic roughness values between 0-100 m (smooth), 50-150 m (intermediate) and 100-300 m (rough).

Whereas Polzin (1999, 2004b, 2009) uses Bell's (1975) model of internal tide generation to compute the parameters ε_0 and h_0 , we here seek simple functions describing $K_b(r)$ and $h_0(r)$ empirically.

The parameters K_b and h_0 are estimated for each of the 273 $\langle K_\rho \rangle$ profiles separately (i.e., with topographic roughness appropriate to each profile, according to eqn (13) with $l = 30$ km) through nonlinear regression using the Gauss-Newton algorithm with Levenberg-Marquardt modifications for global convergence (Seber and Wild, 1989). Figure 18 shows $K_b(r)$ and $h_0(r)$ when both are treated as free parameters in the nonlinear regression in panels (a) and (b). There is considerable scatter yet both plots exhibit some structure. The boundary diffusivities inferred from the regression increase from a range of $O(10^{-6}-10^{-4})$ m^2s^{-1} to a range of $O(10^{-4}-10^{-1})$ m^2s^{-1} as topographic roughness increases from 0 to 400 m and then decrease slightly for higher roughness values. The red curve in panel (a) is a least-squares 3rd order polynomial fit to the boundary diffusivities averaged over 100-m roughness bins. The mean K_b and 95 % bootstrap confidence intervals per bin are also shown (red dots and vertical bars). As before, confidence intervals represent the 3rd and 97th percentile of the distribution resulting from randomly subsampling and averaging 100 times one half of the available data for each bin. The scale heights inferred from the nonlinear regression range from $O(10)$ m to $O(1000)$ m with most of the large decay scales occurring at topographic roughness values less than 400 m.

Repeating the nonlinear regression but now with $K_b(r)$ prescribed as the 3rd order polynomial function shown in red in panel (a) yields a clear pattern in the decay scales as a

function of topographic roughness, see panel (c) of Figure 18. The scale heights now decrease rapidly from roughly 2500 m to 100 m as topographic roughness increases to 400 m and then remain constant for higher roughness values. A least-squares 3rd order polynomial fit to the inferred h_0 averaged over 100-m roughness bins is shown as the red line in panel (c) of Figure 18.

A more conservative estimate for $K_b(r)$ was subsequently constructed based on observed diffusivities within 50 m from the bottom. Given the decay scales parameterized as the polynomial function discussed above, $K_b(r)$ was estimated from observed diapycnal diffusivities within 50 m from the bottom as $K_\rho(h=0)$ using eqn. (14) rather than through linear regression of (14) on the data. These boundary diffusivities were binned in 100-m roughness intervals and parameterized as a least-squares 3rd order polynomial fit to their means (red line in panel (d), Figure 18):

$$K_b(r) = \begin{cases} K_{b0} \exp(k_1(r/r_0)^3 + k_2(r/r_0)^2 + k_3(r/r_0)) & ; r \leq 830 \\ 1.8 \times 10^{-3} & ; r > 830 \end{cases} \quad (15)$$

where $k_1 = 3 \times 10^{-8}$, $k_2 = -5.8 \times 10^{-5}$, $k_3 = 0.0325$, $K_{b0} = \exp(k_4) = 1.87 \times 10^{-5} \text{ m}^2\text{s}^{-1}$. The constant boundary diffusivity for topographic roughness values larger than 830 m was introduced to avoid changes in $K_b(r)$ at large roughness values unconstrained by data. No typical roughness scale could be identified on either an observational or theoretical basis. The normalization constant r_0 introduced for dimensional consistency was therefore assigned a value of 1 m. Using $K_b(r)$ specified by (15), the nonlinear regression was repeated to

determine a new $h_0(r)$. The decay scales obtained from the regression with $K_b(r)$ given by (15) decrease from a maximum at 670 m to 170 m at a roughness value of 540 m after which they remain level. For comparison, Polzin (2004A, 2009) inferred a scale height of 150 m from the Brazil Basin II data. A least squares 3rd order polynomial fit to the scale height averaged over 100-m roughness bins yields (panel (e), Figure 18):

$$h_0(r) = \begin{cases} a_1(r/r_0)^3 + a_2(r/r_0)^2 + a_3(r/r_0) + a_4 & ; r \leq 540 \\ 170 & ; r > 540 \end{cases} \quad (16)$$

where $a_1 = -2.9 \times 10^{-6}$, $a_2 = 0.0046$, $a_3 = -2.5896$ and $a_4 = 670$ m. A constant decay scale for roughness values greater than 540 m was introduced to avoid unphysical behavior at larger roughness values. Further repetition of this procedure, i.e. estimating a new $K_b(r)$ based on observed diffusivities within 50 m of the bottom via (14) with $h_0(r)$ parameterized as (16), yielded no significant changes to the $K_b(r)$ and $h_0(r)$; they will be specified by (15) and (16) henceforth.

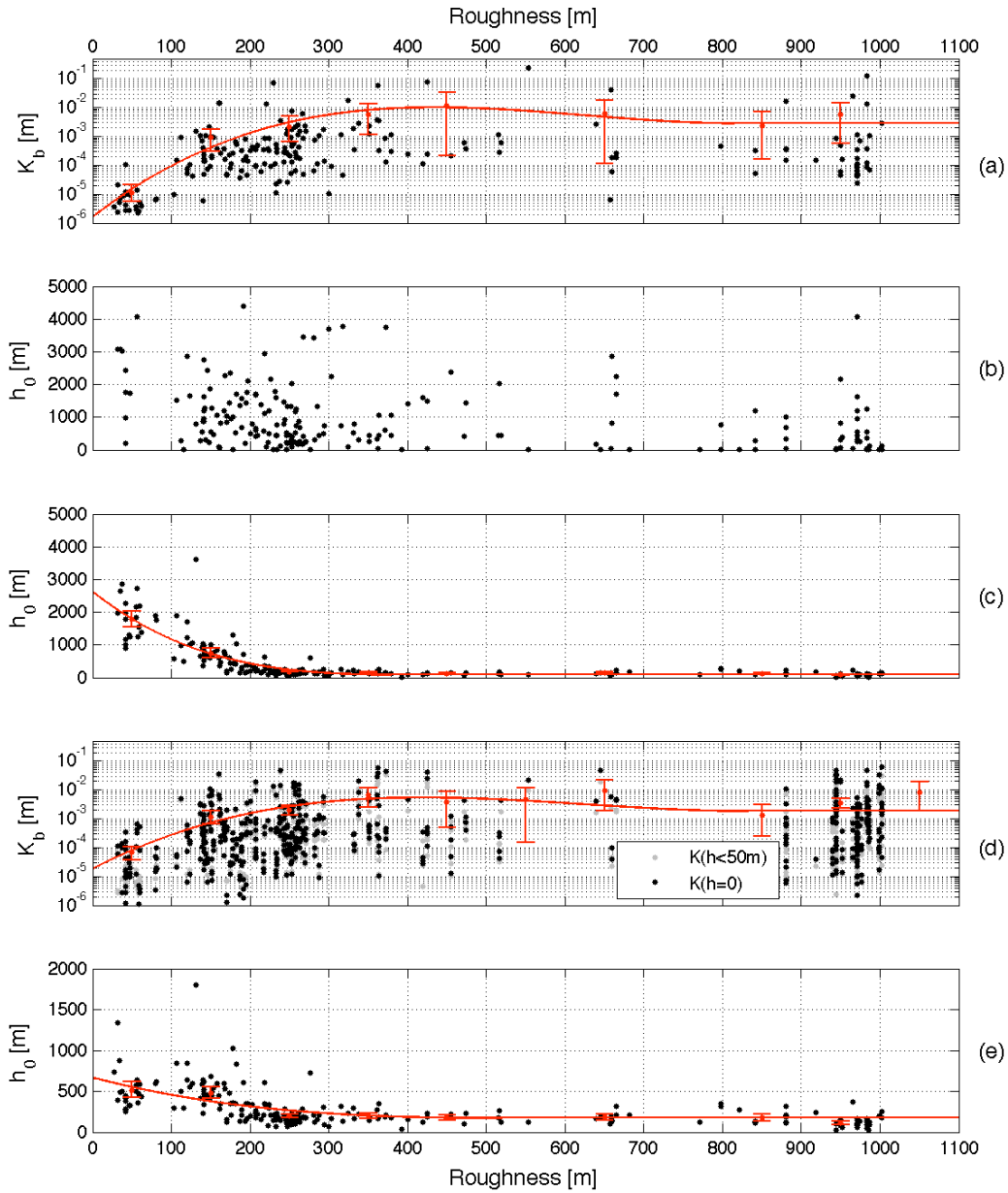


Figure 18: (a) & (b): The boundary diffusivity $K_b(r)$ and decay scale $h_0(r)$ (black dots) when determined simultaneously through nonlinear regression on the $\langle K_p \rangle$ profiles. (a): in red, means of $K_b(r)$ for 100-m roughness bins with 95 % bootstrap confidence intervals. The red line is a 3rd order polynomial fit to the mean $K_b(r)$. (c): Black dots show $h_0(r)$

determined from nonlinear regression on the $\langle K_\rho \rangle$ profiles with $K_b(r)$ fixed to the polynomial fit shown in (a). In red, means of $h_0(r)$ for 100-m roughness bins with 95% bootstrap confidence intervals. The red line is a 3rd order polynomial fit to the mean $h_0(r)$. (d): near-boundary diffusivities $K_\rho(h < 50\text{m})$ inferred from the microstructure data (gray dots) and their projected values at the boundary $K_\rho(h = 0)$ (black dots) using eqn. (14) with decay scales specified by the polynomial in (c). In red, means of the projected $K_b(r)$ for 100-m roughness bins with 95 % bootstrap confidence intervals. The red line is a 3rd order polynomial fit to the mean $K_b(r)$. (e): Black dots show $h_0(r)$ determined from nonlinear regression on the $\langle K_\rho \rangle$ profiles with $K_b(r)$ fixed to polynomial fit shown in (d). In red, means of $h_0(r)$ for 100-m roughness bins with 95 % bootstrap confidence intervals. The red line is a 3rd order polynomial fit to the mean $h_0(r)$. The polynomial fits for $K_b(r)$ and $h_0(r)$ shown in (d) and (e) are used for the RDM.

The joint variation of the maximum boundary diffusivity and decay scale with topographic roughness leads to simple vertical profiles of diapycnal diffusivity as shown in Figure 19 for several roughness values. Over smooth topography, the diffusivities are weak near the bottom and decay slowly (large decay scales ≥ 500 m) towards background values whereas the enhanced diffusivities over rough topography are associated with fast decay (small decay scales ~ 150 m). The inclusion of a background diffusivity has no effect on the decay scales inferred from nonlinear regression for roughness values greater than 100 m. For lower roughness values, decay scales inferred without a background diffusivity are larger by several hundred meters. Mean diffusivity profiles over smooth topography are approximately independent of height of bottom, except the first few 100 m near the bottom (e.g., Figure 17). In order to prevent diffusivities from decaying below observed values 1000 meters plus from the bottom, a regression without a background diffusivity yields large scale heights. Note that for small roughness values, our choice of background diffusivity ($K_{back} = 5.6 \times 10^{-6} \text{ m}^2 \text{ s}^{-1}$)

allows the modeled diffusivity to be less than $10^{-5} \text{ m}^2\text{s}^{-1}$, considered by many authors (e.g., Munk and Wunsch, 1998; St Laurent et al., 2002) to be a reasonable background diffusivity in the open ocean. In fact, the diffusivities estimated from the microstructure data frequently have values smaller than $10^{-5} \text{ m}^2\text{s}^{-1}$ away from rough topography.

Figure 20 compares the mean of the diapycnal diffusivity profiles predicted by the RDM at the locations of all microstructure profiles to the observed mean vertical profile for each microstructure survey considered here. These mean predicted profiles differ from the observed mean profiles by no more than a factor of two for each survey. The predicted profile for all the data shows that the simple model captures the mean structure of the observed diffusivity to within 95 % confidence intervals in the first 1500 m above bottom and may be on the conservative side (i.e., weaker than observed) higher up in the water column. Note that an exponential decay with a fixed decay scale of 500 m as in the LS02 parameterization (see the blue profile in Figure 21) underestimates the mean observed diffusivity from 1000 m above the bottom onwards and differs by factors of 5 between 2000 and 3000 m from the bottom. Predictions from the RDM agree with the mean of all data to within a factor of 2 at all heights above bottom. For simplicity, a factor of 2 will be used to indicate a plausible uncertainty range for the predicted mean diffusivity profiles.

The lower right panel of Figure 20 compares the mean of diapycnal diffusivity profiles predicted by the RDM to the observations for topographic roughness intervals ranging from smooth to rough. The predicted profile for the smooth range (0-100m) overestimates the observations in the first 1200 m above bottom but remains within a factor of 2. For the

intermediate (50-150m) and rough (100-300m) ranges, the predictions are within the 95 % confidence intervals for the first 1500 m above bottom and are on the conservative side (that is, smaller) higher up in the water column. The fits for heights greater than 1500 m above bottom may be improved by allowing the decay scale to vary as a function of height above bottom and stratification as suggested by the analysis in Polzin (2004b, 2009). The dependence of the decay scale on height above bottom or buoyancy frequency could not be inferred from the limited amount of data analyzed here. This is an avenue for further refinement when more microstructure data will be available. Overall, the comparison illustrates that specifying the boundary diffusivity and decay scale as simple functions of topographic roughness is a promising hypothesis. A dependence of the boundary diffusivity on topographic roughness is not a new idea (e.g., SL02, Kunze et al., 2006a). The choice of an appropriate vertical scale height has thus far been problematic in constructing parameterizations of $K_p(x,y,z)$, with previous empirical estimates ranging from 150 m (Polzin, 2004a, 2009) to 500 m (SL02) to 5000 m (Kunze et al., 2006a). Allowing the decay scale to vary with topographic roughness may form a simple improvement over the usual choice of a constant decay scale.

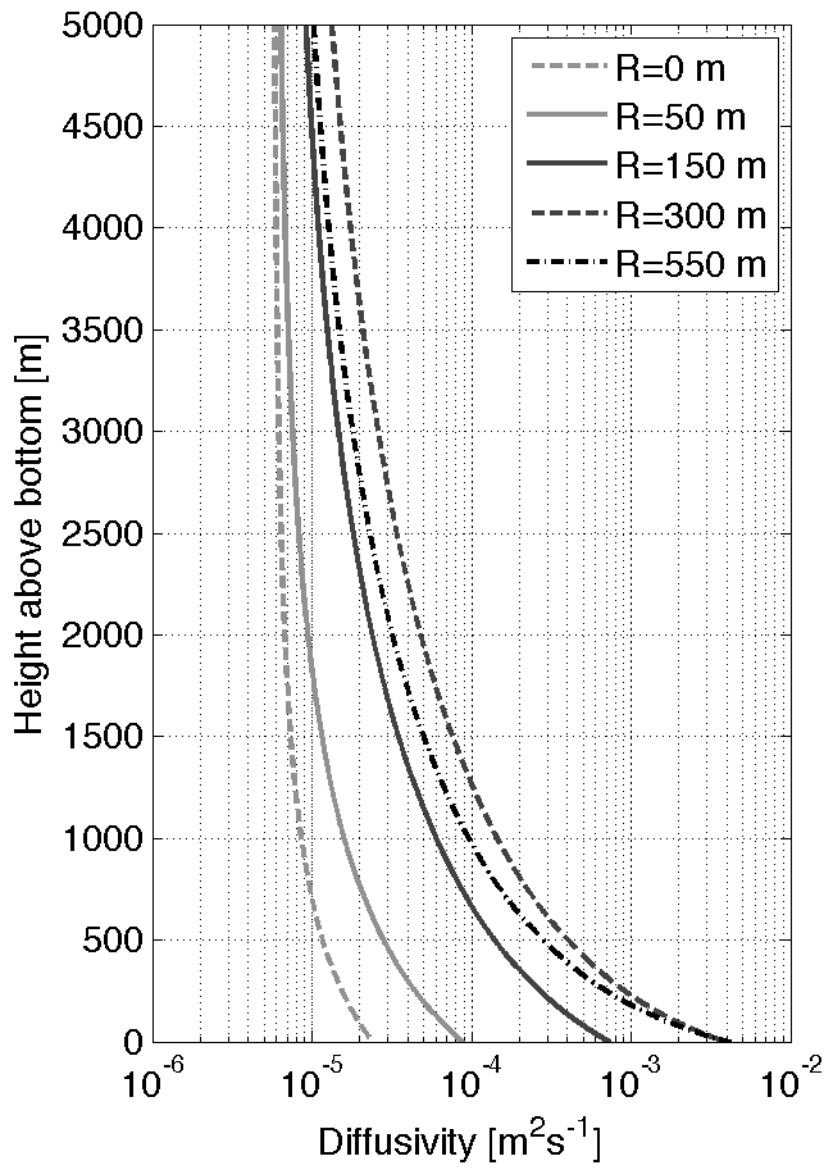


Figure 19: Vertical profiles of diapycnal diffusivity obtained from the RDM for various roughness values. Note that the profile with $r=550$ m has a smaller decay scale than the profile for $r=300$ m and thus decays faster.

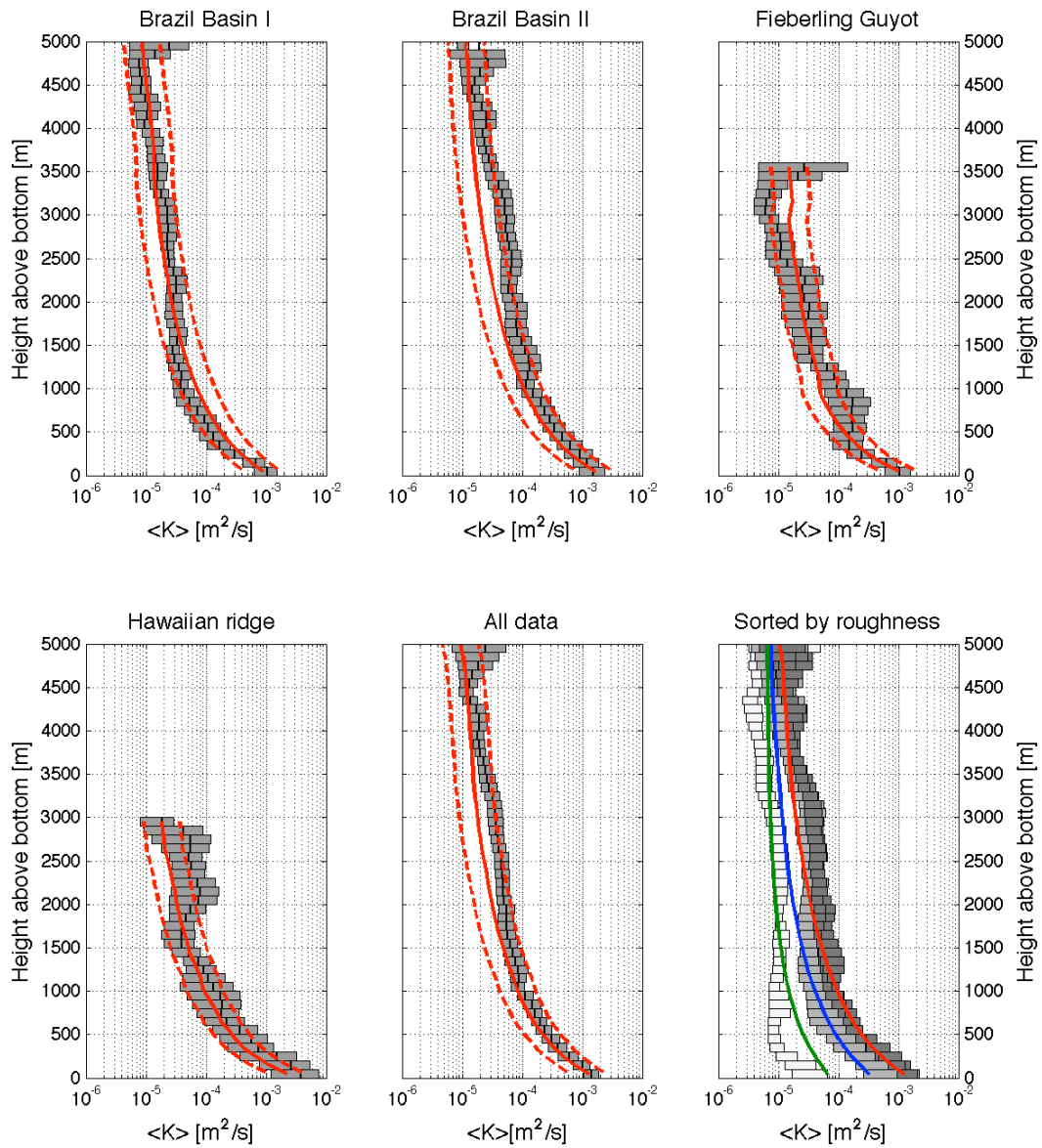


Figure 20: Mean diapycnal diffusivity profiles (red) predicted from the RDM and factors of 2 thereof (dashed red) compared to mean profiles for each microstructure data set with 95% bootstrap confidence intervals in gray. Lower right panel shows 95% bootstrap confidence intervals of mean diffusivity profiles for different roughness ranges as in Figure 5 and mean predictions from the RDM for the smooth range (green), intermediate range (blue) and rough range (red).

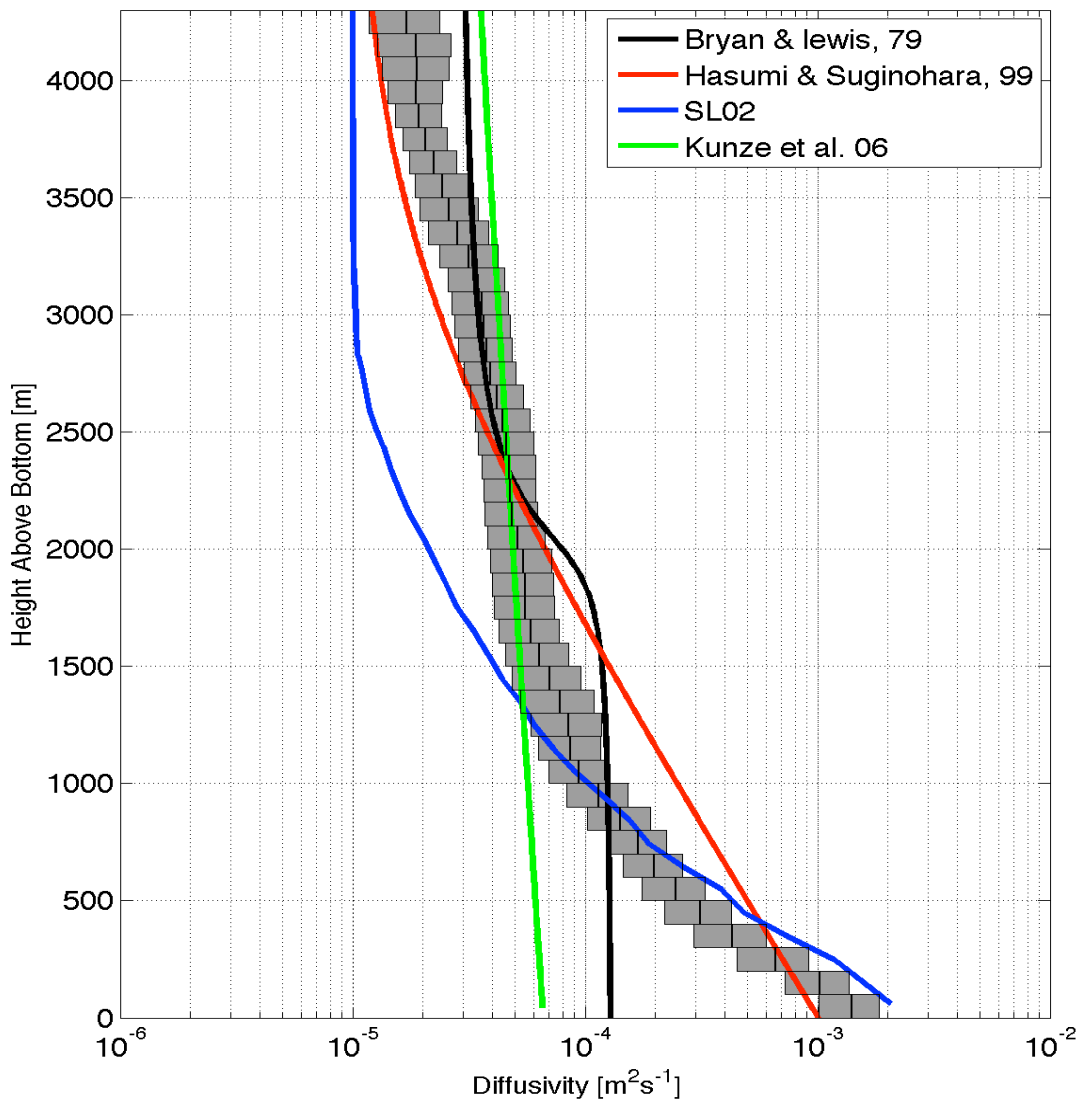


Figure 21: Comparison of various proposed vertical structure functions to the mean diapycnal diffusivity profile inferred from the observed TKE dissipation rates. Gray bins indicate 95% bootstrap confidence intervals for 100-m height above bottom bins. The Bryan and Lewis, 1979 profile is independent of position. Hasumi and Suginothara, 1999 used the profile shown for areas considered rough and the Bryan and Lewis profile for smooth areas. The Jayne and St. Laurent, 2001 (SL02) and Kunze et al., 2006a profiles have a maximum boundary value varying geographically depending on the expected magnitude of the barotropic tide and topographic roughness but use constant decay scale heights of 500 m and 5500 m respectively, independent of location.

2.5. Comparison of the SL02 tidal parameterization to the microstructure data

As discussed in section 1.6, the SL02 tidal parameterization has been widely implemented in OGCMs (e.g., Simmons et al., 2004b; Saenko and Merryfield, 2005; Koch-Larrouy et al., 2007; Jayne, 2009) yet has not been extensively validated against observations. Often, the SL02 tidal parameterization is implemented as a surrogate for topography-catalyzed diapycnal mixing resulting from a number of processes (e.g., Saenko, 2006). In this section, diffusivity profiles predicted by the SL02 parameterization are compared against the microstructure datasets at our disposition. In order to do this, barotropic tidal velocity time series of all major constituents for one year at the time of the microstructure surveys were extracted from the global TPXO7.1 tidal inverse solution⁹ (Egbert and Erofeeva, 2002) at the location of each microstructure profile. These were used to compute the rate of energy conversion $E(x,y)$ in eqn (7). The bottom stratification was obtained from the local stratification profile at each microstructure profile location. Topographic roughness was computed according to the metric proposed by Jayne and St Laurent, 2001. Note that this particular roughness metric must be used since the SL02 parameterization was tuned to minimize the difference between modeled and observed barotropic tides with this metric, resulting in their choice of topographic wavenumber κ of $O(2\pi/(10\text{km}))$. The SL02 predicted deep dissipation varies nearly linearly with this quantity (Jayne and St Laurent, 2001).

⁹ <http://www.coas.oregonstate.edu/research/po/research/tide/index.html>

The SL02 choice of a 500 m scale height was based on the Brazil Basin II dataset (right panel of Figure 22). For heights above bottom less than 1000 m, an exponential vertical structure function with a 500 m scale height is adequate, at least for the Brazil Basin data sets as well as the Hawaiian Ridge. Further away from the bottom, the resulting decay is too fast, by up to factors of 5 (e.g., right panel of Figure 22 (Brazil Basin II) and left panel of Figure 24 (all data)). The SL02 parameterization overestimates the mean diffusivity profile at Fieberling Guyot by a factor of 5 or more the first ~500 m from the bottom. Inspection of the individual terms going into (7) reveals that the likely culprit is the SL02 roughness metric. The energy conversion term $E(x,y) \cong 1/2\rho N_b \kappa h^2 \langle u_{bt}^2 \rangle$ depends quadratically on the amplitude scale h . The latter is computed as the mean square residual height difference between the SS97 bathymetry and a polynomial sloping surface fit $Z=a+bx+cy+dxy$ over 0.5 by 0.5 degree, non-overlapping cells. For an isolated acute topographic feature such as Fieberling Guyot, these are $O(1000\text{m})$, resulting in high energy conversion values of $O(500 \text{ mW/m}^2)$.

Lastly, the righthand panel of Figure 24 shows the SL02 diffusivity predictions binned for three roughness intervals as in Figure 17. The SL02 exponential vertical structure function with 500 m scale height significantly underestimates the extent to which enhanced diffusivities penetrate into the stratified ocean interior over rough topography. For heights above bottom greater than 2500 m, the SL02 predictions have all decayed to background values, irrespective of topographic roughness. Consequently, the SL02 predictions are depth-independent above 2500 from the bottom in contrast to the observations and the RDM predictions. Given the dynamical

importance of vertical gradients of K_p , one may expect this to have some bearing on circulation simulations, for instance on predictions of dense-to-light conversion at thermocline depths (Saenko, 2009, personal communication).

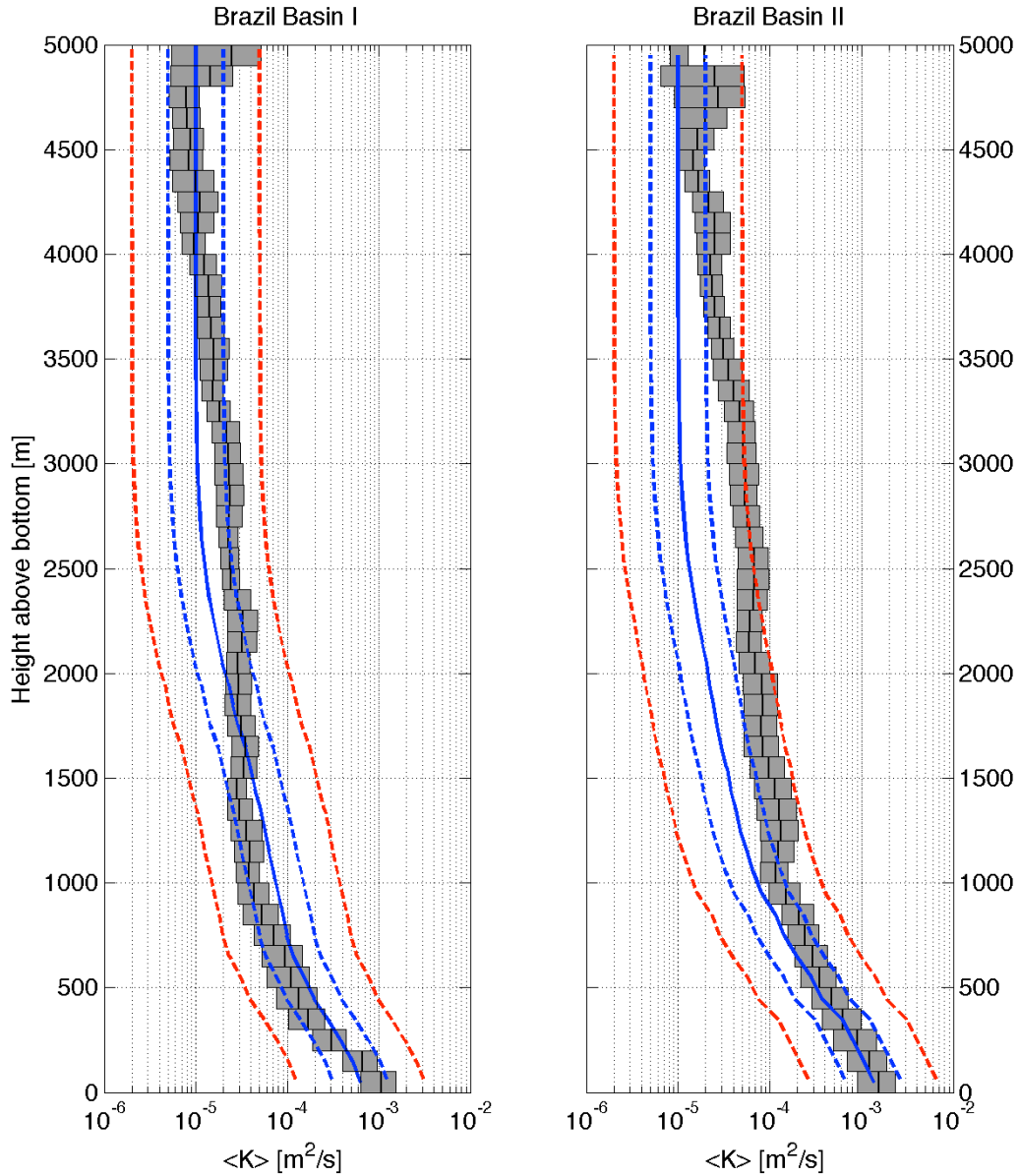


Figure 22: Mean diapycnal diffusivity profiles predicted by the SL02 tidal parameterization (solid blue line), factors of 2 thereof (dashed blue line) and factors of 5 thereof (dashed red line) compared to the mean profiles for each microstructure data set with 95% confidence intervals in gray.

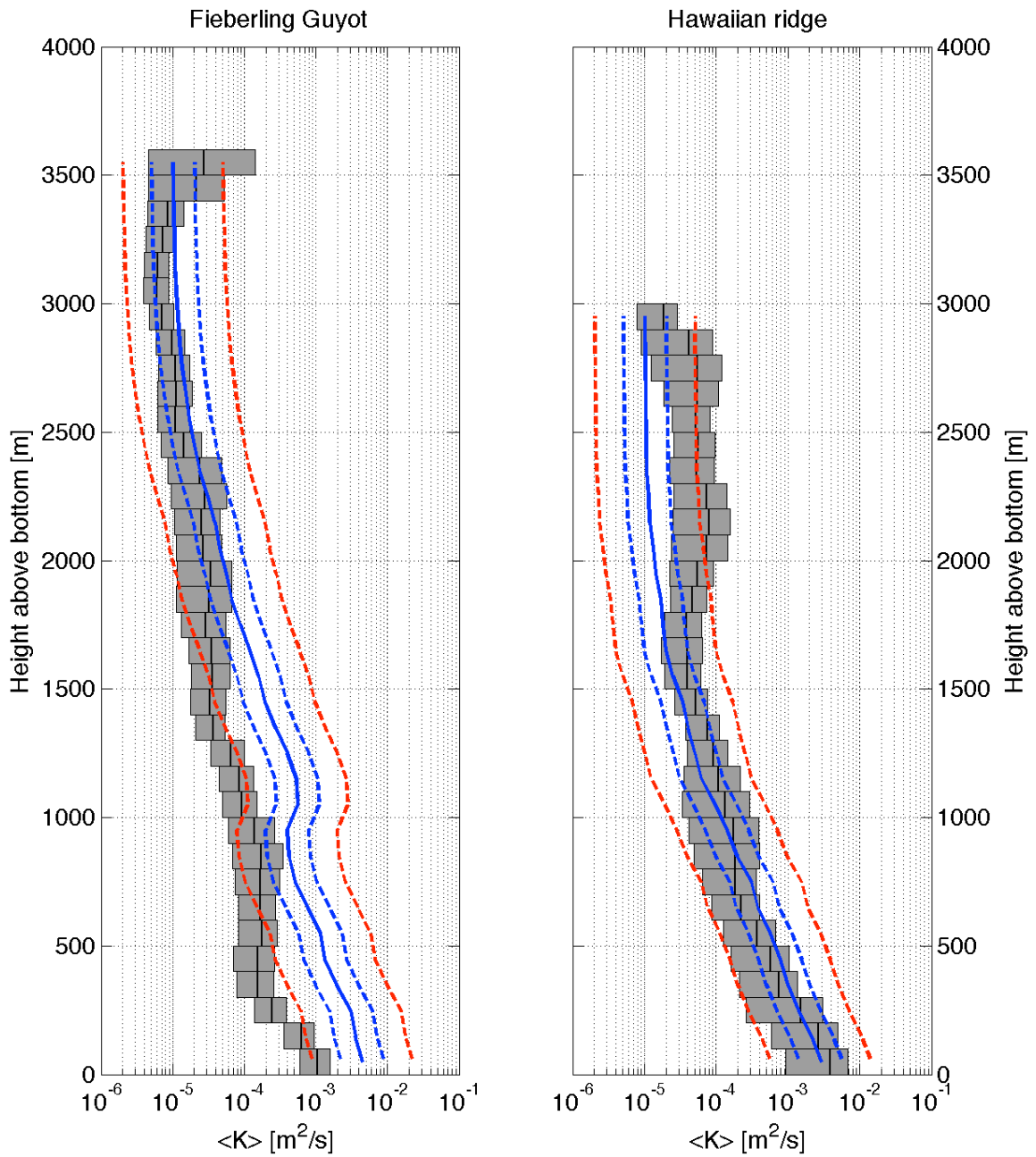


Figure 23: Mean diapycnal diffusivity profiles predicted by the SL02 tidal parameterization (solid blue line), factors of 2 thereof (dashed blue line) and factors of 5 thereof (dashed red line) compared to the mean profiles for each microstructure data set with 95% confidence intervals in gray.

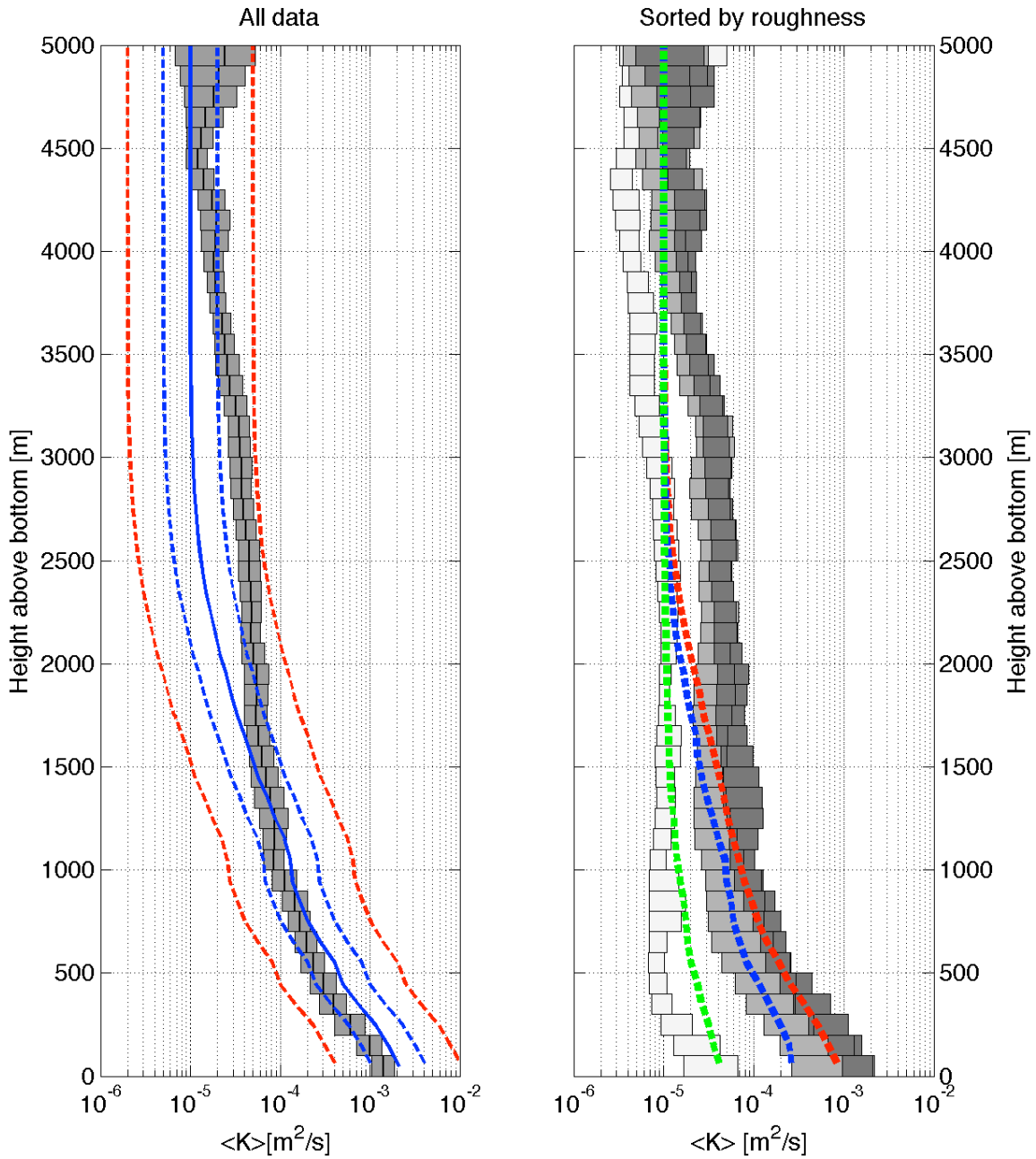


Figure 24: left panel: Mean diapycnal diffusivity profiles predicted by the SL02 tidal parameterization (solid blue line), factors of 2 thereof (dashed blue line) and factors of 5 thereof (dashed red line) compared to the mean profile for all microstructure data set with 95% confidence intervals in gray. right panel: SL02 predictions for different roughness ranges as in Figure 17. Green corresponds to smooth topography ($0 < r < 100$), blue to intermediate ($50 < r < 150$) and red to rough topography ($100 < r < 300$).

2.6. *General comments about the spatial distribution predicted by the RDM*

Three-dimensional distributions of the turbulent diapycnal diffusivity can now be constructed based on the roughness diffusivity model (RDM; eqns. (14), (15) & (16)) and the topographic roughness derived from SS97 bathymetry (eqn (13) with $l = 30$ km). Given the stratification, the diffusivities can be converted to TKE dissipation rates using the Osborn (1980) relation $\varepsilon = K_\rho N^2 / \Gamma$ with $\Gamma = 0.2$ as before. The buoyancy frequency profiles used here to obtain ε are $1^\circ \times 1^\circ$ averages derived from the 2005 World Ocean Atlas temperature and salinity profiles. Figure 26 shows the globally averaged (between 40°S - 48°N) diapycnal diffusivity profile and TKE dissipation rate profile predicted by the RDM as a function of depth. This is the global effective profile assuming that the products of locally enhanced mixing near rough topography are exported (via mesoscale and sub-mesoscale circulation features) along neutral surfaces to the ocean interior away from the topography. This is the scenario implied by the boundary mixing hypothesis (see section 1.3). The predicted global effective diffusivity profile increases in an almost perfect exponential fashion with depth until about 6200 m. It reaches the canonical value of $10^{-4} \text{ m}^2\text{s}^{-1}$ (required by Munk and Wunsch (1998) to maintain the stratification at depths between 1 and 4 km in the domain 40°S - 48°N) only by a depth of about 3.2 km; but the profile does exceed $0.5 \times 10^{-4} \text{ m}^2\text{s}^{-1}$ at all depths greater than about 2 km. It can be safely concluded, especially considering that the RDM errs on the conservative (smaller than observations) side, that topography-catalyzed diapycnal mixing is an important contributor to the maintenance of the abyssal stratification from the tropics to mid-latitudes. The globally averaged TKE dissipation rate profile

decreases with depth, reaching a minimum of $5 \times 10^{-10} \text{ W kg}^{-1}$ at a depth of 3 km. At greater depths, the influence of bottom enhanced mixing counteracts the effect of the decreasing stratification resulting in a slight increase to about $10^{-9} \text{ W kg}^{-1}$ at a depth of 4.5 km below which the TKE dissipation rate remains approximately constant.

Figure 26 shows global maps of K_ρ and ε predicted by the RDM at depths of 1 and 3 km. Whether any specific high-roughness region actually exhibits the levels of mixing and dissipation shown in Figure 26 of course depend on the nature of available energy sources such as the tides, wind-generated internal waves and low-frequency mesoscale variability, whose individual energy levels may vary significantly as a function of location. Our RDM and resultant dissipation rates are primarily intended to provide a more systematic extrapolation of the sparse observed diffusivities than has been accomplished previously. They are not intended to provide definitive maps of the spatial dependencies of K_ρ and ε in the deep ocean. The RDM is based on ~ 300 microstructure profiles. While this is a large number of profiles by microstructure study standards, it is a very small amount to attempt a global extrapolation. It must be kept in mind that the maps shown in Figure 26 are only meaningful in as far as the mixing observed in the Brazil Basin, around Hawaii and Fieberling Guyot is representative of mixing in general. Clearly, more observations are needed to verify this implicit assumption. Note that by including Fieberling Guyot and Hawaii in the calibration of the RDM, the RDM is less Brazil-Basin-centric than the SL02 parameterization and the Polzin (2009) recipe, whose calibrations are entirely based on data from the Brazil Basin.

The horizontal spatial distribution predicted by the RDM exhibits many similarities with published maps of predicted intensified mixing due to local dissipation at internal tide generation sites (e.g., St Laurent et al., 2002; Simmons et al., 2004a). Figure 27 shows global maps of the boundary diffusivity distribution predicted by the RDM and the SL02 tidal parameterization. The differences, most pronounced over the Pacific-Antarctic Ridge and the South East Indian Ridge, provide suggestions for locations where future explorations of non-tidal mixing phenomena might be profitably focused. An interesting difference between the RDM and published maps of tidalgenic mixing based on the SL02 parameterization arises from the difference in vertical structure functions. A distinct horizontal structure remains apparent in the RDM predictions at 1 km of depth, see Figure 28. In contrast, diffusivities predicted by the SL02 parameterizations at 1 km have mostly decayed to background values. Note that both the vertical structure function of the RDM and the SL02 parameterization result are biased low compared to the mean observed profile upward of 1500 m from the bottom (see Figure 21). The exponential decay employed in the JSL01 parameterization differs by up to a factor of 5 whereas the RDM remains within a factor of 2 from the observations. The numerical studies by Saenko and Merryfield (2005) and Jayne (2009) suggest that the diapycnal diffusivity at this depth and shallower have a bearing on the poleward heat transport. Furthermore, given the approximate area of the low-latitude ocean at 1 km of depth ($\sim 2.35 \times 10^{14} \text{ m}^2$ between 40°S and 48°N based on SS97 bathymetry), the average predicted diffusivity of $K_\rho = 3 \times 10^{-5} \text{ m}^2\text{s}^{-1}$ by the RDM can account for about 7 Sv [$A \times w \approx K_\rho \times \frac{A}{h}$, with $h=1 \text{ km}$] of dense-to-light water conversion (Saenko O. A., personal communication, 2009). This supports the observations that a significant fraction of NADW is

converted to lighter water classes at the base of the pycnocline (e.g., Talley et al., 2003; Talley, 2003) with the remaining conversion presumably occurring in the Southern Ocean.

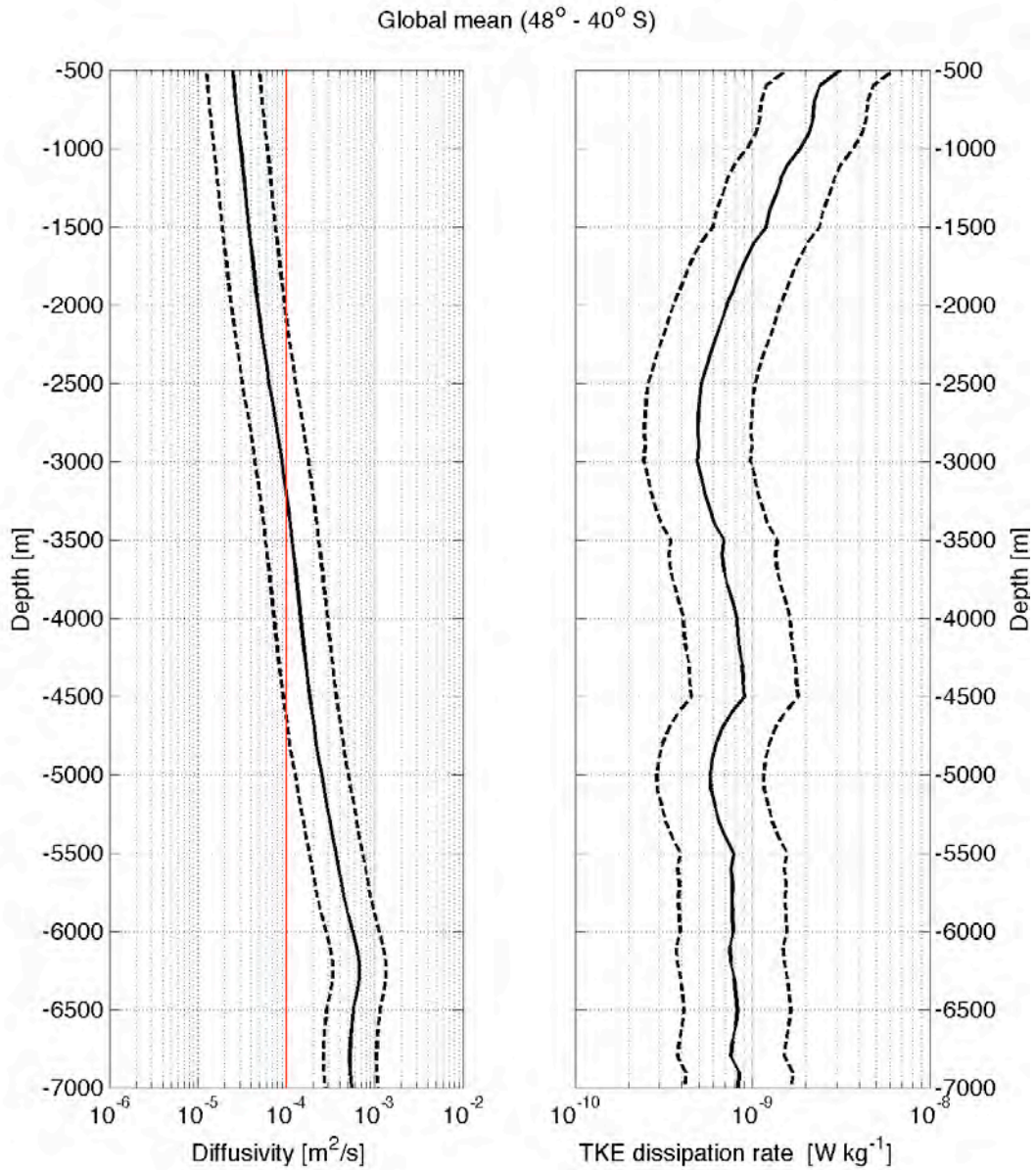


Figure 25: Globally averaged diapycnal diffusivity and TKE dissipation rate profile predicted by the RDM for the latitude bounds used by Munk and Wunsch, 1998 in their definition of the abyssal ocean (see Figure 3). The canonical average value of $10^{-4} \text{ m}^2 \text{ s}^{-1}$ found by MW98 to be consistent with global density distribution for 1-4 km of depth is shown as the thin red line for reference.

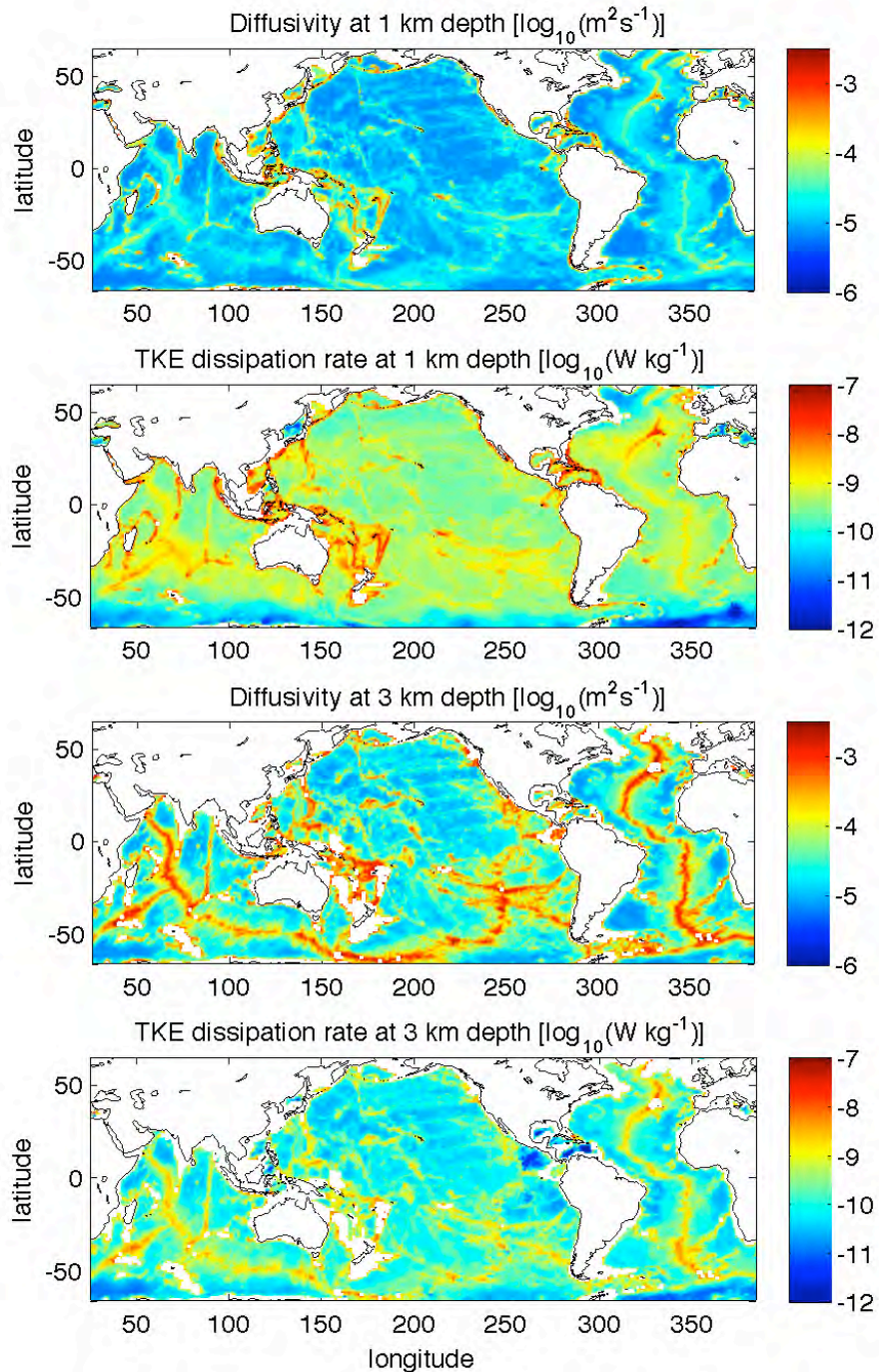


Figure 26: Global diapycnal diffusivity and TKE dissipation rate obtained from the RDM at depths of 1 km and 3 km. Note that the spatial variation of the TKE dissipation rates at 1 km depth are not only dependent on topographic roughness, but also on the lateral variability of the stratification. At the 3 km depth level, the TKE dissipation rates vary mainly as a function of topographic roughness. Values shown here are 1x1 degree averages, blank areas are shallower than the given depth.

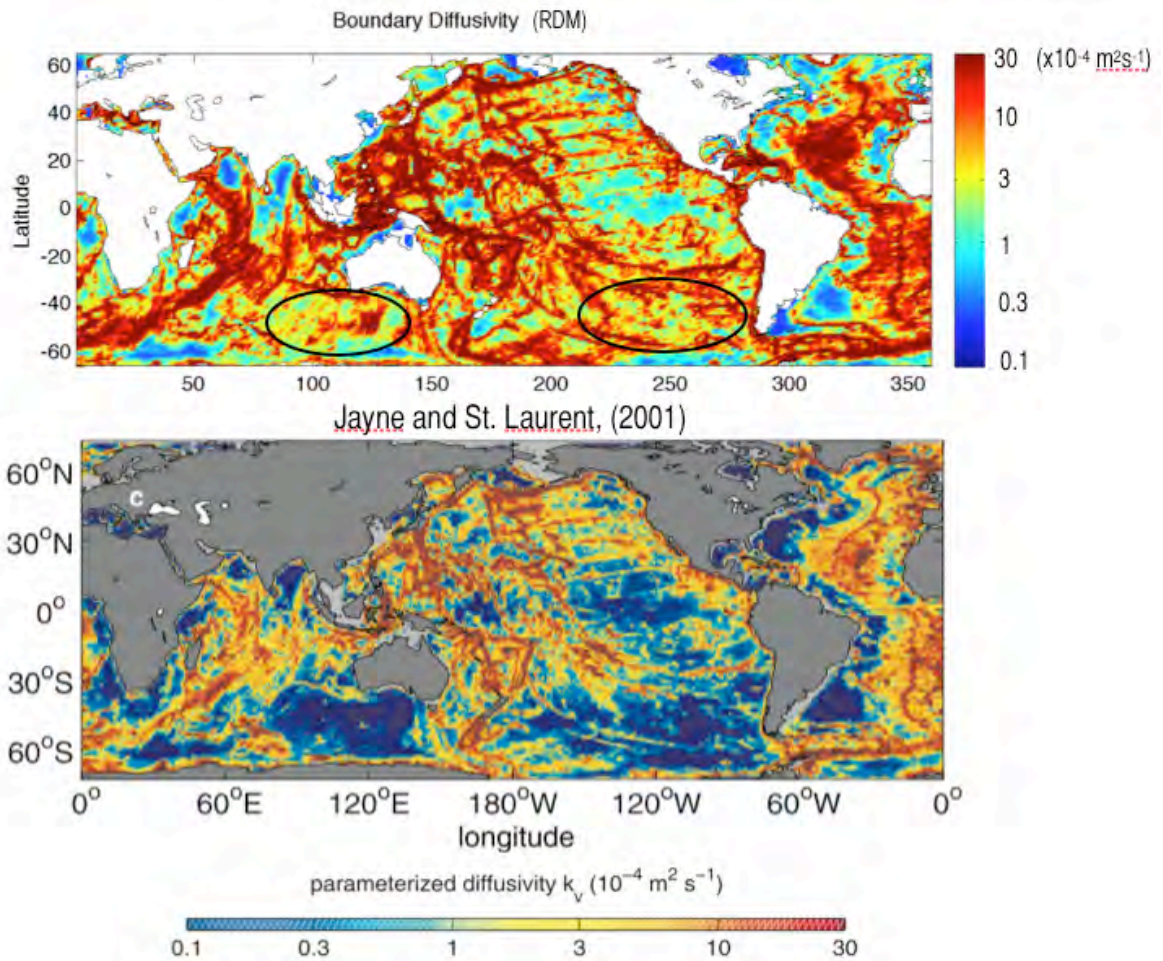


Figure 27: Comparison of the boundary diffusivities predicted by the RDM (top) to the SL02 tidal parameterization. Black ellipses in top panel indicate regions where the differences are clearest.

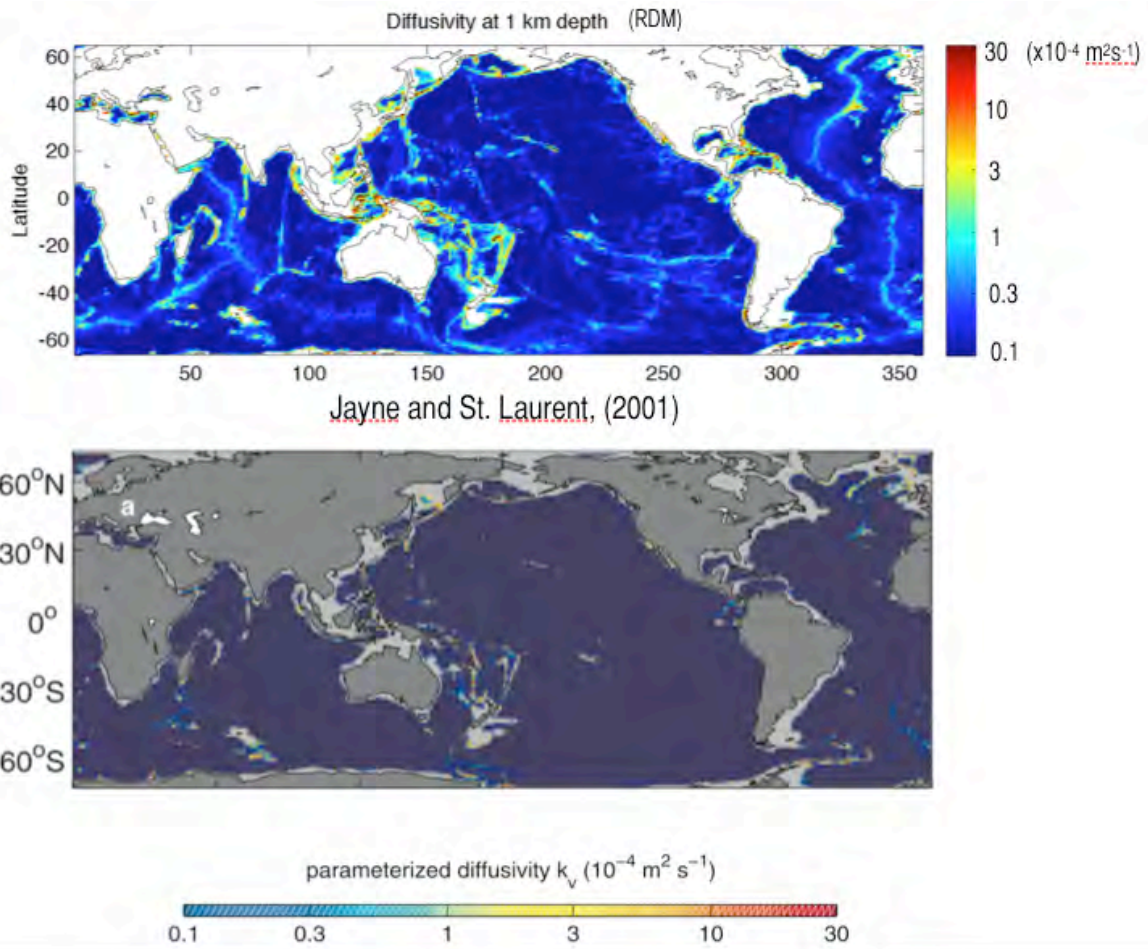


Figure 28: Comparison of the diffusivities predicted by the RDM (top) to the SL02 tidal parameterization at 1 km of depth.

2.7. *Comparison of the RDM to inverse model results*

Inverse models do not yield high resolution vertical profiles of diapycnal mixing but instead give estimates of the mean diffusivity over large ocean volumes. This section is devoted to comparing the RDM predictions to the global inversions by Lumpkin and Speer, 2007 and Ganachaud, 2003, two of the few independent data sets available against which we can check the RDM predictions.

2.7.1. Comparison of RDM to Lumpkin and Speer, 2007

Lumpkin and Speer, 2007 (LS07 hereafter) estimated the decade-mean global ocean circulation using inverse techniques, incorporating air-sea buoyancy fluxes, from recent WOCE hydrographic sections and from direct current measurements. The LS07 inversion yielded net diapycnal advection (in Sv) across 40 neutral density layers driven by interior mixing, and separately by air-sea buoyancy fluxes. The effective diffusivity estimates are based on the area-averaged diapycnal transport across layers driven by interior mixing, as determined from the inversions, and estimates of the mean area of these surfaces based on the Gouretski and Jancke, 1998 climatology.

Global comparison

The global effective diffusivity inferred by LS07 is shown in Figure 29 as a function of neutral density in black with standard error bars shaded. The nonlinear neutral density scale is constructed such that each layer contains approximately equal ocean volumes between 32°S-48°N. The RDM diffusivity predictions for the same ocean volume are shown in red. The global LS07 profile and the RDM predictions are similar for low densities but increase at a slower rate with neutral density than the effective diffusivities estimated by LS07. That RDM predictions for deep waters are lower than the estimates by LS07 may very well be due to the predicted vertical decay of diffusivity being too fast for heights greater than 1500 m above the bottom, as discussed earlier. However, the RDM estimates are within a factor of 2 of the standard error bars obtained by LS07, certainly suggesting that topography-catalyzed mixing explains a major fraction of the large average diffusivities called for by heat budgets and inverse models. For comparison, Kunze et al., 2006a argue that topographically enhanced mixing can not be invoked to explain the “missing” abyssal mixing based on the diffusivities inferred from the Gregg-Henyey scaling applied to WOCE data. Kunze, using an exponential structure function with constant scale height to extrapolate the observations, finds abyssal diffusivities an order of magnitude lower than those of Lumpkin and Speer, 2003 (the same as LS07 here but only for the North Atlantic). This discrepancy is likely due to a combination of the choice of an exponential vertical structure function and the dubious quality of diffusivity estimates based on the Gregg-Henyey scaling in the abyssal ocean. As discussed in section 2.2.2, these estimates

often underestimate mixing by more than order of magnitude compared to estimates based on microstructure data and Thorpe scale analysis.

Figure 30, Figure 31 and Figure 32 compare the RDM predictions to the LS07 estimates for the Atlantic, Indian and Pacific oceans respectively.

As for the global comparison, the RDM estimates for the Atlantic ocean are within a factor of 2 of the standard error bars obtained by LS07. In the Indian Ocean, the LS07 estimates and RDM predictions differs by factors of ~ 4 for a good portion of the water column. Whereas the RDM predicts an effective diffusivity increasing with depth, the LS07 profile is almost independent of depth with $K_p \sim 3 \times 10^{-4} \text{ m}^2 \text{ s}^{-1}$. MacKinnon et al., 2008 inferred a mean diapycnal diffusivity well in excess of $10^{-2} \text{ m}^2 \text{ s}^{-1}$ at several hundred meters from the bottom using Thorpe scale analysis and the Gregg-Henyey finescale parameterization applied to LADCP/CTD data in the Atlantis II fracture zone on the Southwest Indian Ridge. This large mean diffusivity is an order of magnitude greater than mean diffusivities observed in the microstructure surveys used for the construction of the RDM here. In addition, Saenko, 2008 presents numerical evidence that over vast areas of the deep interior, particularly in the Indian Ocean, annual-mean circulation represents a small residual of much stronger seasonal flows. In many places the seasonal horizontal velocities are of the order of 10^{-2} ms^{-1} , reaching locally to 10^{-1} ms^{-1} . An interaction of these relatively strong flows (of nontidal origin) with bottom topography may contribute to diapycnal mixing in the abyssal ocean. There is thus no doubt that intense mixing is to be expected in the Indian ocean. The quasi-independence of depth in the LS07 estimates is a puzzle however, since the observations by MacKinnon et al.,

2008 display a decay with height above bottom similar to that in the datasets on which the RDM is based. No observations of mixing due to the seasonal wind-driven flows in the deep ocean suggested by Saenko, 2008 exist but there is no a priori reason why these should decay differently. It could be that the red sea overflow (e.g., Beal, 2000), not explicitly accounted for in the LS07 inversion, is “parametrically disguised” in the diffusivity estimates.

The RDM predictions agree with the LS07 to within a factor of 2 for the deeper layers in the Pacific ocean. For the shallower layers, the LS07 estimates display a suspicious decrease that is unlikely to be physical (R. Lumpkin, 2009. Personal communication).

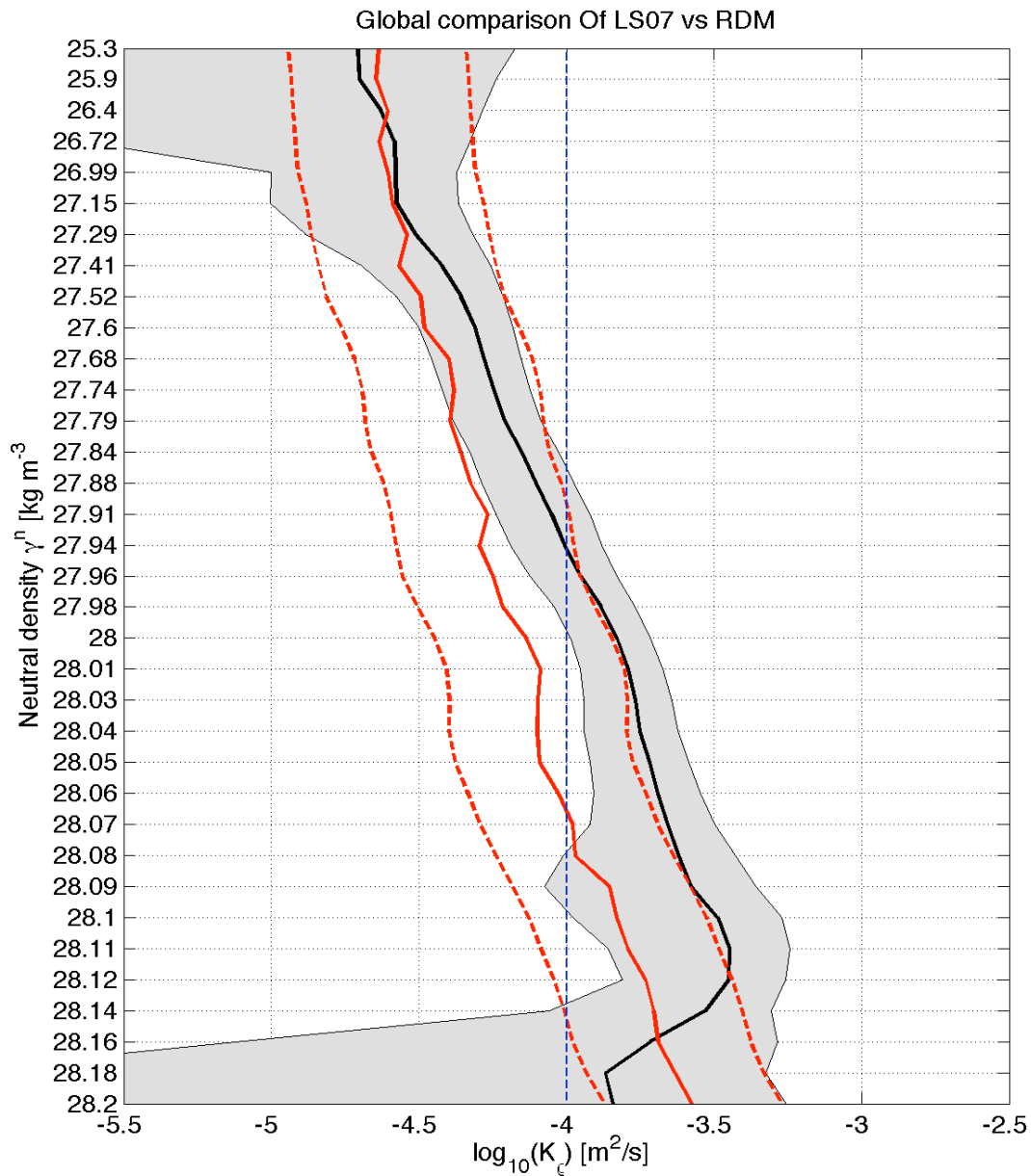


Figure 29: Global (48°N-32°S) comparison of effective diffusivities inferred by LS07 (black line with standard error shaded) compared to the RDM predictions (red line, dashed lines are factors of 2). The nonlinear scale for neutral density is constructed such that each layer contains an equal ocean volume based on the SAC/Hamburg climatology (Gouretski and Jancke, 1998). The canonical abyssal diffusivity of $10^{-4} \text{ m}^2 \text{ s}^{-1}$ inferred by MW98 is shown as the thin dashed blue line for reference.

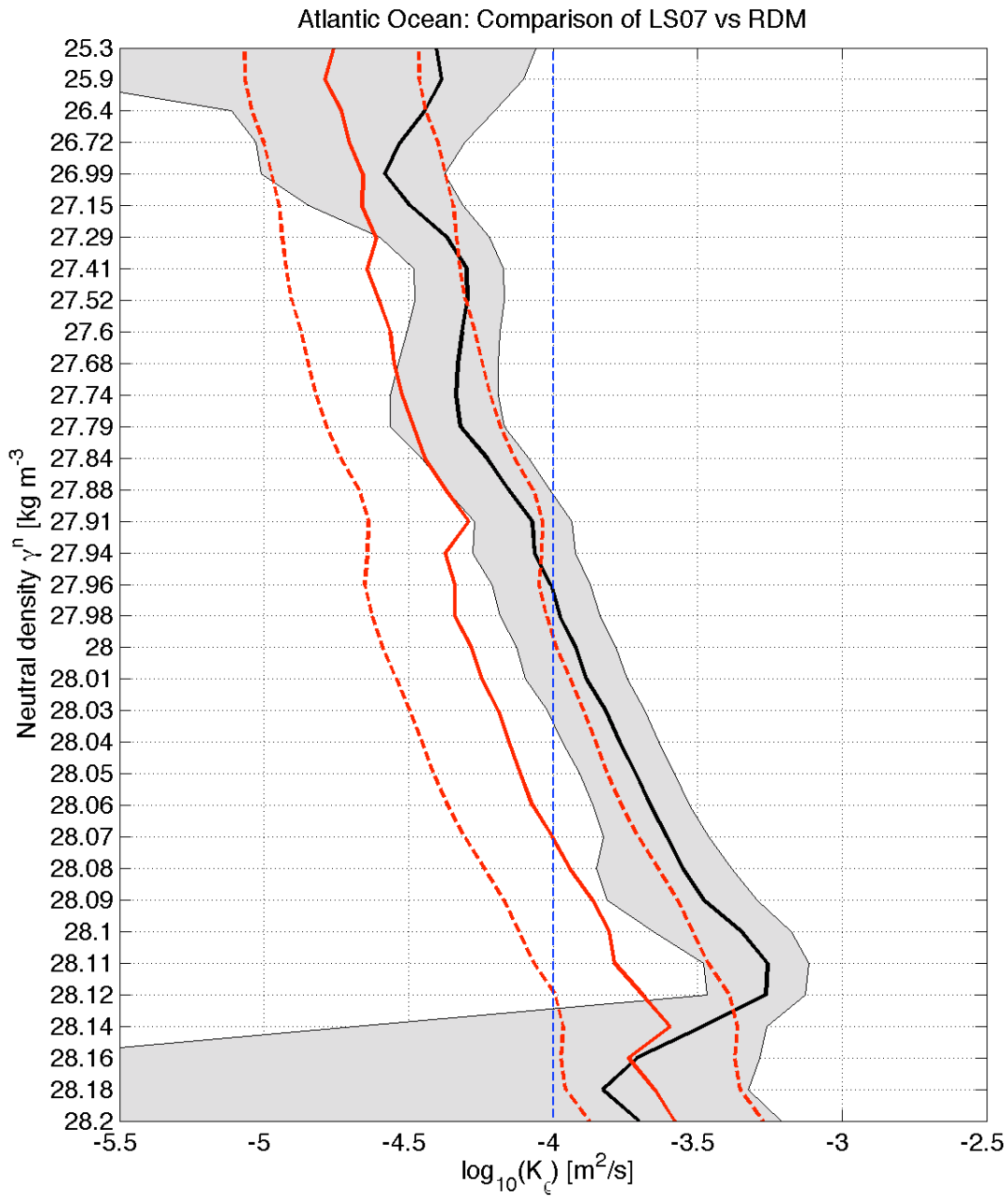


Figure 30: Comparison of effective diffusivities inferred by LS07 (black line with standard error shaded) compared to the RDM predictions (red line, dashed lines are factors of 2) for the Atlantic ocean (48°N-32°S). The canonical abyssal diffusivity of $10^{-4} \text{ m}^2 \text{ s}^{-1}$ inferred by MW98 is shown as the thin dashed blue line for reference.

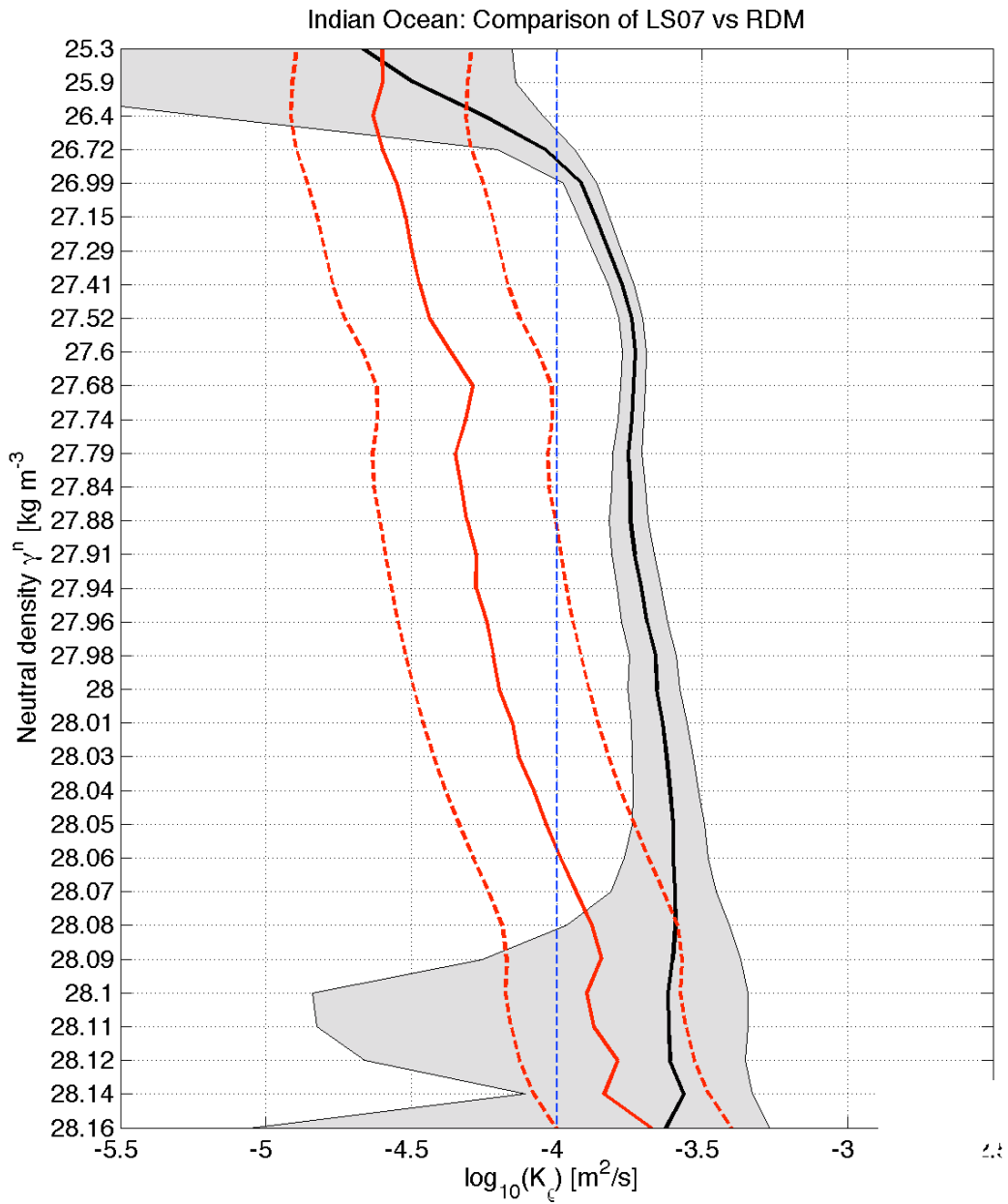


Figure 31: Comparison of effective diffusivities inferred by LS07 (black line with standard error shaded) compared to the RDM predictions (red line, dashed lines are factors of 2) for the Indian ocean (48°N-32°S). The canonical abyssal diffusivity of $10^{-4} \text{ m}^2 \text{ s}^{-1}$ inferred by MW98 is shown as the thin dashed blue line for reference.

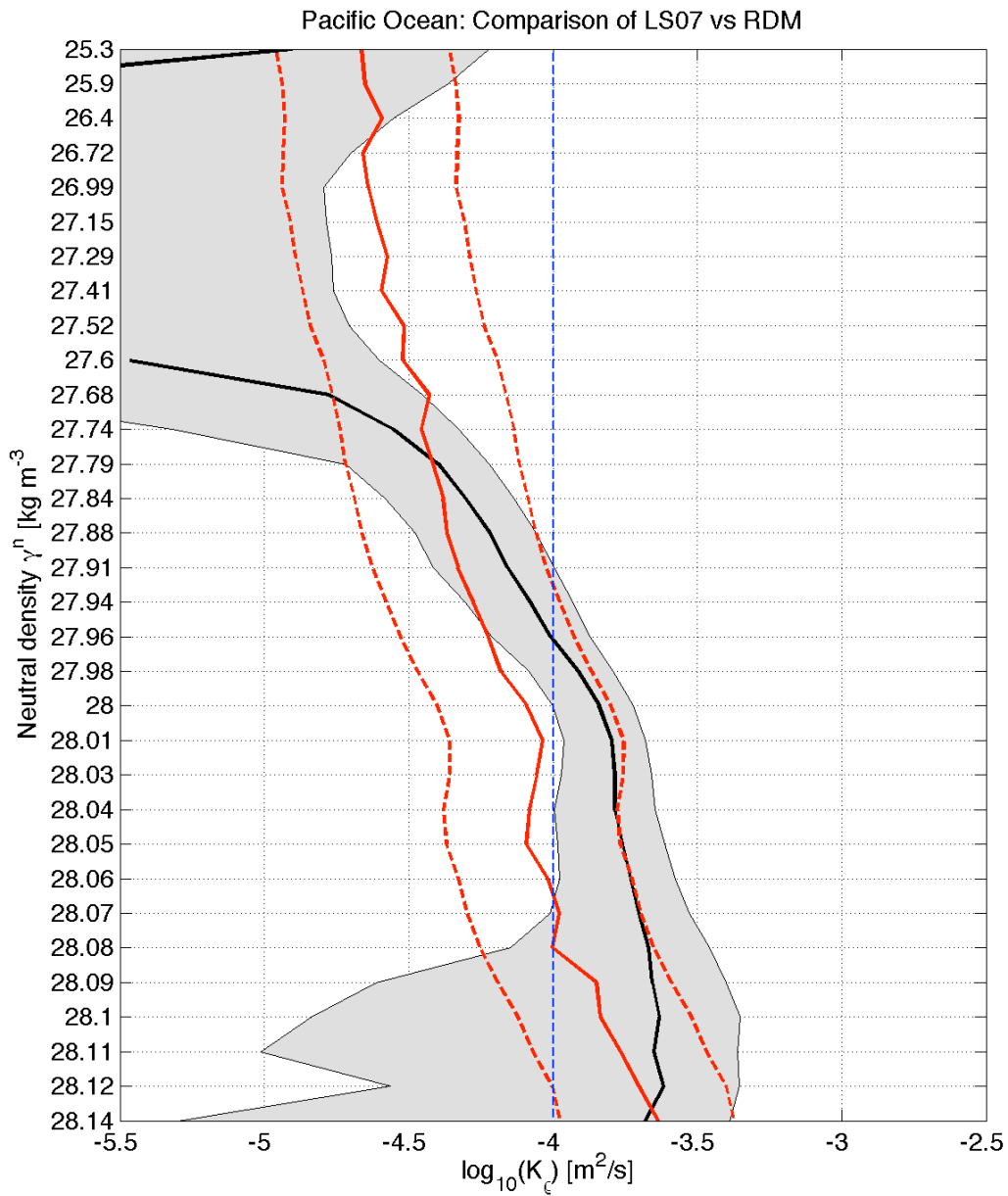


Figure 32: Comparison of effective diffusivities inferred by LS07 (black line with standard error shaded) compared to the RDM predictions (red line, dashed lines are factors of 2) for the Indian ocean (48°N-32°S). The canonical abyssal diffusivity of $10^{-4} \text{ m}^2\text{s}^{-1}$ inferred by MW98 is shown as the thin dashed blue line for reference.

2.7.2. Comparison of RDM to Ganachaud, 2003

Before discussing the box-by-box comparison to Ganachaud, 2003 (GA03 hereafter), a brief discussion of the globally averaged diffusivities tabulated in the frequently cited paper by Ganachaud and Wunsch, 2000 is in order. Ganachaud and Wunsch, 2000 report globally averaged diffusivities for deep waters ($27.96 < \gamma^{\theta} < 28.07 \text{ kg m}^{-3}$) and bottom waters ($\gamma^{\theta} > 28.10 \text{ kg m}^{-3}$) between 30°S - 47°N of $(3.7 \pm 0.7) \times 10^{-4} \text{ m}^2\text{s}^{-1}$ and $(9 \pm 2) \times 10^{-4} \text{ m}^2\text{s}^{-1}$ respectively. Our estimates for these volumes, $8.6 \times 10^{-5} \text{ m}^2\text{s}^{-1}$ and $2.7 \times 10^{-4} \text{ m}^2\text{s}^{-1}$ respectively, are factors of 4 and 3 less than the Ganachaud and Wunsch, 2000 estimates. This may indicate that there are intense mixing hot spots in the deep ocean that are not well represented in the microstructure surveys considered here. In particular, deep flow through bathymetric constrictions comes to mind. For instance, Ferron et al., 1998 and Polzin et al., 1996 infer a mean diapycnal diffusivity of $O(10^{-2})$ to $O(10^{-1}) \text{ m}^2\text{s}^{-1}$ for bottom waters in the Romanche Fracture Zone. Roemmich et al., 1996 document extraordinarily high mixing rates in the Samoan Passage, of $O(10^{-1}) \text{ m}^2\text{s}^{-1}$ for bottom waters. Some more evidence suggesting that mixing in such locations may be important follows in the box-by-box comparison to GA03 in the next few sub-sections.

Indian ocean

An overview of the box geometry used in GA03 for the Indian ocean is shown Figure 33.

Figure 34 through Figure 39 show the horizontal distributions of K_p , predicted by the RDM for several depth levels and compare the vertical profiles inferred by GA03 to the RDM

predictions for the Subtropical Indian ocean, Tropical Indian and Northern Indian ocean boxes respectively. GA03 inferred downwelling at the base of the surface layers of the Subtropical and North Indian ocean. Most of the deep upwelling was found to take place in the North Indian boxes, about 10 ± 5 Sv. Deep upwelling in the Subtropical and Tropical Indian ocean was not significantly different from zero (diapycnal advection figures not shown here, see GA03).

In the Subtropical Indian ocean box (Figure 34 and Figure 35), the RDM predictions are consistent with the GA03 estimates below 1500 m of depth. At shallower depths, between 500 m and ~ 2000 m, GA03 inferred negative diffusivities and no meaningful comparison is possible. Negative diffusivities do not show up in the figures shown here because we use a logarithmic scale but the error bars in GA03 are sufficiently large that the maximum diffusivity within their error bars does (e.g., Figure 35 between 500 m and 1500 m of depth).

In the Tropical Indian ocean box (Figure 36 and Figure 37), the RDM predictions and GA03 estimates are consistent where GA03 estimates are positive (downgradient).

In the North Indian ocean box (Figure 38 and Figure 39), GA03 inferred downgradient mixing consistently over all the deep interfaces, although there was no requirement that the mixing be positive. The average diffusivity deeper than $\gamma' = 27.36 \text{ kg m}^{-3}$ or ~ 1000 m, is $8.6 \pm 4 \times 10^{-4} \text{ m}^2 \text{ s}^{-1}$, much larger than the canonical $1 \times 10^{-4} \text{ m}^2 \text{ s}^{-1}$ required by a global 1-dimensional balance (Munk and Wunsch, 1998). Owing to large uncertainties in the horizontal area of neutral surfaces, the latter value is very uncertain (Ganachaud, 1999). The

large values and weak depth dependence of the inferred K_p are consistent with the LS07 estimates for the entire Indian Ocean. As discussed in 2.7.1, we suspect that Red Sea overflow may be biasing mixing results high for the Indian Ocean. The difference in the vertical K_p structure in the North Indian compared to the vertical structures in the Tropical and Subtropical boxes is suspicious.

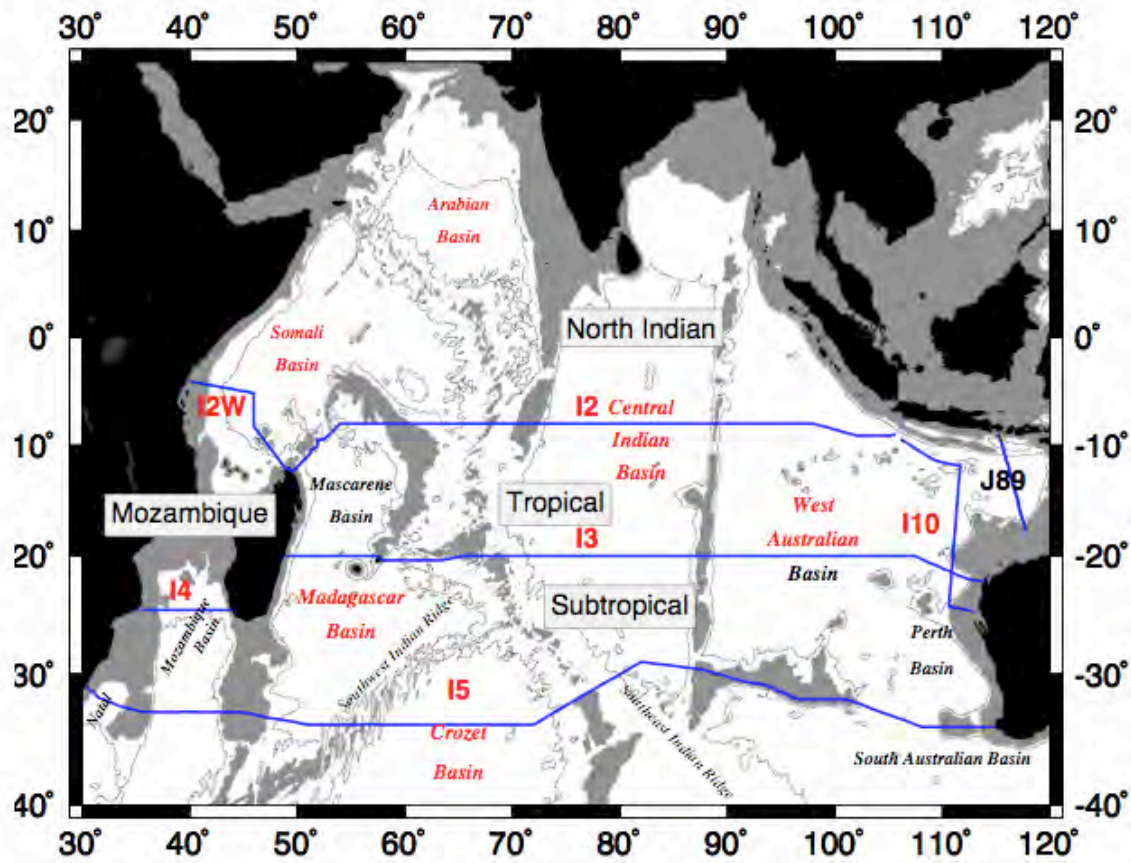


Figure 33: Indian Ocean sections and topography. The 4000 m isobath is contoured and areas shallower than 3000 m are shaded. Figure from Ganachaud (1999).

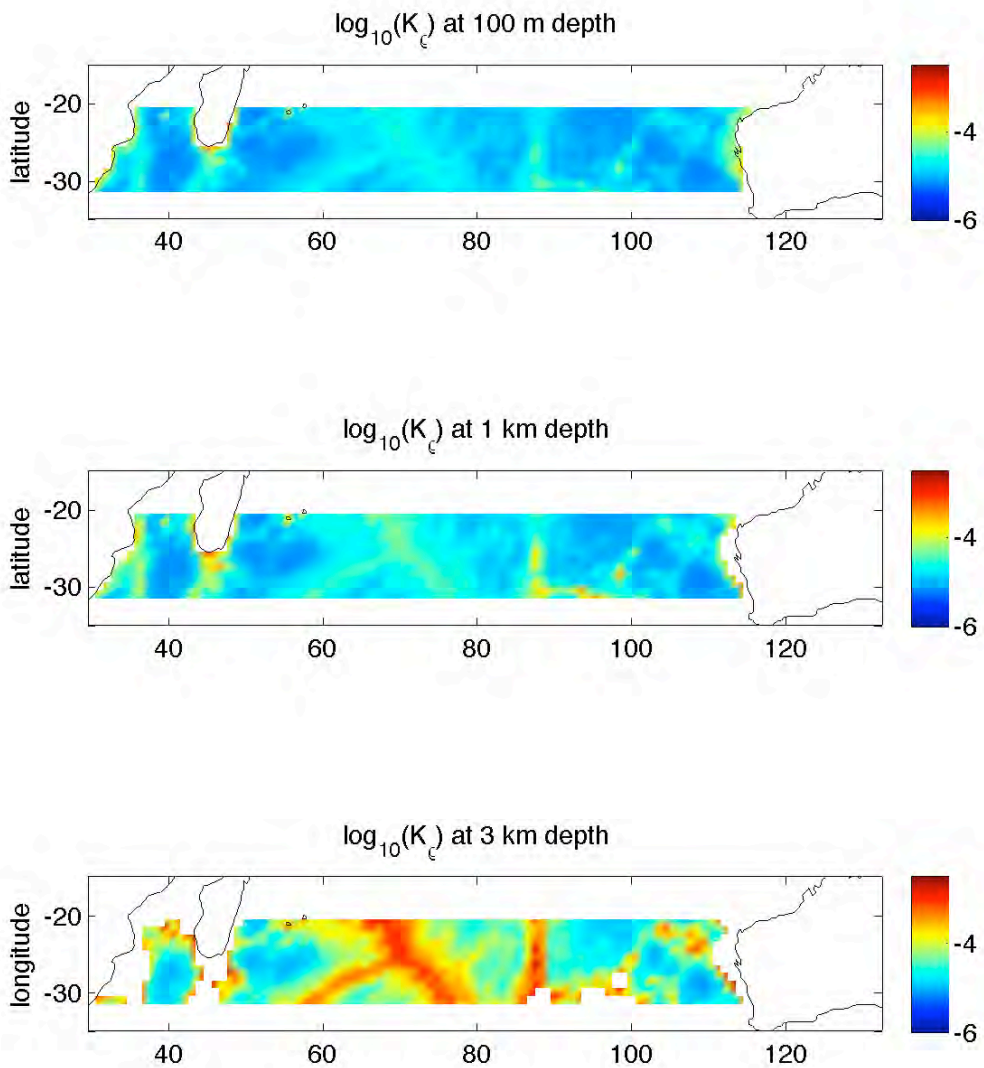


Figure 34 : Subtropical Indian Ocean (32°S-20°S). Diapycnal diffusivities predicted by the RDM at 100 m, 1000 m and 3000 m of depth for the Subtropical Indian Ocean (32°S-20°S).

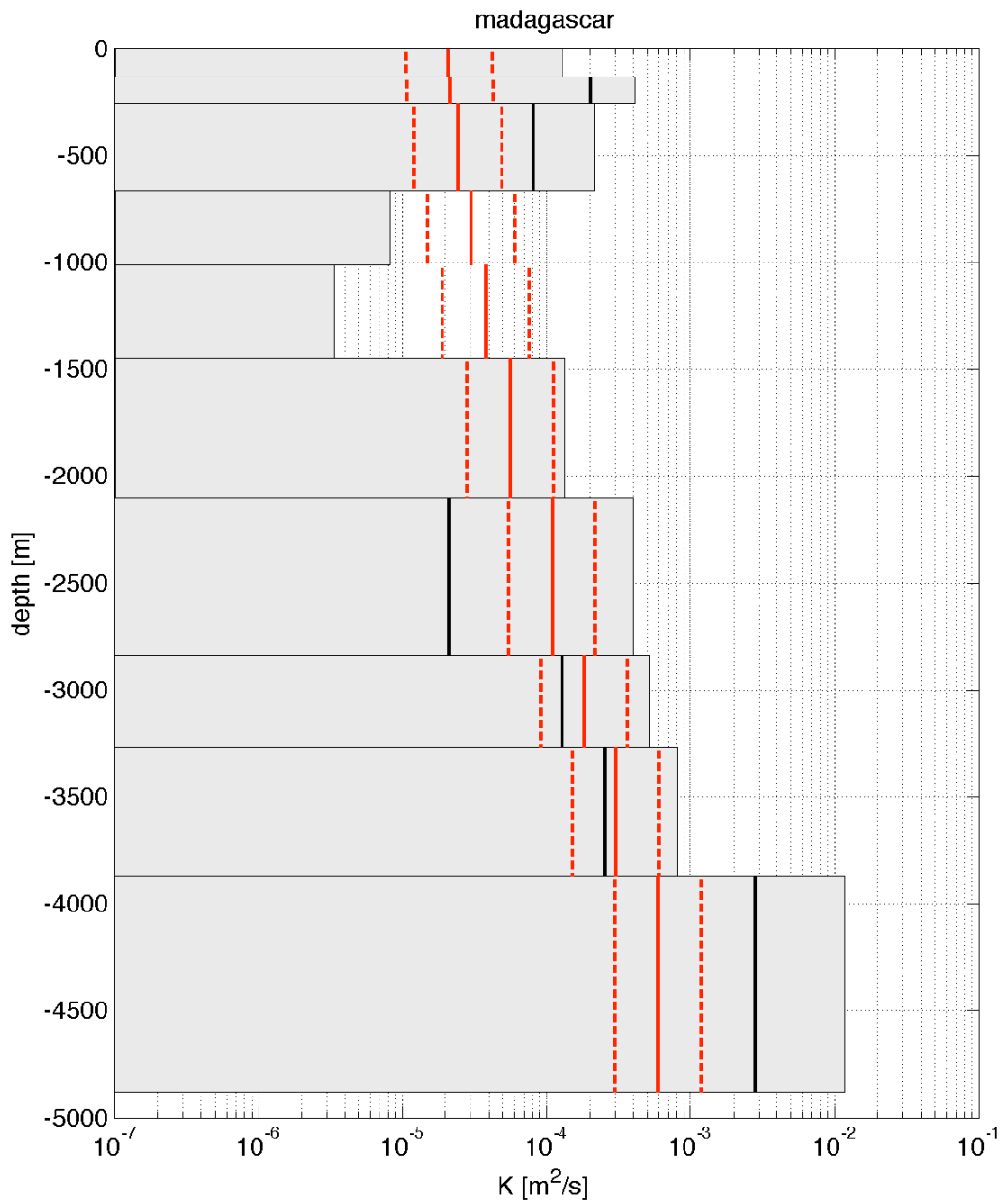


Figure 35: Diffusivities inferred from inversion of hydrography (gray boxes) and average diffusivities predicted by the RDM (solid red, factors of two in dashed red) for the Subtropical Indian Ocean (32°S-20°S).

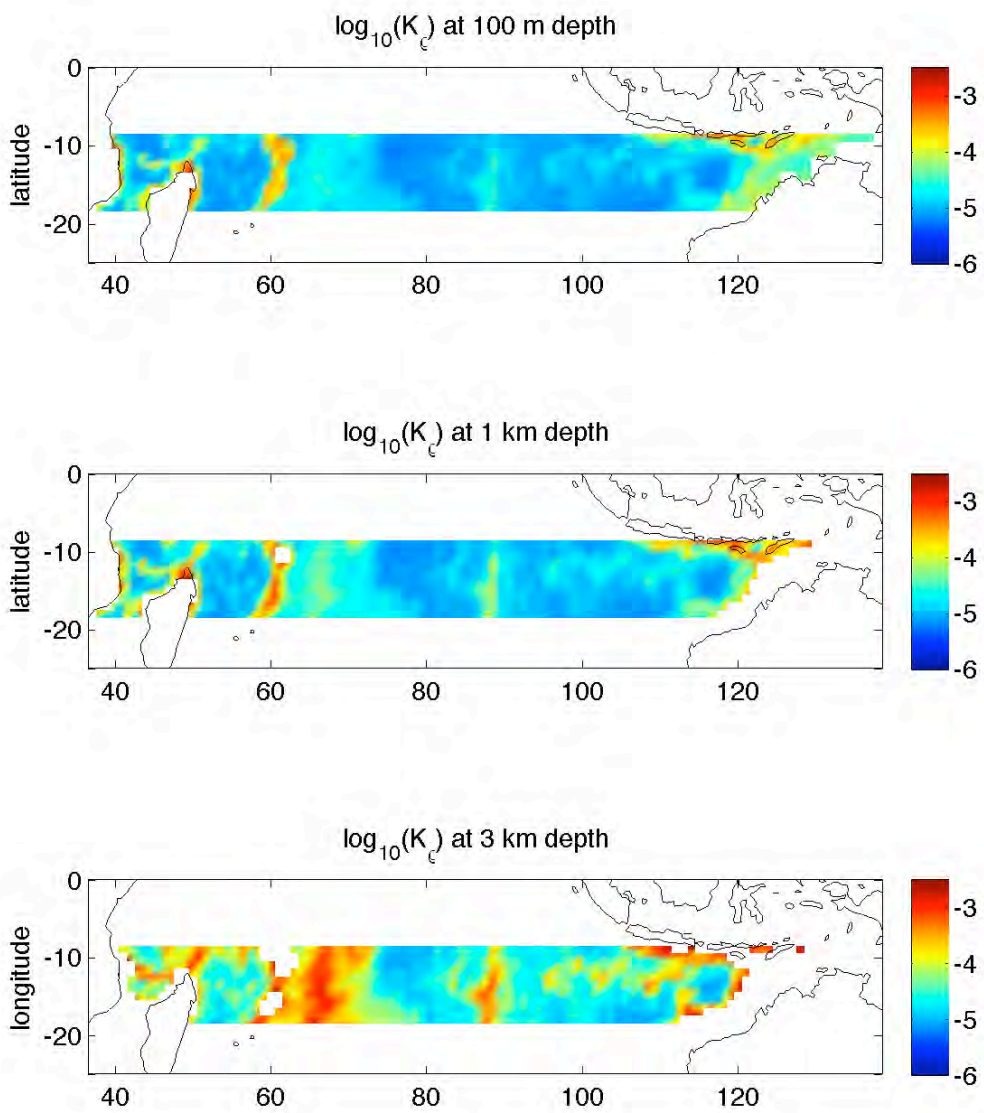


Figure 36: Tropical Indian Ocean (20°S-8°S). Diapycnal diffusivities predicted by the RDM at 100 m, 1000 m and 3000 m of depth.

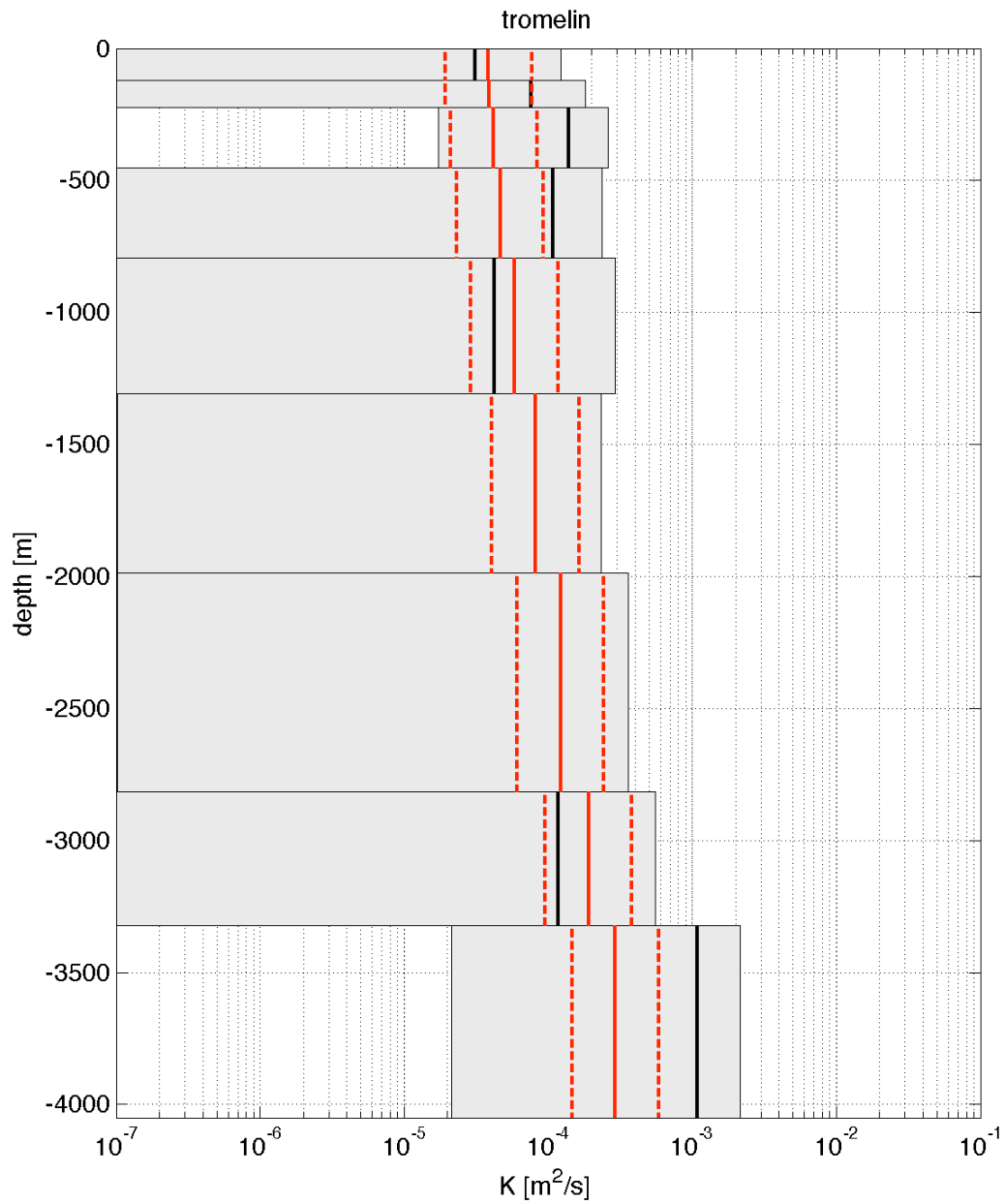


Figure 37: Diffusivities inferred from inversion of hydrography (gray boxes) and average diffusivities predicted by the RDM (solid red, factors of two in dashed red) for the Tropical Indian Ocean (20°S-8°S).

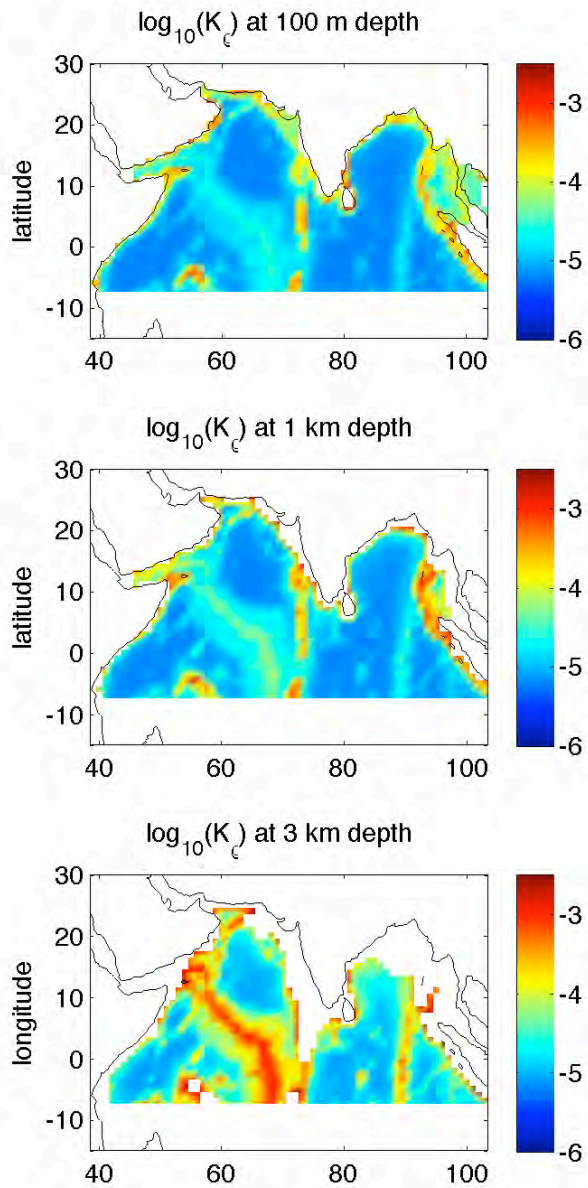


Figure 38: North Indian Ocean (8°S-JADE89-coast). Diapycnal diffusivities predicted by the RDM at 100 m, 1000 m and 3000 m of depth.

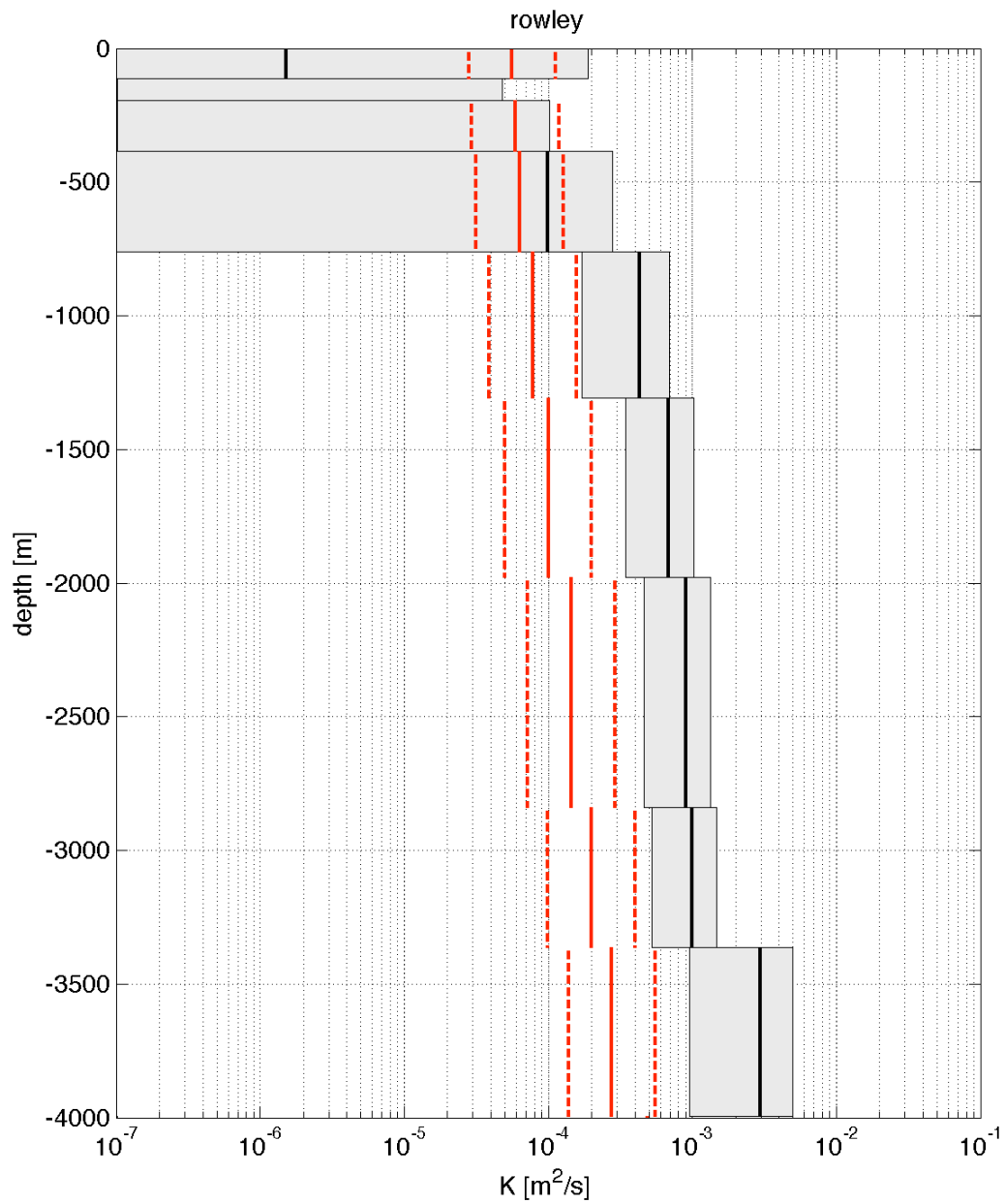


Figure 39: Diffusivities inferred from inversion of hydrography (gray boxes) and average diffusivities predicted by the RDM (solid red, factors of two in dashed red) for the North Indian Ocean (8°S-JADE89-coast)

Atlantic Ocean

Figure 40 shows the box geometry for the Atlantic ocean used in the analysis of GA03.

Figure 41 to Figure 54 show the horizontal distributions of K_p predicted by the RDM for several depth levels and compare the vertical profiles inferred by GA03 to the RDM predictions for the North Atlantic to the Tristan da Cunha box (South Atlantic).

GA03 inferred upwelling in the bottom layers almost everywhere. At deep levels, upwelling is mainly found in the Equatorial box, the Rio box and the Tristan da Cunha box, totaling 5-7 Sv. At intermediate depths, upwelling is found in the Tristan da Cunha box, while downwelling is found in the Equatorial box, with -10 ± 2 Sv at 1300 db. This is consistent with the southward North Atlantic Deep Water increase from entrainment of Antarctic Bottom Waters (Ganachaud, 1999). In the surface layers, GA03 finds significant downwelling over the North Atlantic box, with -13 ± 3 Sv, then upwelling in most other boxes, except in the Tristan da Cunha box, -5 ± 2 Sv downwelling. (Diapycnal advection not shown here, see GA03 for figures).

GA03 found diapycnal diffusivities to be systematically positive (negative diffusivities are not prohibited by inversion constraint) in the deep layers and with values in the range $0-50 \times 10^{-4} \text{ m}^2 \text{ s}^{-1}$, depending on location. The highest diffusivities were found in the bottom layers with values up to $50 \pm 50 \times 10^{-4} \text{ m}^2 \text{ s}^{-1}$ in the North Atlantic box (Figure 41). The RDM predictions are consistent with GA03 diffusivities in the North Atlantic for the deep layers. The RDM predicts lower diffusivities for the bottom layer. Uncertainties in the GA03 are

highest in the bottom layers however because the area of the neutral density layers are small and subject to large error. The neutral density layers were obtained from the Levitus (1994) climatology and thus subject to the considerable uncertainties in the climatology. GA03 diffusivities are negative between ~ 1500 m and ~ 3500 m, precluding comparison to the RDM.

GA03 found diffusivities to be significant in the North Tropical box (Figure 43). Diffusivities are $O(10^{-3}) \text{ m}^2\text{s}^{-1}$ deeper than ~ 3500 m of depth and almost depth-independent. The RDM predictions are significantly lower for those depths. A possible explanation for this discrepancy is intense mixing in the Vema Fracture Zone at 11N. The Vema Fracture Zone, with a sill depth of more than 4500 meters, allows transport of Antarctic Bottom Water and North Atlantic Deep Water from the Western to the Eastern North Atlantic. The observed isopycnal field is consistent with an internal hydraulic jump. Overturns as large as 400 m have been inferred in the sill vicinity (Mecking et al., in preparation). This type of mixing can not be captured by the RDM.

For the Equatorial box (Figure 45), GA03 finds diffusivities of $5\text{-}20 \times 10^{-4} \text{ m}^2\text{s}^{-1}$ deeper than 1500 m, again displaying little depth dependence. The RDM predictions are consistent for the deepest layers but significantly lower between 1500 and 3500 m of depth. This is likely related to the intense mixing in the Romanche Fracture Zone (e.g., Polzin et al., 1996; Ferron et al., 1998). The Romanche Fracture Zone is deep enough to allow significant eastward flow of Antarctic bottom water from the Brazil Basin into the Sierra Leone and Guinea Abyssal plains. Intense mixing is documented in the Romanche Fracture Zone, Ferron et al., 1998

report a mean diapycnal diffusivity of $10^{-1} \text{ m}^2\text{s}^{-1}$, and strong mixing up to a 1000 m from the bottom at the northern exit of the fracture zone (in the area of the RFZ they studied). Polzin et al., 1996 suggest flow is hydraulically controlled in the Romanche Fracture Zone.

In the Helena box (A8 to A9, Figure 47), the RDM predictions and the GA03 estimates are consistent.

In the Rio box (A9 to A10, Figure 51), GA03 finds the highest values at approximately the depths of the crest of the Mid-Atlantic Ridge and attributes that to enhanced mixing by tidally generated internal waves and cites the microstructure studies in the Basin Basin. The RDM, calibrated on those very data, does not predict a maximum between 2500 m and 3500 m of depth as suggested by the GA03 estimates although the RDM was shown earlier to reproduce the diffusivities in the Brazil Basin to within factors of two. It is also unlikely that the vertical structure in the Helena box, which is also traversed by the Mid-Atlantic Ridge, is so different from the vertical structure in the Rio box if indeed that mid-depth maximum is the signature of bottom-intensified mixing over the Ridge. The difference between the RDM and the GA03 estimates in the Rio box is more likely related to intense mixing in the Vema Channel. Antarctic bottom water piles up in the Argentine Basin behind the sill in the Vema Channel at about 31° S . There is then a discontinuity in bottom water density between the Argentine Basin and the Brazil Basin as AABW flows through the Vema Channel and mixes as it descends into and fills the Brazil Basin (Hogg et al., 1982 Bryden and Nurser, 2003).

In the Tristan da Cunha box (Figure 53), most of the GA03 diffusivity estimates are negative. The RDM is however consistent within the uncertainties of the GA03 estimates.

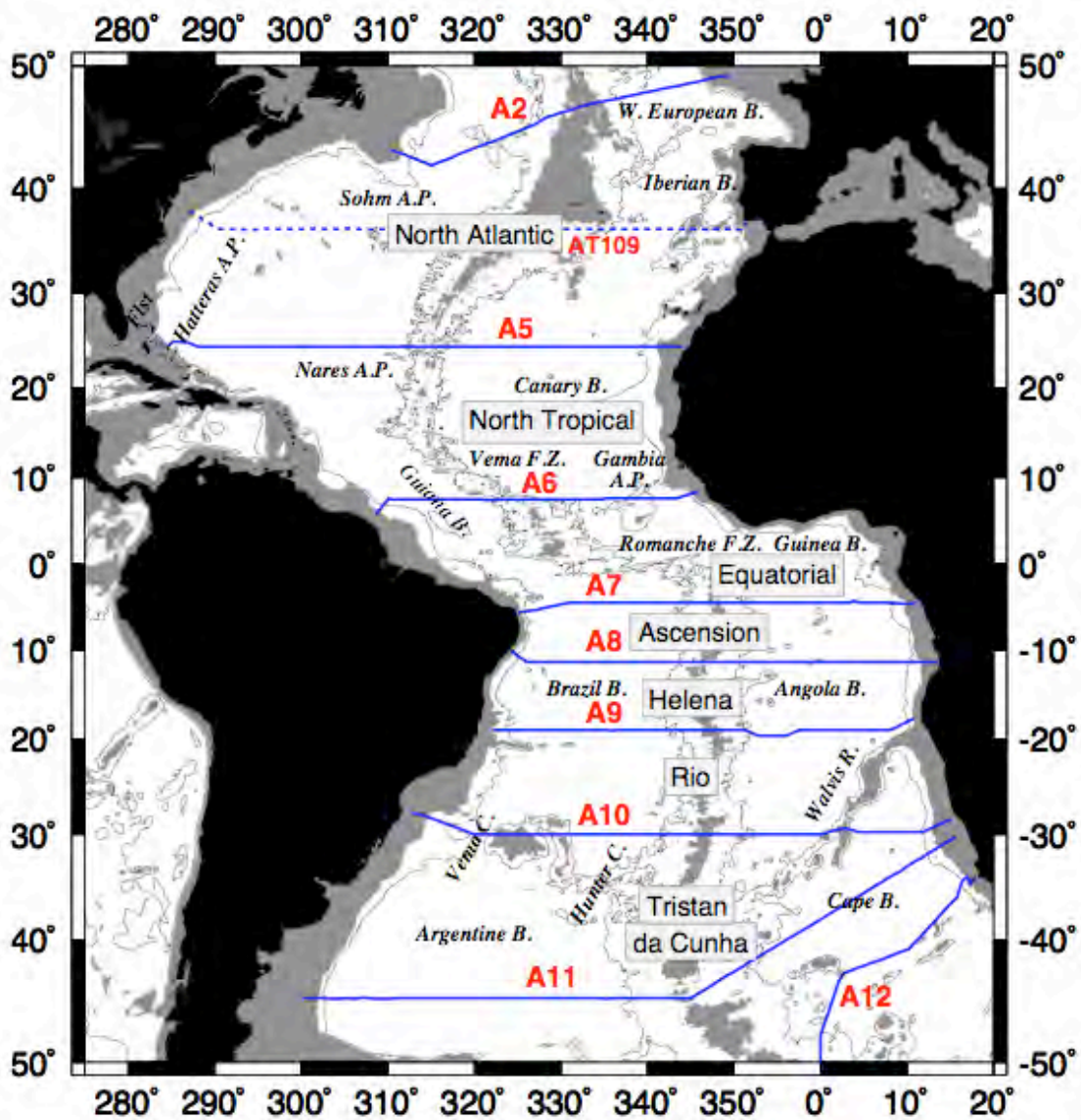


Figure 40: Atlantic ocean hydrographic (blue) sections and topography. The 4000 m isobath is contoured and areas shallower than 3000 m are shaded. Figure from Ganachaud (1999).

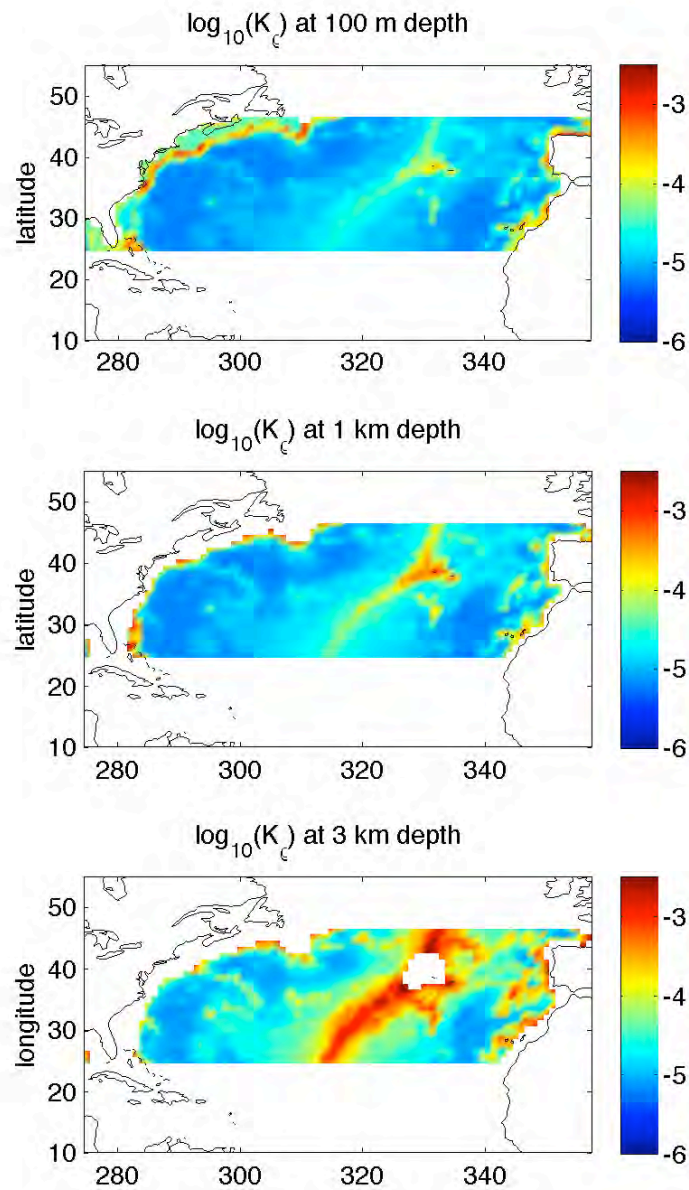


Figure 41: North Atlantic (A2 to A5). Diapycnal diffusivities predicted by the RDM at 100 m, 1000 m and 3000 m of depth.

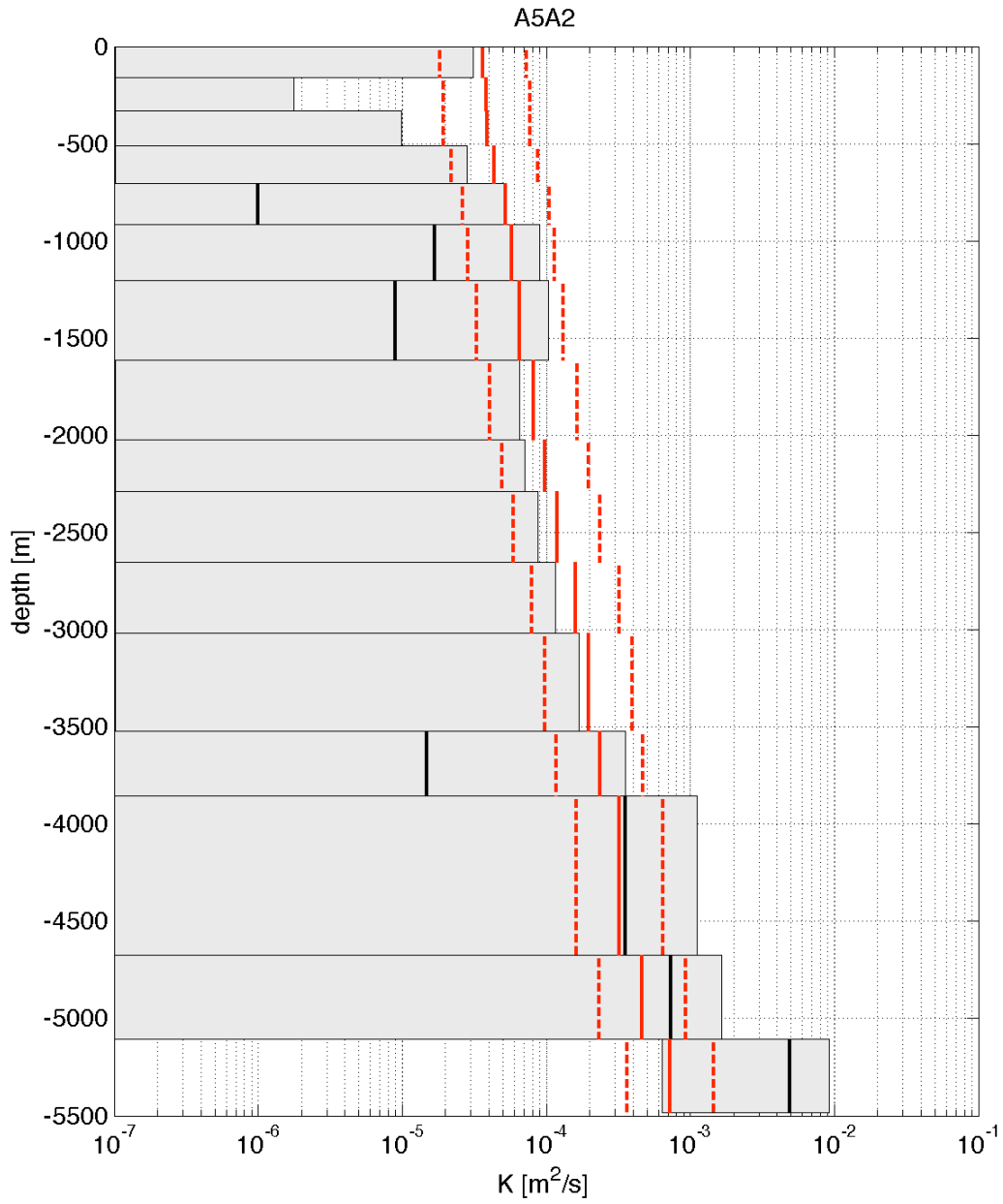


Figure 42: Diffusivities inferred from inversion of hydrography (gray boxes) and average diffusivities predicted by the RDM (solid red, factors of two in dashed red) for the North Atlantic (A2 to A5).

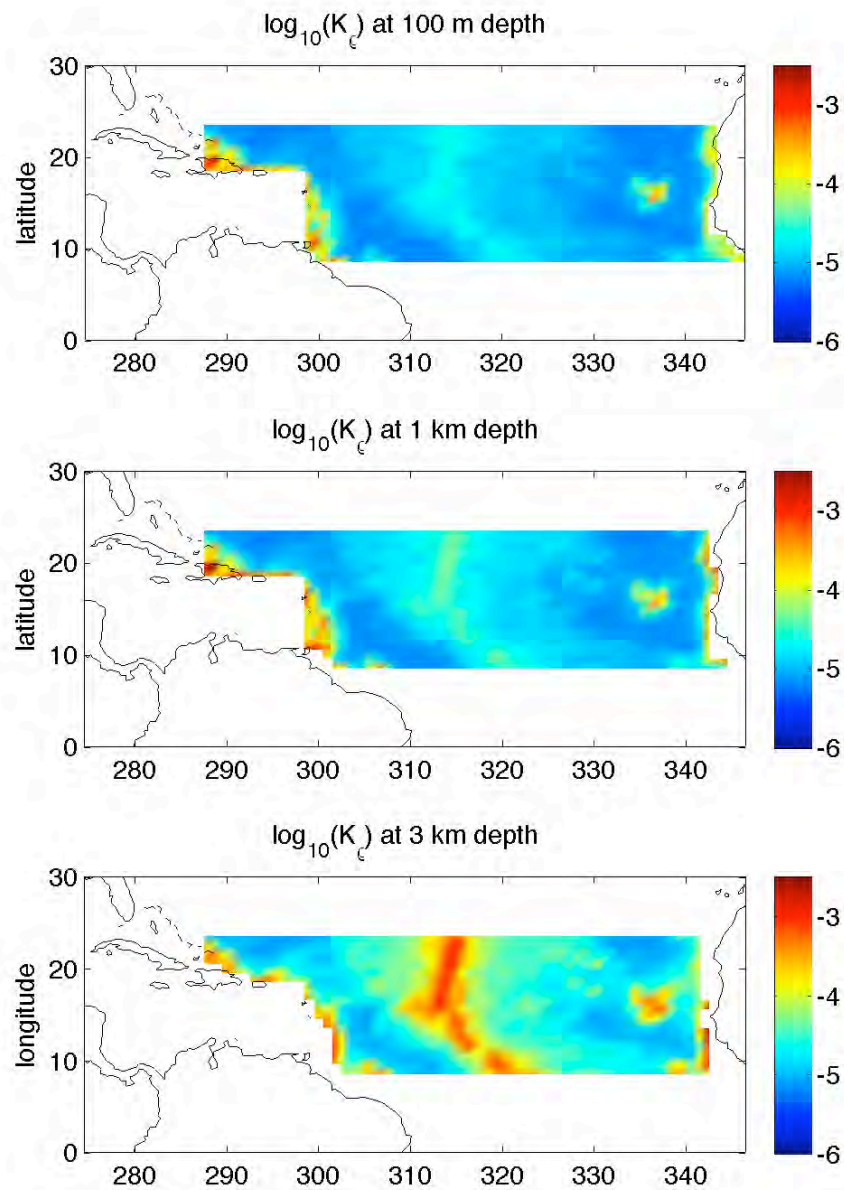


Figure 43: North Tropical Atlantic (A5 to A6). Diapycnal diffusivities predicted by the RDM at 100 m, 1000 m and 3000 m of depth.

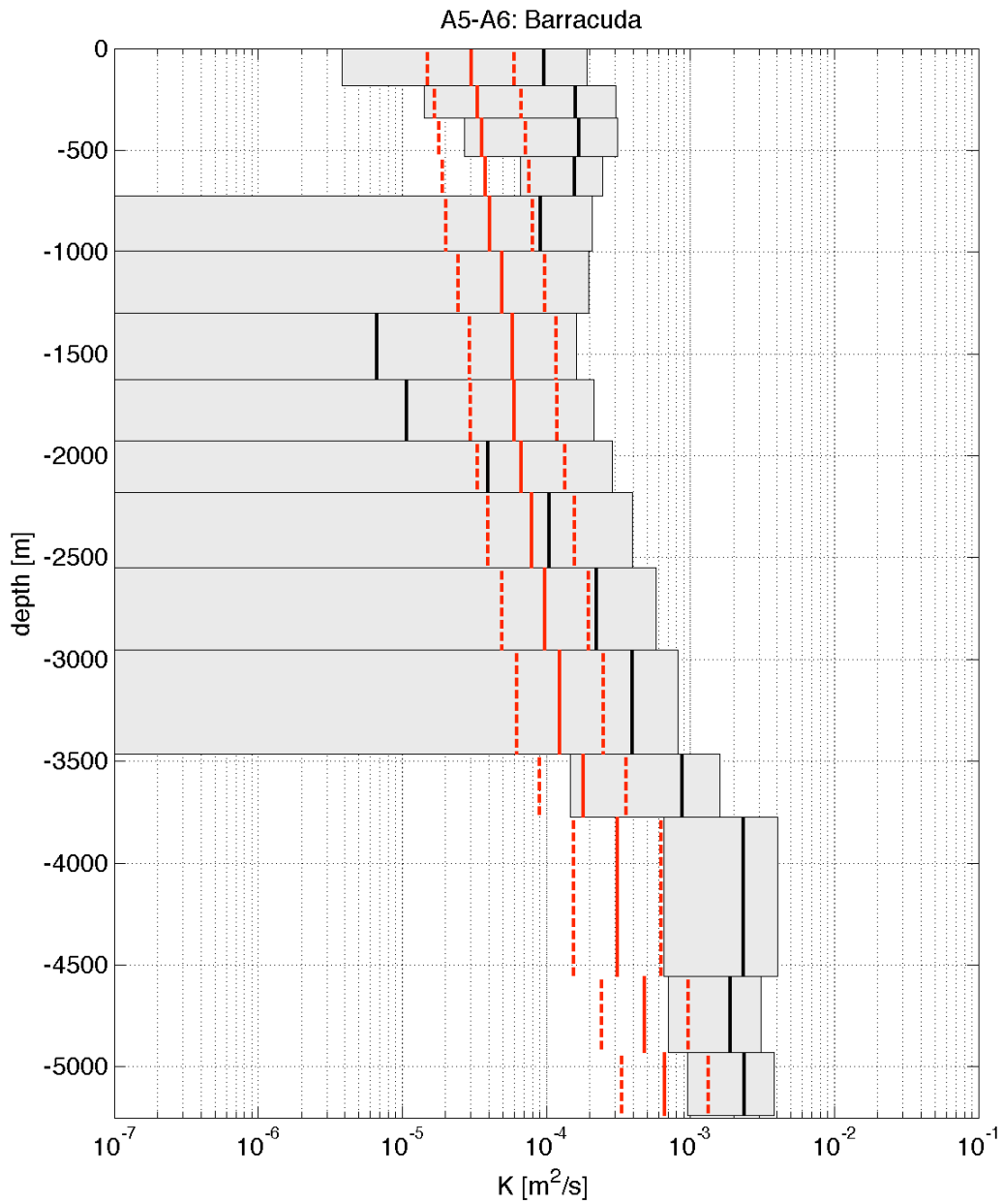


Figure 44: Diffusivities inferred from inversion of hydrography (gray boxes) and average diffusivities predicted by the RDM (solid red, factors of two in dashed red) for the North Tropical Atlantic (A5 to A6).

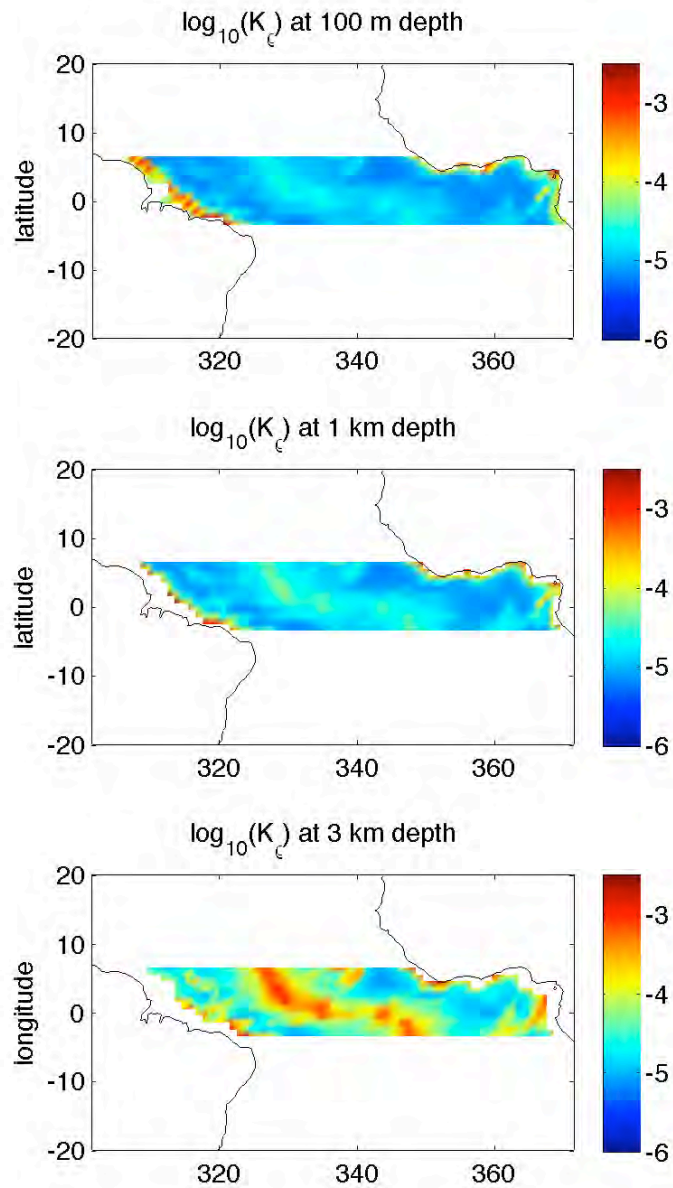


Figure 45: Equatorial Atlantic (A6 to A7). Diapycnal diffusivities predicted by the RDM at 100 m, 1000 m and 3000 m of depth.

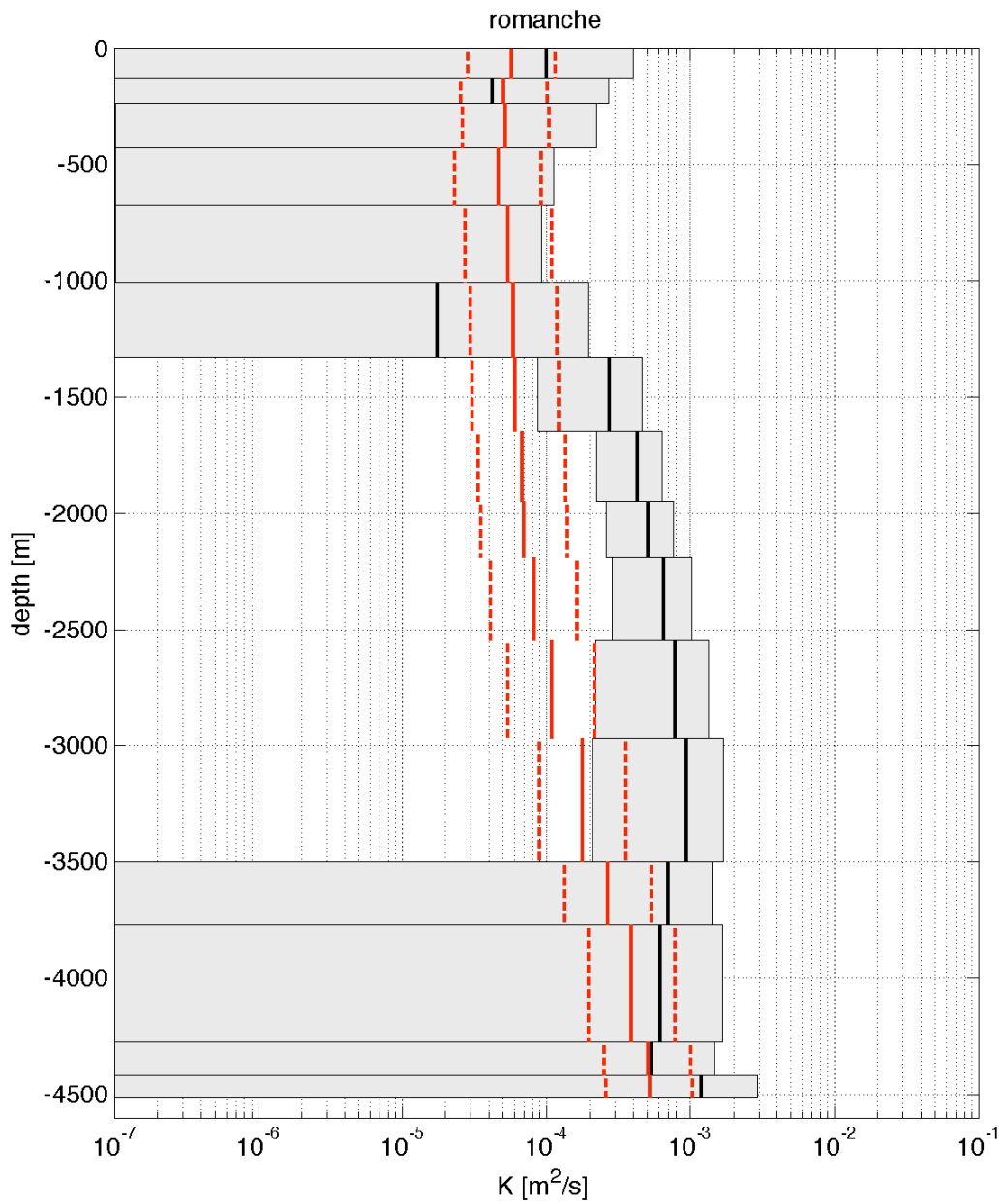


Figure 46: Diffusivities inferred from inversion of hydrography (gray boxes) and average diffusivities predicted by the RDM (solid red, factors of two in dashed red) for the Equatorial Atlantic (A6 to A7).

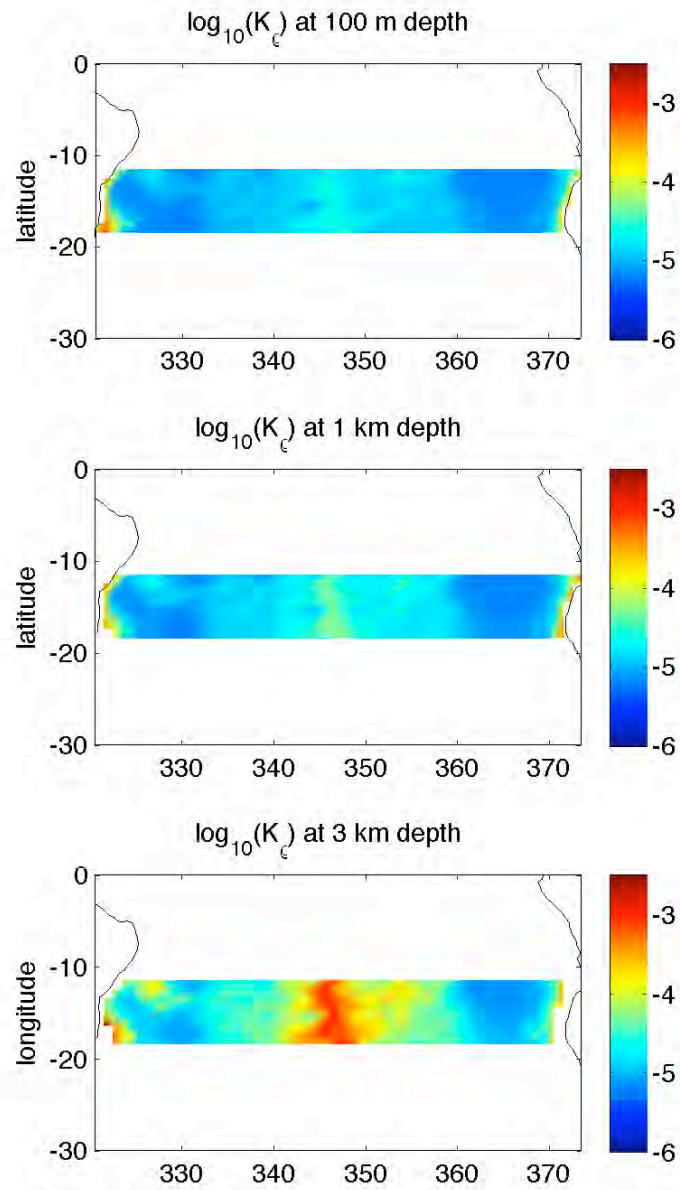


Figure 47: South Atlantic (A8 to A9). Diapycnal diffusivities predicted by the RDM at 100 m, 1000 m and 3000 m of depth.

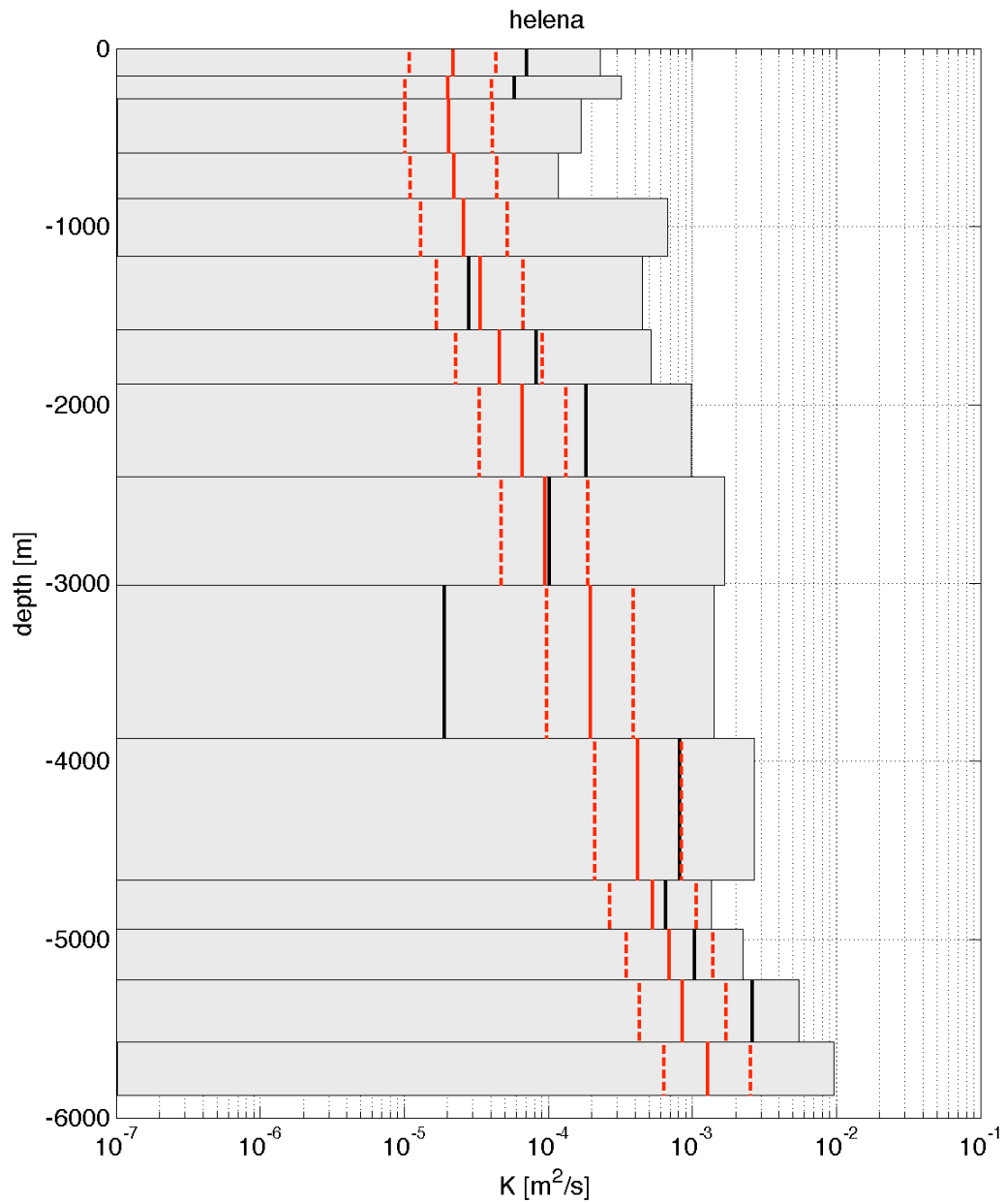


Figure 48: Diffusivities inferred from inversion of hydrography (gray boxes) and average diffusivities predicted by the RDM (solid red, factors of two in dashed red) for the South Atlantic (A8 to A9).

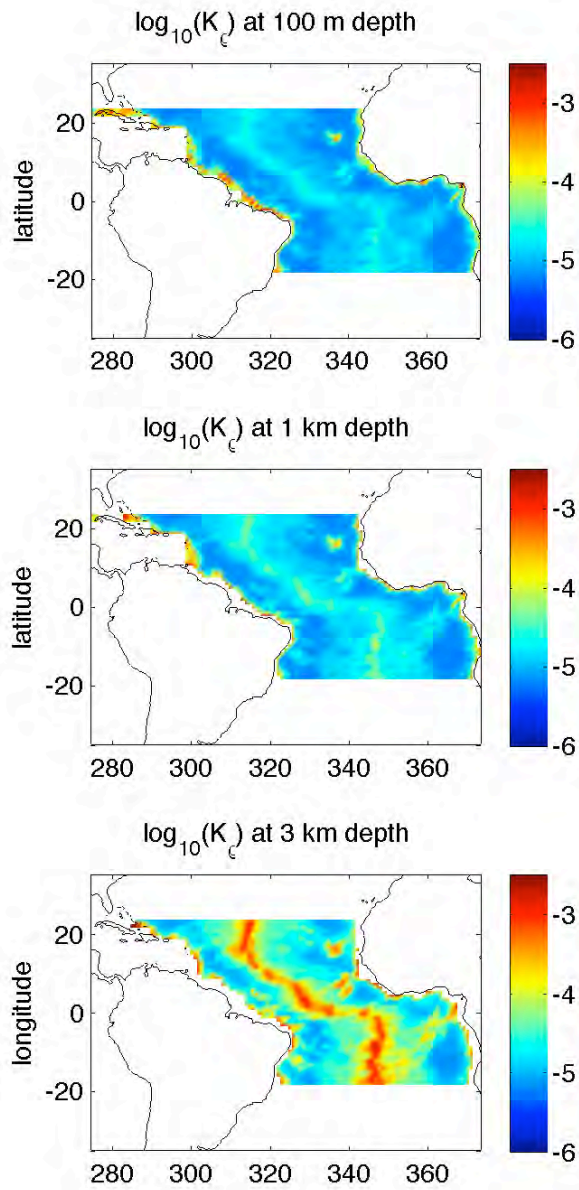


Figure 49: Atlantic ‘superbox’ (A5 to A9). Diapycnal diffusivities predicted by the RDM at 100 m, 1000 m and 3000 m of depth.

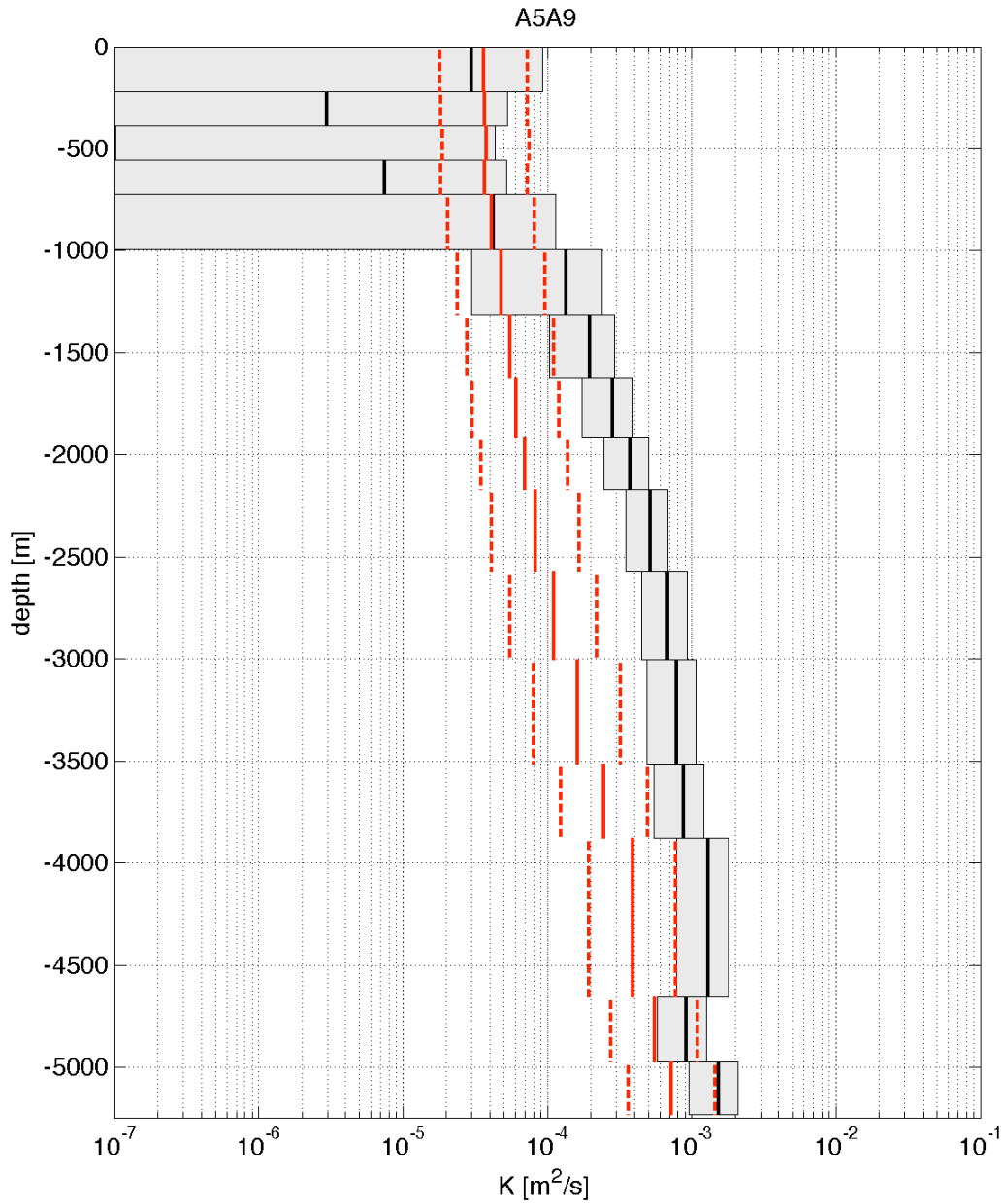


Figure 50: Diffusivities inferred from inversion of hydrography (gray boxes) and average diffusivities predicted by the RDM (solid red, factors of two in dashed red) in the central Atlantic ‘superbox’ (A5 to A9)..

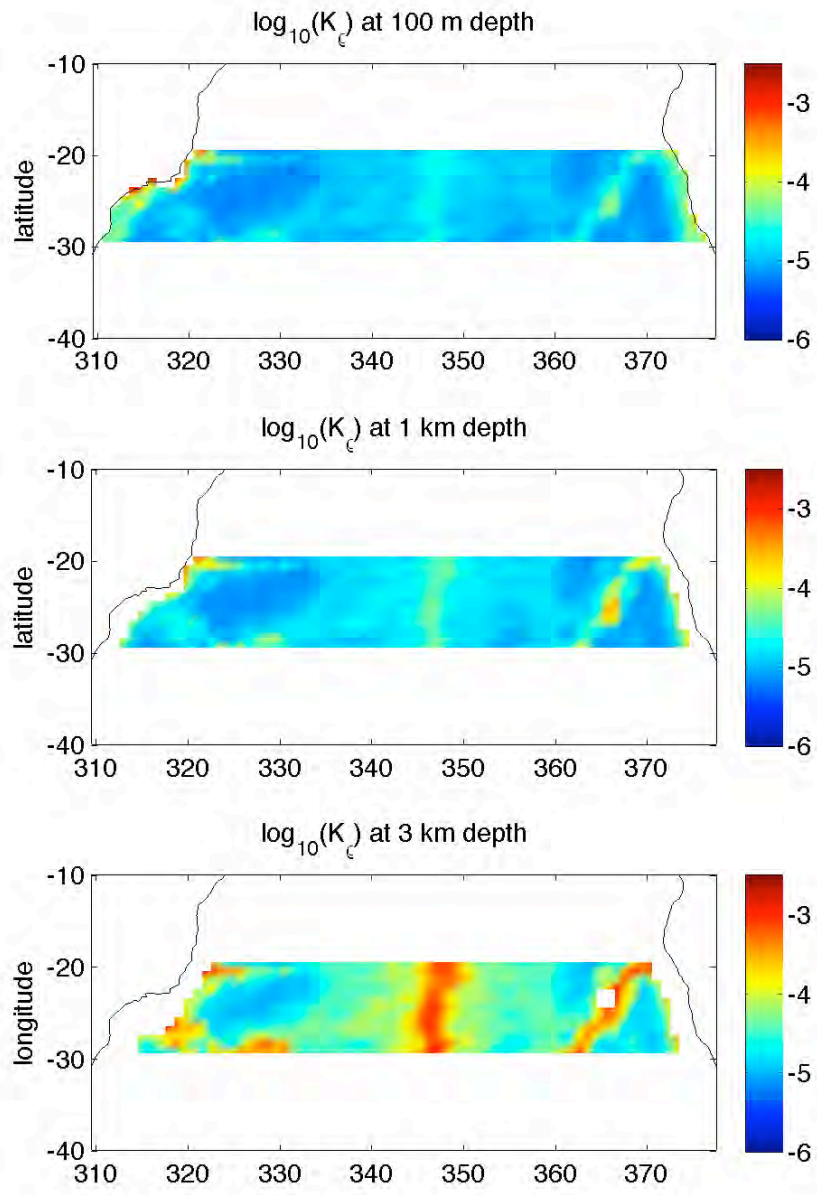


Figure 51: South Atlantic (A9 to A10). Diapycnal diffusivities predicted by the RDM at 100 m, 1000 m and 3000 m of depth.

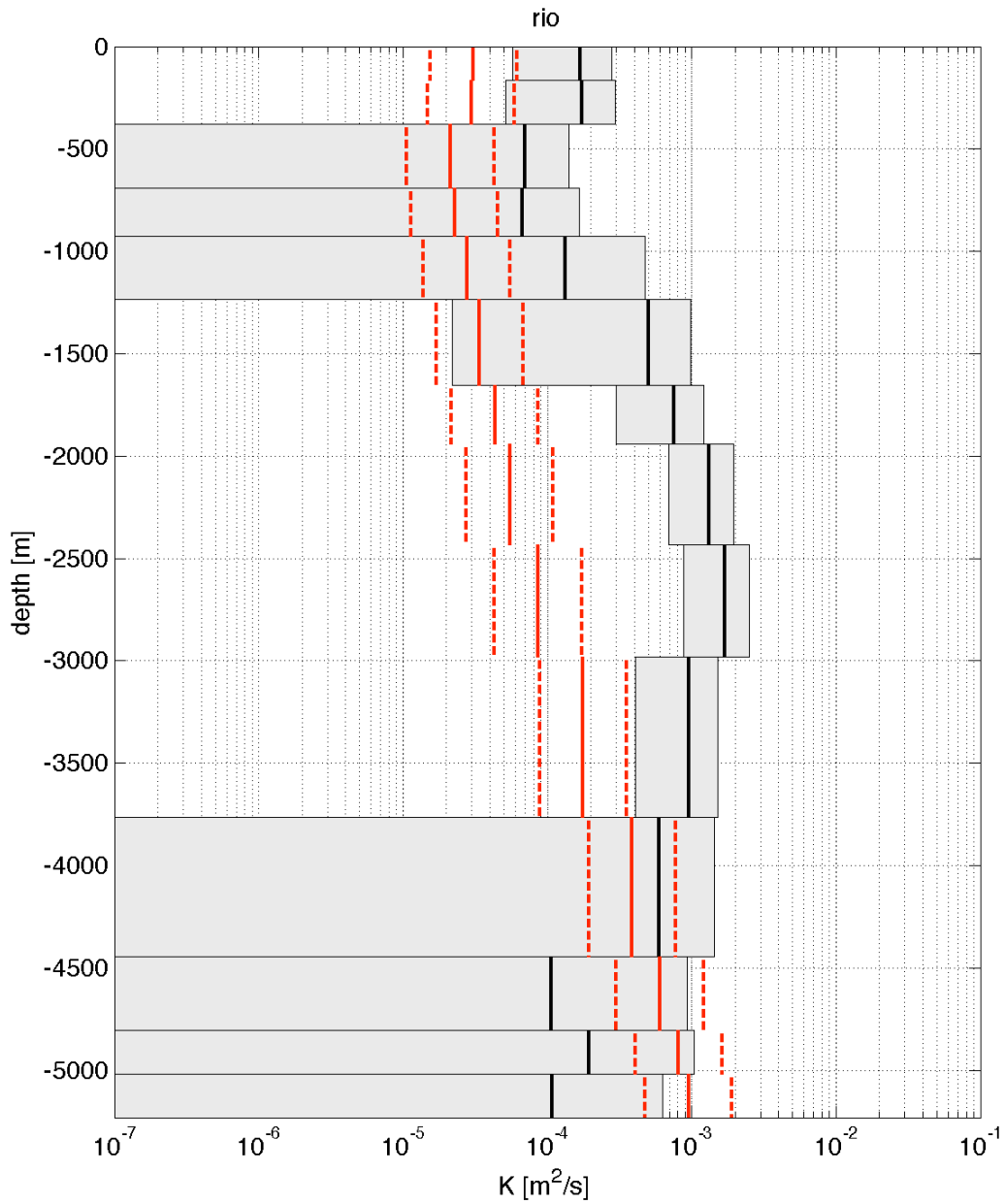


Figure 52: Diffusivities inferred from inversion of hydrography (gray boxes) and average diffusivities predicted by the RDM (solid red, factors of two in dashed red) for the South Atlantic (A9 to A10).

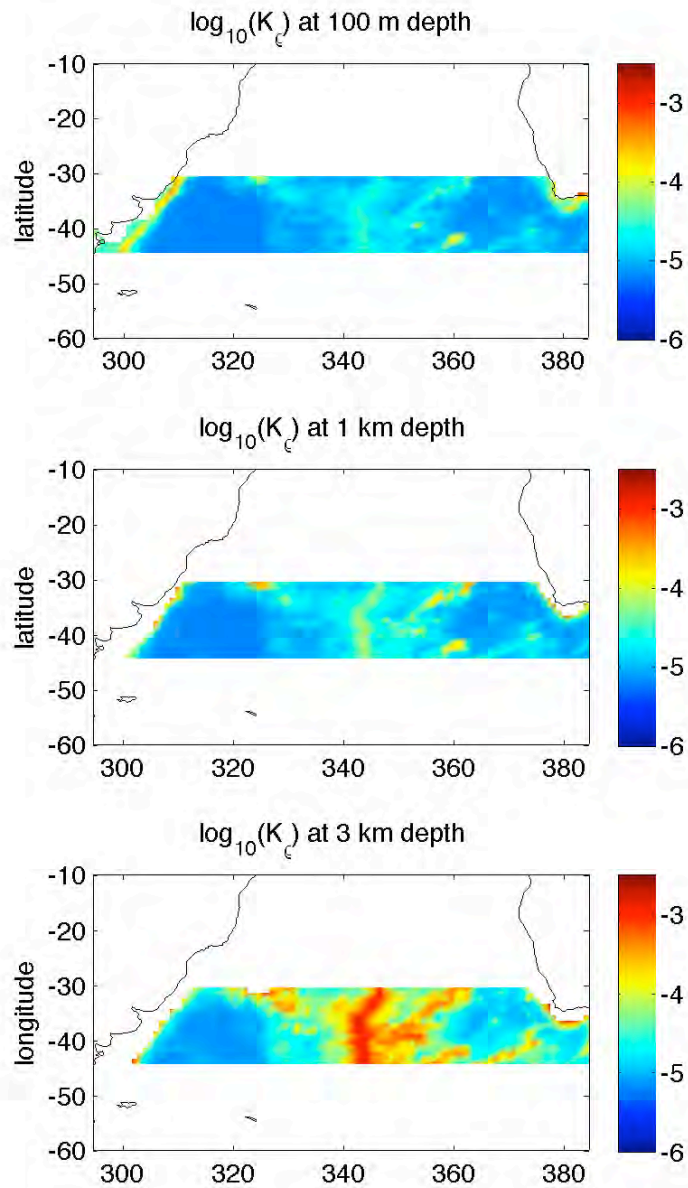


Figure 53: Diapycnal diffusivities predicted by the RDM at 100 m, 1000 m and 3000 m of depth for the South Atlantic (A10 to A11).

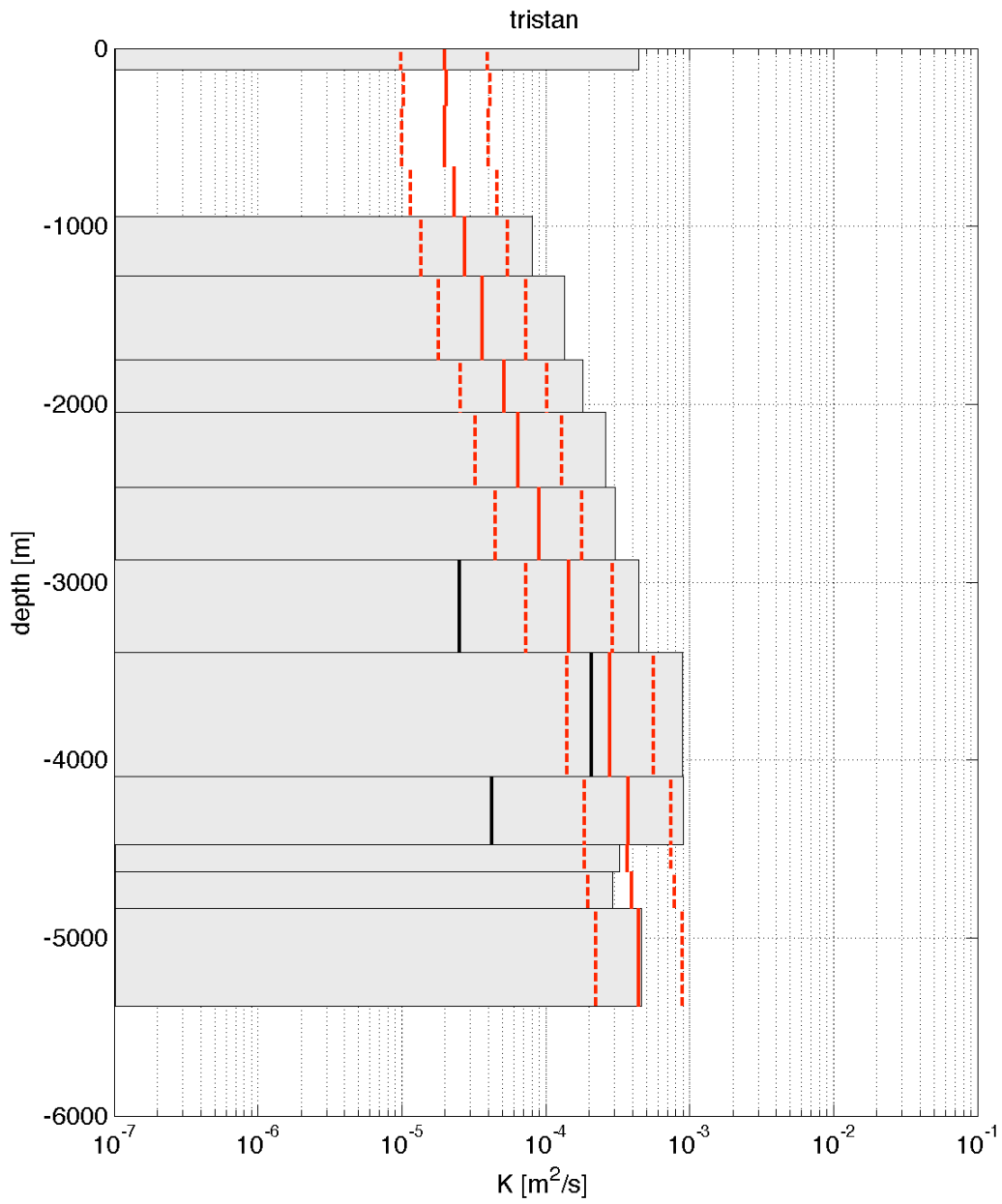


Figure 54: Diffusivities inferred from inversion of hydrography (gray boxes) and average diffusivities predicted by the RDM (solid red, factors of two in dashed red).

Pacific Ocean

Figure 55 shows the box geometry for the Pacific ocean used in GA03.

Figure 56 to Figure 61 show the horizontal distributions of K_p predicted by the RDM for several depth levels and compare the vertical profiles inferred by GA03 to the RDM predictions for the North Pacific, Central Pacific and South Subtropical Pacific respectively.

GA03 found diapycnal mass transfers indicative of upwelling at the surface in the Central Pacific, 45 ± 6 Sv, and downwelling in the subtropical gyres, -16 ± 5 Sv in the South Pacific and -17 ± 3 Sv, in North Pacific respectively. At depth, there is upwelling below 2000 db associated with systematic and significant diffusivities ranging from 1 to $8 \pm 2 \times 10^{-4} \text{ m}^2 \text{ s}^{-1}$ between 2000 db and 4500 db (diapycnal advection figures not shown here, see GA03).

The RDM predictions are consistent with the GA03 estimates in the North Pacific and Central Pacific boxes. In the South Subtropical Pacific, the RDM underpredicts compared to the GA03 estimates for the bottom-most layer. This is likely due to the diapycnal diffusivities of $60\text{-}1000 \times 10^{-4} \text{ cm}^2 \text{ s}^{-1}$ in the deep layers downstream of the Samoan Passage as documented by Roemmich et al. (1996).

On a different note, there is not much evidence for the latitude dependence of diapycnal mixing as suggested by Gregg et al., 2003. Because of the curvature of the Earth, $\sim 30\%$ of the area of the Central Pacific box (Figure 58) is within 5° of the equator. According to the latitudinal dependent factor in Gregg et al., 2003, the diffusivities should be reduced by

factors of 5 to a 100 in that latitude range. In contrast, the GA03 estimates are rather strong, even higher than the RDM predictions which does not include the latitudinal dependence.

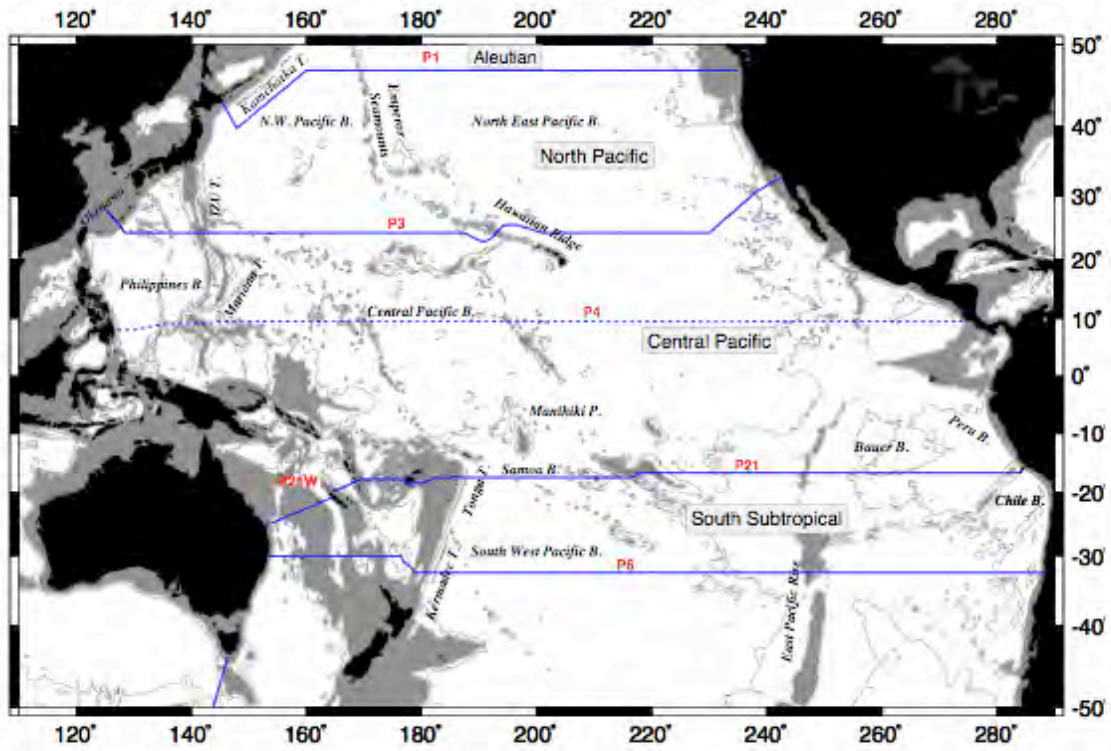


Figure 55: Pacific Ocean sections and topography. The 4000 m isobath is contoured and areas shallower than 3000 m are shaded. Figure from Ganachaud (1999).

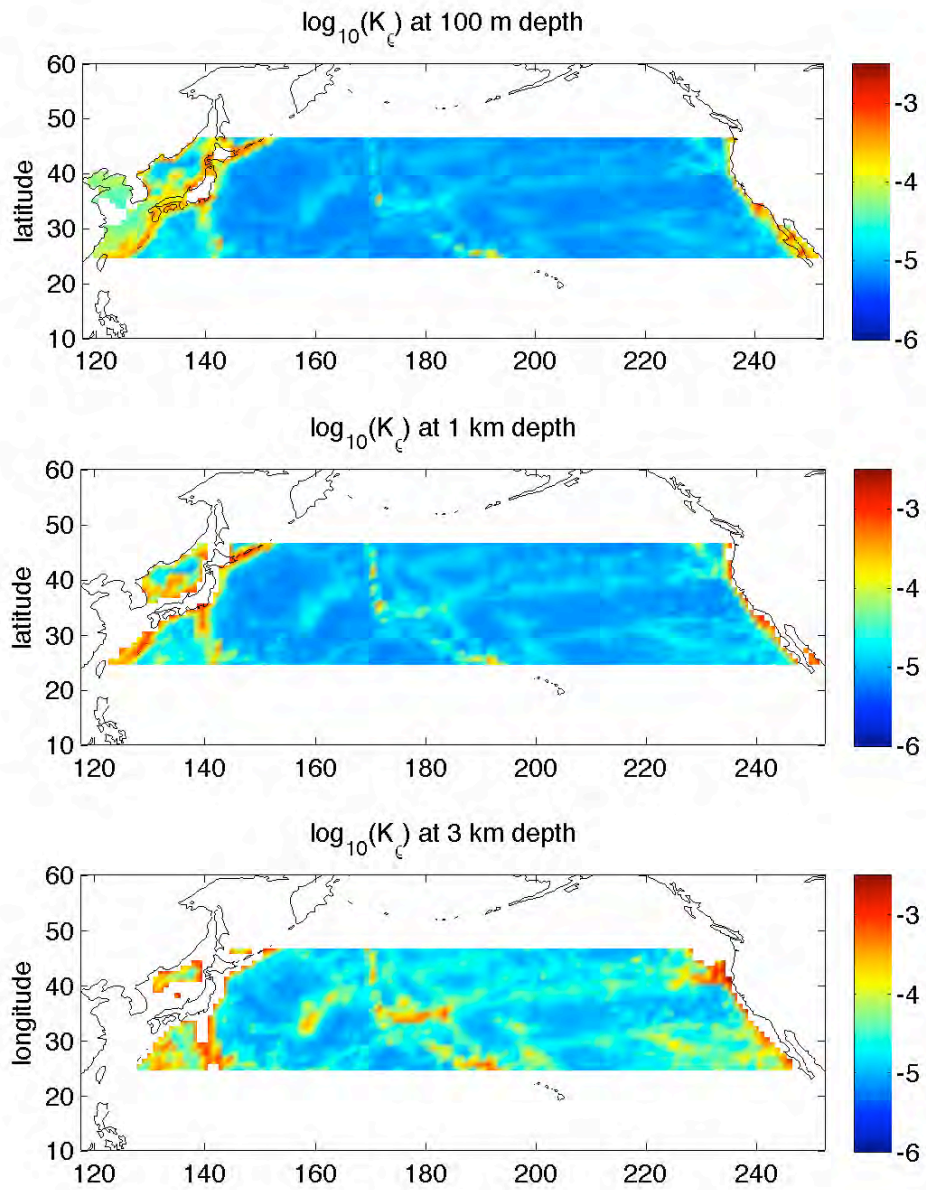


Figure 56: North Pacific (24°N-47°N). Diapycnal diffusivities predicted by the RDM at 100 m, 1000 m and 3000 m of depth.

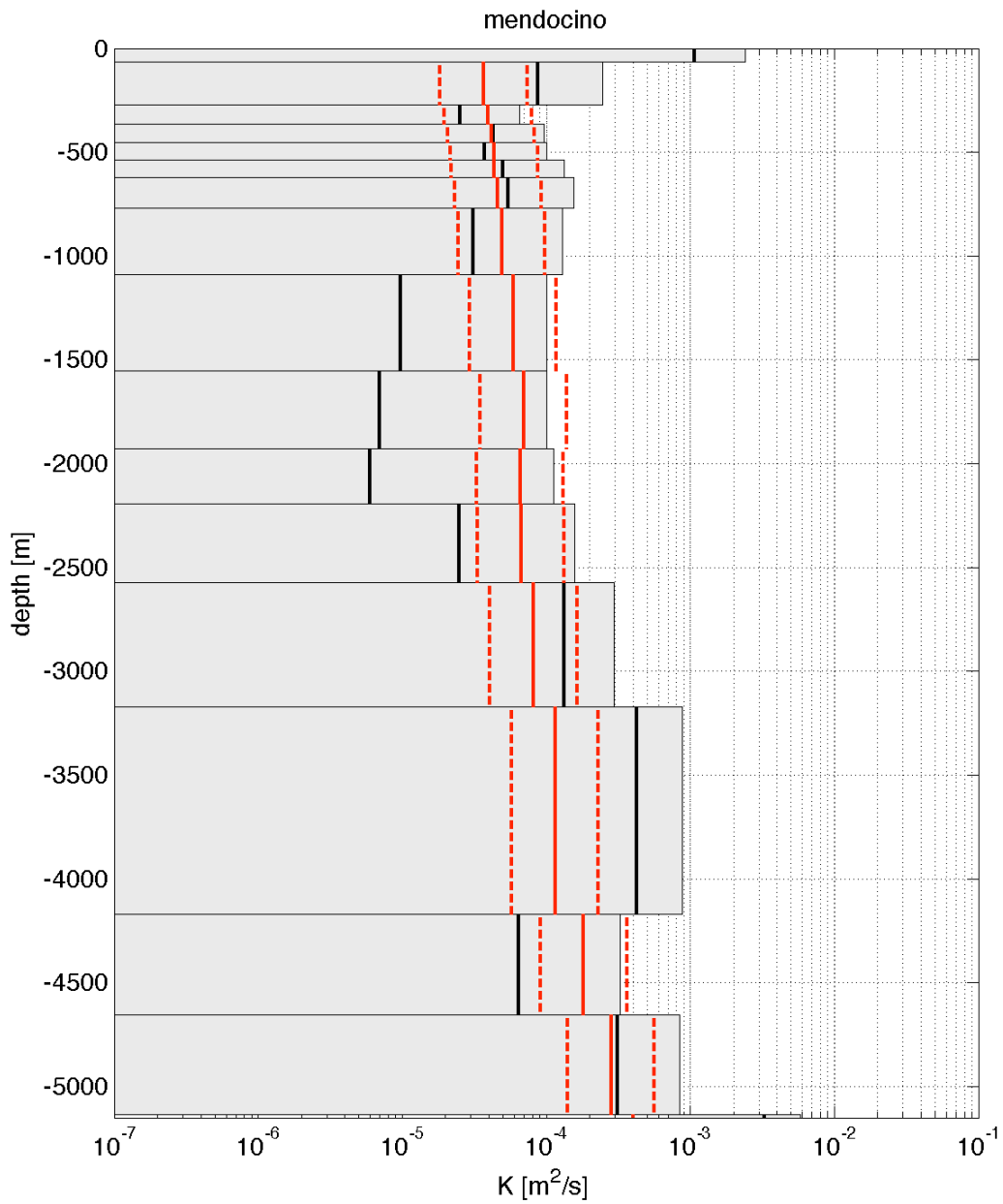


Figure 57: Diffusivities inferred from inversion of hydrography (gray boxes) and average diffusivities predicted by the RDM (solid red, factors of two in dashed red).

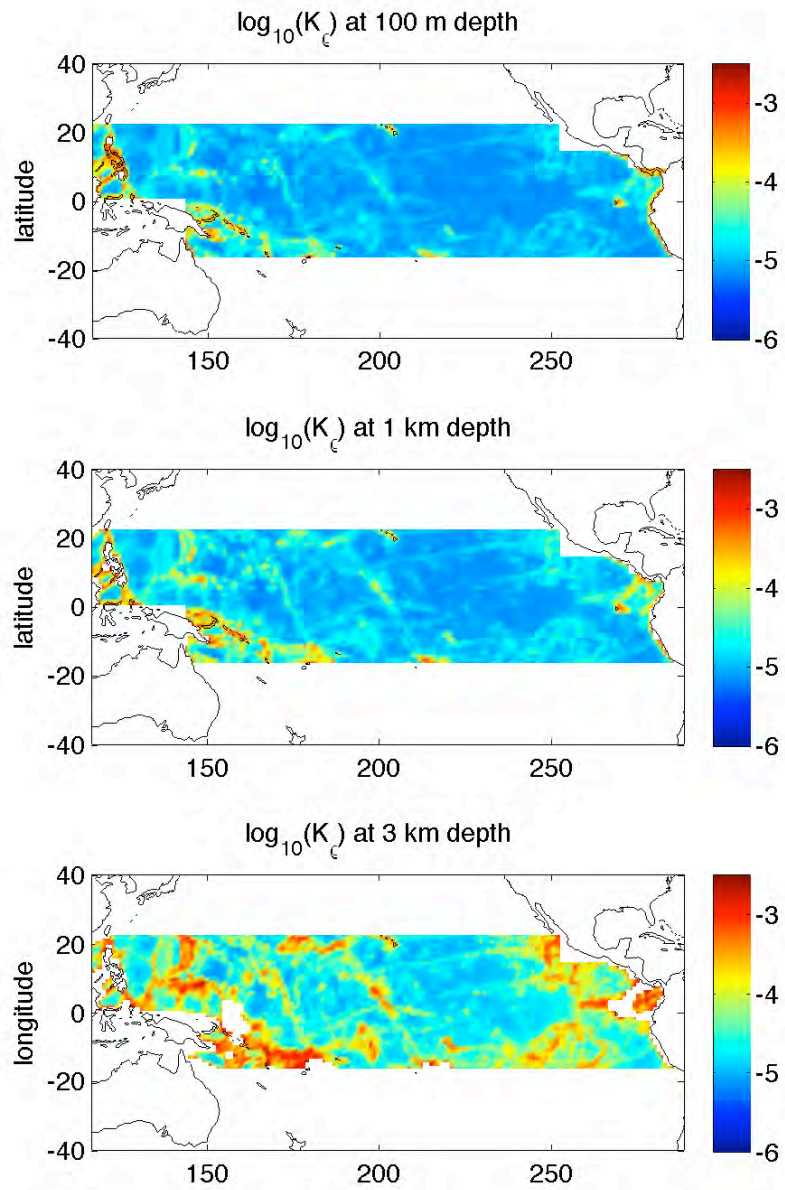


Figure 58: Central Pacific (17°S-24°N). Diapycnal diffusivities predicted by the RDM at 100 m, 1000 m and 3000 m of depth. Central Pacific (17°S-24°N).

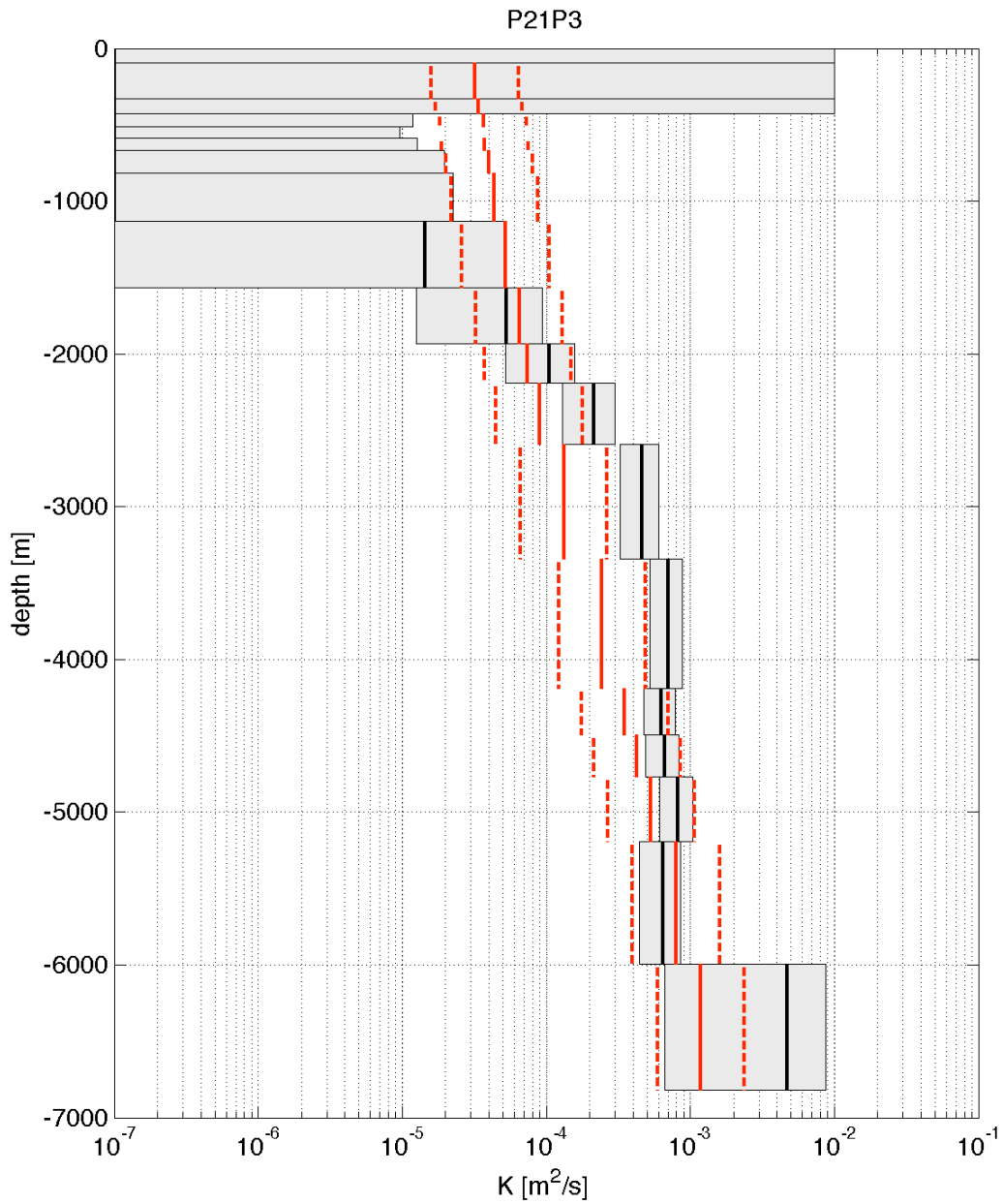


Figure 59: Diffusivities inferred from inversion of hydrography (gray boxes) and average diffusivities predicted by the RDM (solid red, factors of two in dashed red) for the Central Pacific (17°S-24°N).

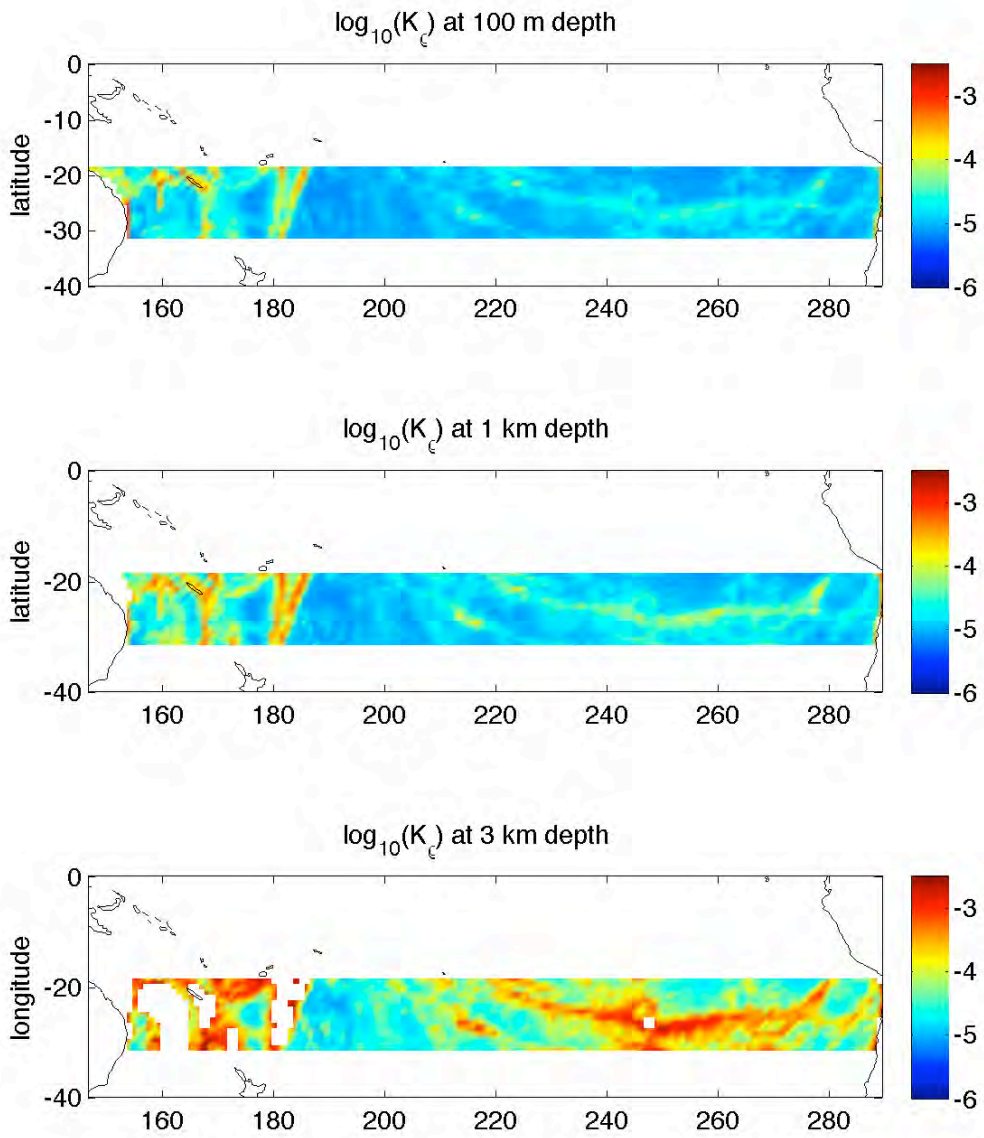


Figure 60: South Subtropical Pacific (32°S-17°S). Diapycnal diffusivities predicted by the RDM at 100 m, 1000 m and 3000 m of depth.

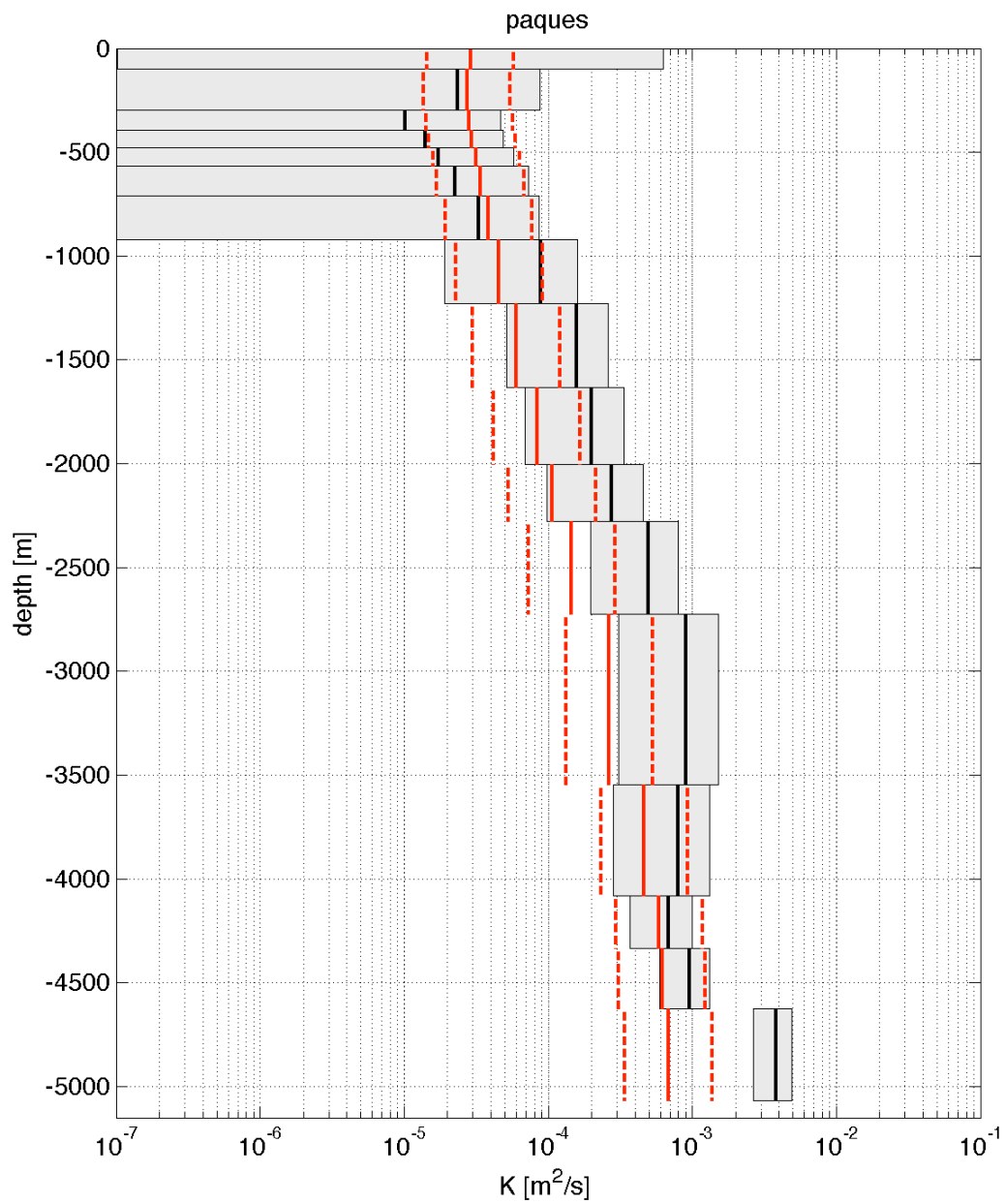


Figure 61: Diffusivities inferred from inversion of hydrography (gray boxes) and average diffusivities predicted by the RDM (solid red, factors of two in dashed red) for the South Subtropical Pacific (32°S-17°S).

Chapter Three

3. Some inferences about diapycnal mixing based on the RDM

The simple empirical model for the spatial distribution of diapycnal mixing developed in this dissertation has the functional form :

$$K_{\rho}(h,r) = K_b(r)(1 + h/h_0(r))^{-2} + K_{back}$$

The RDM was calibrated on microstructure data from the Brazil Basin, Hawaii and Fieberling Guyot. The RDM was then extrapolated globally based on topographic roughness values inferred from the SS97 bathymetry. A good analogy of this process is attempting to map a forest based on knowledge of a few trees and the soil on which they grow. Nonetheless, comparison to inverse model results indicate that the diapycnal diffusivity structure implied by the RDM may be a reasonable first-order approximation. We here summarize some of the lessons learned along the way. In the last section of this chapter, we inquire into how much power would be required to sustain mixing as parameterized by the RDM. The power consumption estimate is compared to the 2.1 TW proposed by Munk and Wunsch, 1998. It is found that allowing for spatially varying mixing lowers the power requirement by a factor of five, as discussed in detail later.

3.1. *Vertical structure of diapycnal mixing*

The vertical structure function used in the RDM is directly adopted from K. Polzin's work (Polzin, 2004; Polzin, 2009). The inverse square decay was shown to be an improvement over the usual choice of exponential vertical decay (e.g., Figure 21). Exponential decay is faster than the observed decay and results in background, depth independent diffusivities at heights greater than 2500 m above topography of all roughness values. This is at odds with the observations and potentially of dynamical importance given that vertical gradients of K_p influence upwelling. The RDM captures the far-field observations better.

Allowing the scale height to vary as a function of topographic roughness improves fits to observed mean diffusivity profiles (cf. Figure 20 to Figure 23).

Of course, there is room for improvement. The decay implied by the RDM is still faster than observed at heights above bottom greater than about 1000 m. This may be remedied by allowing the scale height to grow with height above bottom. Polzin's analysis suggests that the scale height is a function of both height above bottom and buoyancy frequency. Some exploration of this idea was done, mostly inconclusive. More data would be required to verify Polzin's predictions empirically.

Indirect estimates of mixing in the weakly stratified Southern Ocean suggest mixing to be intense throughout the entire water column (Polzin and Firing, 1997; Garabato et al., 2004; Sloyan, 2005), implying much larger decay scales than would be predicted by the RDM. If

true, this may be an indication of the stratification dependence of the scale height. Microstructure measurements are underway in the Southern Ocean (DIMES)¹⁰ which will likely yield much insight.

3.2. Horizontal distribution of diapycnal mixing

The horizontal distribution of time mean ε and K_p predicted by the RDM show a spatial variation in the horizontal with similarities to the global dissipation and diffusivity maps based on tidal mixing parameterizations. However, notable regions of dissimilarity exist, such as at the East Pacific Rise, the Pacific-Antarctic Ridge, the Mid-Indian Ridge and the South-East Indian Ridge. These regions are potential mixing hotspots missed by tidal parameterizations. Whether they actually exhibit intensified mixing due to non-tidal mixing phenomena will require further observations to verify.

The comparison to the diffusivities inferred through inversion of the WOCE data by A. Ganachaud indicates that intense mixing at bathymetric constrictions such as the for instance Romanche Fractures Zone ought to be taken into account. This would likely require a separate parameterization, in addition to the RDM.

¹⁰ <http://dimes.ucsd.edu/>

3.3. *Missing diapycnal Mixing ?*

The comparisons to the inverse model results by Lumpkin and Speer, 2007 suggest topography-catalyzed mixing as parameterized by the RDM can account for a large fraction of the large values called for by indirect estimates. The more localized comparison to the inverse estimates by Ganachaud, 2003 suggests likewise, except in regions where intense mixing resulting from deep flow through bathymetric constrictions is known to occur. It is likely that adding a parameterization specific for this type of mixing would do away with the idea of missing mixing once and for all.

3.4. *Power consumed by spatially varying diapycnal mixing*

Munk and Wunsch, 1998 (MW98 hereafter) estimated the rate at which the global abyssal ocean mixes in much the same way as did Munk, 1966. MW98 found $K_\rho \approx 10^{-4} \text{ m}^2\text{s}^{-1}$ to be a reasonable average for the global abyssal ocean as well. They further estimated the power required to sustain the hypothesized mixing as 2.1 TW (10^{12} W) and attempted to infer what mechanisms drive the mixing by examining the energy sources capable of supplying such amounts of mechanical energy to the deep ocean. Their well-known conclusion is that the $O(1 \text{ TW})$ of wind work alone is not sufficient and thus another source of mechanical energy is required. The tides are the only other major contender as an energy source, possibly contributing $O(1 \text{ TW})$ to mix the abyss, and thus MW98 linked the tides to the general circulation of the ocean.

Webb and Sugimotohara, 2001 (WS01 hereafter) noted that a large fraction of deep and bottom water injected into the deep ocean upwells by Ekman suction along isopycnals in the Southern Ocean in OGCM simulations, as pointed out by Toggweiler and colleagues (see the discussion in 1.41.4). WS01 argue there is no need for ~30 Sv to upwell by diapycnal mixing as assumed by MW98. WS01 make a rough estimated of only ~8 Sv needing to be upwelled by diapycnal mixing in the abyssal ocean. Scaling down the MW98 power consumption estimate of 2.1 TW, WS01 proposed that less than 0.6 TW are required.

The power consumed by diapycnal mixing is given by (St Laurent and Simmons, 2006):

$$P = (1 + 1/\Gamma) \int \rho K_{\rho}(x, y, z) N^2(x, y, z) dV \quad (17)$$

A number of simplifications to (17) are made by MW98. First, the oceanic buoyancy field is integrated in a crude manner in MW98. MW98 assumed

$$\int N^2(x, y, z) dV \approx A \int N^2(z) dz \approx Ag\Delta\rho \quad (18)$$

where A is the area of the ocean and g is the acceleration due to gravity. Taking the ocean area to be $3.6 \times 10^{14} \text{ m}^2$ and the density difference $\Delta\rho$ between 1 and 4 km of depth as 1 kg m^{-3} , MW98 found the now iconic value of $(1 + 1/\Gamma)Ag\Delta\rho \times 10^{-4} \approx 2.1 \text{ TW}$ to be consumed by mixing in the abyssal ocean. MW98 explicitly defined the abyssal ocean as the volume between 40°S and 48°N and 1 to 4 km of depth, where isopycnals generally outcrop only in

the convective regions themselves. The value for the ocean area used in MW98 (i.e., 3.6×10^{14} m²) is actually the pole-to-pole area of the ocean at the surface. Using the more appropriate average ocean area between the latitude and depth range of the abyssal ocean, 2.35×10^{14} m² as estimated from Smith and Sandwell, 1997) bathymetry, reduces the 2.1 TW estimate to 1.4 TW. Furthermore, using $N^2(x,y,z)$ estimated from WOA 2005 climatology rather than the coarse approximation (18) reduces the 1.4 TW estimate to 0.83 TW (see Table 1). Both the MW98 and WS01 estimates of power consumption in the abyssal ocean thus appear to be overestimates by at least a factor of 2.

If we now allow for a spatially variable diffusivity, as observed, the power consumed by mixing is generally further reduced. That is, $\int \rho \overline{K}_\rho N^2(x,y,z) dV \geq \int \rho K_\rho(x,y,z) N^2(x,y,z) dV$ due to the stratification generally decreasing with depth whereas the observed diffusivity decreases with height above bottom. If we use the $K_\rho(x,y,z)$ predicted by the RDM, the power consumption in the abyssal ocean domain is 0.37 TW (see Table 1). Both the MW98 and WS01 estimates of power consumption in the abyssal ocean associated with a uniform diffusivity thus appear to be overestimates by a factor of 5 .

A more recent estimate of power consumption was presented by St Laurent and Simmons, 2006. They divided the ocean between 30°S-47°N into 3 volumes (bottom, deep and ventilated) along neutral density surfaces as in Ganachaud and Wunsch, 2000 and assigned a constant diffusivity value to each volume based on the inverse studies by Ganachaud and Wunsch, 2000 and Lumpkin and Speer, 2003. Their estimate of power consumption for the deep waters is 0.20-0.61 TW and for bottom water is 0.15-0.49 TW. Power consumption

estimates derived from the roughness diffusivity model for the same ocean volumes are 0.1 TW for the deep and 0.04 TW for the bottom waters, factors of 2-6 and 3-10 times smaller, respectively (see Table 2). We suspect a major factor in the discrepancy is the assumption of a constant diffusivity over large ocean volumes in St Laurent and Simmons, 2006). Estimates based on a constant, volume-averaged diffusivity quickly diverge from estimates based on a spatially variable diffusivity (e.g., compare columns 2 and 4 of Table 1). In the case of bottom-intensified mixing, again, we generally find that

$$\int \rho \overline{K}_\rho N^2(x,y,z) dV \geq \int \rho K_\rho(x,y,z) N^2(x,y,z) dV$$

where \overline{K}_ρ is the volume averaged $K_\rho(x,y,z)$ since the diffusivity and the stratification are inversely correlated. The dependence of power consumption on the spatial distribution of mixing and the lower values associated with non-uniform mixing are nothing new in the literature but perhaps merit more consideration. For instance, Simmons et al., 2004b computed the power consumption (for the entire ocean depth) associated with (i) spatially variable mixing (specified by the SL02 parameterization), (ii) mixing varying only in the vertical (based on the Bryan and Lewis, 1979) profile), and (iii) uniform mixing. The globally averaged diffusivities for all three cases were kept the same but the power consumptions ranged from 1.01 TW (variable mixing), 2.11 TW (varying only in the vertical) and 5.80 TW (uniform mixing). Saenko, 2006 also noted that the power consumed by two climate models having the same mean vertical profile of diffusivity but differing in their distribution (horizontally uniform versus topography intensified) is much greater in the case of the horizontally uniform mixing case. Considering that a large fraction of the power

believed to be available for mixing the abyssal ocean is likely dissipated in the upper ocean (e.g., there are good reasons to suspect that much if not most of the 0.9 TW of open ocean internal tide power is dissipated above 1 km (see, for instance, Althaus et al., 2003 and Klymak et al., 2006), the more modest power consumption estimates associated with bottom-intensified mixing (such as the one provided here based on direct microstructure observations of abyssal turbulence) are more consistent with current best estimates of the maximum power of ~2 TW available for mixing in the deep ocean (e.g., Wunsch and Ferrari, 2004) .

We can here only speculate about the fraction of power supplied by the winds and tides respectively. Assuming that the power consumption by diapycnal mixing below 1 km for mid-latitudes (Table 1, 2^d column, bottom row, 0.42 TW) is within a factor of two of the estimate presented here, i.e. 0.21-0.84 TW, and that 0.3 TW is provided by the tides as argued in St Laurent et al., 2002, a reasonable maximum requirement of 0.54 TW is placed on the wind and other sources.

Table 1: The second column lists the power P consumed by mixing over various depth ranges between 40°S and 48°N as in MW98, estimated with the spatially variable $K_\rho(x,y,z)$ predicted by the RDM. The third column lists the averaged diffusivity over that ocean volume. The fourth column lists the power consumed assuming the constant volume averaged diffusivities from column three. The difference in power consumption between columns 2 and 4 illustrates the bias towards higher power consumption estimates when the spatial variability of diffusivity is neglected. This is especially clear over large ocean volumes (see rows 3 and 5). The last column lists the power consumption estimates when the iconic value of $10^{-4} \text{ m}^2\text{s}^{-1}$ is used. All power consumption estimates here are computed with a spatially varying $N^2(x,y,z)$ derived from WOA 2005 climatology.

Depth range	$P(K_\rho(x,y,z))$	$\overline{K_\rho}$	$P(\overline{K_\rho})$	$P(K_\rho = 10^{-4} \text{ m}^2\text{s}^{-1})$
500-1000 m	0.21 TW	$2.7 \times 10^{-5} \text{ m}^2\text{s}^{-1}$	0.22 TW	0.90 TW
1000-4000 m	0.37 TW	$7.0 \times 10^{-5} \text{ m}^2\text{s}^{-1}$	0.58 TW	0.83 TW
4000m-bottom	0.05 TW	$2.2 \times 10^{-4} \text{ m}^2\text{s}^{-1}$	0.05 TW	0.02 TW
1000m-bottom	0.42 TW	$9.5 \times 10^{-5} \text{ m}^2\text{s}^{-1}$	0.81 TW	0.85 TW

Table 2: Column 2 shows the SS06 midlatitude estimates for ventilated, deep and bottom waters based on constant diffusivities for each density class. Their lower bound diffusivities ($0.1, 1.0$ and $3 \times 10^{-4} \text{ m}^2\text{s}^{-1}$ respectively) are based on Lumpkin and Speer, 2003). Their upper bound diffusivities ($0.1, 3,$ and $10 \times 10^{-4} \text{ m}^2\text{s}^{-1}$ respectively) are based on Ganachaud and Wunsch, 2000). Column 3 shows the estimates based on $K_\rho(x,y,z)$ predicted by the RDM. For comparison, volume averaged diffusivities for each density class based on the RDM are $0.4, 0.95$ and $4.0 \times 10^{-4} \text{ m}^2\text{s}^{-1}$ respectively.

Water class	SS06 (TW)	RDM (TW)
<u>Midlatitudes (30°S-47°N)</u>		
Ventilated water ($26.00 < \gamma^t < 27.96$)	0.55	0.60
Deep water ($27.96 < \gamma^t < 28.10$)	0.20-0.61	0.10
Bottom water ($\gamma^t > 28.10$)	0.15-0.49	0.04

3.5. *Conclusions*

The principal objectives of this work are to contribute towards understanding the impact of topography-catalyzed mixing on the distribution of water properties in the abyssal ocean and to improve mixing schemes for implementation in OGCMs. A simple empirical model for the spatial distribution of diapycnal mixing was developed, based on the premise that topography-catalyzed mixing can be approximated as depending primarily on topographic roughness (RDM). The RDM was calibrated on microstructure data from the Brazil Basin, Hawaii and Fieberling Guyot and then extrapolated globally based on topographic roughness values inferred from the SS97 bathymetry. As mentioned earlier, globally extrapolating a model based on ~300 microstructure profiles is a leap of faith. Nonetheless, comparison to inverse model results indicate that the spatial distribution of diapycnal mixing implied by the RDM is a reasonable first-order approximation for mid-latitudes. An improved vertical structure function was proposed, at least compared to exponential decay generally used in current mixing parameterizations. Regions where nontidal mixing may be important were suggested based on global maps predicted by the RDM. Comparison to inverse models indicated that the type of mixing seen in the microstructure observations analyzed here, i.e., turbulence attributed mostly to breaking internal waves, accounts for a significant fraction of the mixing occurring in the abyssal ocean. Regions where the inverse models and the RDM did not agree were all regions where intense mixing in deep passages and channels have been documented. Turbulent mixing there is frequently attributed to internal hydraulic jumps and is not faithfully represented in the RDM, nor the SL02 and Polzin (2009) tidal

parameterizations. Much work remains to be done before mixing parameterizations will capture all of the mixing processes at work in the ocean.

Lastly, the power consumed by mixing was shown to be sensitive to the spatial distribution. The power consumption estimate based on the RDM is about $1/5^{\text{th}}$ of the canonical 2.1 TW proposed by Munk and Wunsch, 1998 associated with uniform mixing. This implies that both the winds and the tides could possibly sustain abyssal mixing alone. It is perhaps fortunate that Munk and Wunsch, 1998 based their power estimate on uniform mixing since it forced the community to examine the importance of tidal mixing in the abyssal ocean and sparked a very fruitful decade of research on tidally-driven mixing. The sensitivity of the power consumption to the spatial distribution of diapycnal mixing implies that we only have a crude idea of how much total power is in fact required to maintain the observed abyssal stratification. It is still not known what fraction of abyssal mixing is due to either the winds or the tides. It is likely this important question will remain unanswered for many years to come.

References

- Adcroft, A., J. R. Scott, and J. Marotzke, 2001: Impact of geothermal heating on the global ocean circulation. *Geophysical Research Letters*, **28**, 1735-1738.
- Alford, M. H., 2003: Improved global maps and 54-year history of wind-work on ocean inertial motions. *Geophysical Research Letters*, **30**.
- Althaus, A. M., E. Kunze, and T. B. Sanford, 2003: Internal tide radiation from Mendocino Escarpment. *Journal of Physical Oceanography*, **33**, 1510-1527.
- Armi, L., 1978: Some evidence for boundary mixing in the deep ocean. *Journal of Geophysical Research-Oceans*, **83**, 1971-1979.
- Aucan, J. and M. A. Merrifield, 2008: Boundary mixing associated with tidal and near-inertial internal waves. *Journal of Physical Oceanography*, **38**, 1238-1252.
- Aucan, J., M. A. Merrifield, D. S. Luther, and P. Flament, 2006: Tidal mixing events on the deep flanks of Kaena Ridge, Hawaii. *Journal of Physical Oceanography*, **36**, 1202-1219.
- Baker, M. A. and C. H. Gibson, 1987: Sampling Turbulence in the Stratified Ocean - Statistical Consequences of Strong Intermittency. *Journal of Physical Oceanography*, **17**, 1817-1836.
- Beal, L. M., 2000: Spreading of Red Sea overflow waters in the Indian Ocean. *Journal of Geophysical Research*, **105**, 8549-8564.
- Bray, N. A. and N. P. Fofonoff, 1981: Available potential energy for MODE eddies. *Journal of Physical Oceanography*, **11**, 30-46.
- Broersen, P., 2002: Automatic Spectral Analysis with Time Series Models. *IEEE Transactions on Instrumentation and Measurement*, **51**, 211-216.
- Bryan, F., 1987: Parameter Sensitivity of Primitive Equation Ocean General-Circulation Models. *Journal of Physical Oceanography*, **17**, 970-985.
- Bryan, K. and L. Lewis, 1979: A water mass model of the world ocean. *Journal of Geophysical Research-Oceans*, **84**, 2503-2517.
- Bryden, H. L. and A. J. G. Nurser, 2003: Effects of strait mixing on ocean stratification. *Journal of Physical Oceanography*, **33**, 1870-1872.
- Carter, G. S. and M. C. Gregg, 2002: Intense, variable mixing near the head of Monterey Submarine Canyon. *Journal of Physical Oceanography*, **32**, 3145-3165.
- Carter, G. S., M. C. Gregg, and M. A. Merrifield, 2006: Flow and mixing around a small seamount on Kaena Ridge, Hawaii. *Journal of Physical Oceanography*, **36**, 1036-1052.
- Chelton, D., 2001: Report of the High-Resolution Ocean Topography Science Working Group Meeting.
- Davis, R. E., 1994: The Osborn-Cox model. *Journal of Physical Oceanography*, **24**, 2560-2576.
- De Szoeko, R. A. and A. F. Bennet, 1993: Microstructure fluxes across density surfaces. *Journal of Physical Oceanography*, **23**, 2254-2264.
- Decloedt, T. and D. S. Luther, 2009: On a Simple Empirical Parameterization of Topography-Catalyzed Diapycnal Mixing in the Abyssal Ocean. *Journal of Physical Oceanography*, **early online release**.

- Dewar, W. K., R. J. Bingham, R. L. Iverson, D. P. Nowacek, L. C. St Laurent, and P. H. Wiebe, 2006: Does the marine biosphere mix the ocean? *Journal of Marine Research*, **64**, 541-561.
- Doos, K. and A. C. Coward, 1997: The Southern Ocean as the major upwelling zone of the North Atlantic Deep Water. *WOCE Newsletter*, **27**, 3-17.
- Efron, B. and G. Gong, 1983: A leisurely look at the bootstrap, the jackknife, and cross-validation *Amer. Stat.*, **37**, 36-48.
- Egbert, G. D. and A. Erofeeva, 2002: Efficient inverse modeling of barotropic ocean tides. *Journal of Atmospheric and Oceanic Technology*, **19**.
- Eriksen, C. C., 1998: Internal wave reflection and mixing at Fieberling Guyot. *Journal of Geophysical Research-Oceans*, **103**, 2977-2994.
- Ferrari, R. and C. Wunsch, 2009: Ocean Circulation Kinetic Energy: Reservoirs, Sources, and Sinks. *Annual Review of Fluid Mechanics*, **41**, 253-282.
- Ferron, B., H. Mercier, K. Speer, A. Gargett, and K. Polzin, 1998: Mixing in the Romanche Fracture Zone. *Journal of Physical Oceanography*, **28**, 1929-1945.
- Finnigan, T. D., D. S. Luther, and R. Lukas, 2002: Observations of enhanced diapycnal mixing near the Hawaiian ridge. *Journal of Physical Oceanography*, **32**, 2988-3002.
- Frisch, U., 1996: *Turbulence: A tribute to A. N. Kolmogorov*. First South Asian Edition 1999 ed. Cambridge university Press.
- Ganachaud, A., 1999: Large-scale oceanic circulation and fluxes of freshwater, heat, nutrients and oxygen., MIT/WHOI joint program, 296 pp.
- , 2003: Large-scale mass transports, water mass formation, and diffusivities estimated from World Ocean Circulation Experiment (WOCE) hydrographic data. *Journal of Geophysical Research*, **108**.
- Ganachaud, A. and C. Wunsch, 2000: Improved estimates of global ocean circulation, heat transport and mixing from hydrographic data. *Nature*, **408**, 453-457.
- Garabato, A. C. N., D. P. Stevens, and K. J. Heywood, 2003: Water mass conversion, fluxes, and mixing in the Scotia Sea diagnosed by an inverse model. *Journal of Physical Oceanography*, **33**, 2565-2587.
- Garabato, A. C. N., K. L. Polzin, B. A. King, K. J. Heywood, and M. Visbeck, 2004: Widespread intense turbulent mixing in the Southern Ocean. *Science*, **303**, 210-213.
- Gargett, A. E. and G. Holloway, 1992: Sensitivity of the GFDL ocean model to different diffusivities for heat and salt. *Journal of Physical Oceanography*, **22**, 1158-1178.
- Garrett, C., 1979: Comment on 'Some evidence for boundary mixing in the deep ocean' by Laurence Armi. *Journal of Geophysical Research*, **84**, 5095-5096.
- Gibson, C. H., 1982: Alternative interpretations for microstructure patches in the thermocline. *Journal of Physical Oceanography*, **12**, 374-383.
- Gille, S. T., M. M. Yale, and D. T. Sandwell, 2000: Global correlation of mesoscale ocean variability with seafloor roughness from satellite altimetry. *Geophysical Research Letters*, **27**, 1251-1254.
- Gnanadesikan, A., 1999: A simple predictive model for the structure of the oceanic pycnocline. *Science*, **283**.
- Gnanadesikan, A. and R. W. Hallberg, 2002: Physical Oceanography, thermal structure and general circulation. *Encyclopedia of Physical Science and Technology*, Academic Press, 189-210.

- Goff, J. A. and T. H. Jordan, 1988: Stochastic modeling of seafloor morphology: Inversion of sea beam data for second-order statistics. *Journal of Geophysical Research*, **93**, 13589-13608.
- Gouretski, V. and K. Jancke, 1998: A new climatology for the world ocean. *WOCE Hydrographic Program Special Analysis Centre Tech. Rep. 3*, 40 pp.
- Gregg, M. C., 1987: Diapycnal Mixing in the Thermocline - a Review. *Journal of Geophysical Research-Oceans*, **92**, 5249-5286.
- Gregg, M. C. and T. B. Sanford, 1980: Signatures of Mixing from the Bermuda Slope, the Sargasso Sea and the Gulf-Stream. *Journal of Physical Oceanography*, **10**, 105-127.
- Gregg, M. C. and J. K. Horne, 2009: Turbulence, Acoustic backscatter and pelagic nekton in Monterey Bay. *Journal of Physical Oceanography*, **39**, 1097-1114.
- Gregg, M. C., H. E. Seim, and D. B. Percival, 1993: Statistics of Shear and Turbulent Dissipation Profiles in Random Internal Wave Fields. *Journal of Physical Oceanography*, **23**, 1777-1799.
- Gregg, M. C., T. B. Sanford, and D. P. Winkel, 2003: Reduced mixing from the breaking of internal waves in equatorial waters. *Nature*, **422**, 513-515.
- Hasumi, H. and N. Sugimoto, 1999: Effects of locally enhanced vertical diffusivity over rough bathymetry on the world ocean circulation. *Journal of Geophysical Research-Oceans*, **104**, 23367-23374.
- Heisenberg, W., 1948: Zur Statistischen Theorie der Turbulenz. *Zeitschrift für Physik*, **124**, 628-657.
- Henye, F., J. Wright, and S. Flute, 1986: Energy and action flow through the internal wave field: An eikonal approach. *Journal of Geophysical Research*, **91**, 9686-9698.
- Hogg, N. G., E. Biscaye, E. Gardner, and J. W. Schmitz, 1982: On the transport of Antarctic Bottom Water in the Vema Channel. *Journal of Marine Research*, **40**, 231-263.
- Huang, R. X. and X. Z. Jin, 2002: Deep circulation in the South Atlantic induced by bottom-intensified mixing over the midocean ridge. *Journal of Physical Oceanography*, **32**, 1150-1164.
- Huntley, M. E. and M. Zhou, 2004: Influence of animals on turbulence in the sea. *Marine Ecology-Progress Series*, **273**, 65-79.
- Ivey, G. N., 1987: The Role of Boundary Mixing in the Deep Ocean. *Journal of Geophysical Research-Oceans*, **92**, 11873-11878.
- Jayne, S. R., 2009: The impact of abyssal mixing parameterizations in an Ocean General Circulation Model. *Journal of Physical Oceanography*, **early online release**.
- Jayne, S. R. and L. C. St Laurent, 2001: Parameterizing tidal dissipation over rough topography. *Geophysical Research Letters*, **28**, 811-814.
- Kantha, L. H. and C. C. Tierney, 1997: Global Baroclinic Tides. *Progress in Oceanography*, **40**, 163-178.
- Katija, K. and J. Dabiri, 2009: A viscosity-enhanced mechanism for biogenic ocean mixing. *Nature*, **460**, 624-627.
- Katsman, C. A., 2006: Impacts of localized mixing and topography on the stationary abyssal circulation. *Journal of Physical Oceanography*, **36**, 1660-1671.
- Klymak, J., R. Pinkel, and L. Rainville, 2007: Direct breaking of the internal tide near topography: Kaena Ridge. *Journal of Physical Oceanography*, **in press**.
- , 2008: Direct breaking of the internal tide near topography: Kaena Ridge. *Journal of Physical Oceanography*, **38**, 380-399.

- Klymak, J. M., J. N. Moum, J. D. Nash, E. Kunze, J. B. Girton, G. S. Carter, C. M. Lee, T. B. Sanford, and M. C. Gregg, 2006: An estimate of tidal energy lost to turbulence at the Hawaiian Ridge. *Journal of Physical Oceanography*, **36**, 1148-1164.
- Koch-Larrouy, A., G. Madec, P. Bouruet-Aubertot, T. Gerkema, L. Bessieres, and R. Molcard, 2007: On the transformation of Pacific Water into Indonesian Throughflow Water by internal tidal mixing. *Geophysical Research Letters*, **34**.
- Kolmogorov, A. N., 1941: Local structure of turbulence in an incompressible fluid at very high Reynolds numbers. *Doklady AN SSSR*, **30**, 299-303.
- Kuhlbrodt, T., 2008: On Sandstrom's inferences from his tank experiments: a hundred years later. *Tellus Series a-Dynamic Meteorology and Oceanography*, **60**, 819-836.
- Kuhlbrodt, T., A. Griesel, M. Montoya, A. Levermann, M. Hofmann, and S. Rahmstorf, 2007: On the driving processes of the Atlantic meridional overturning circulation. *Reviews of Geophysics*, **45**.
- Kunze, E., 2003: Yes. we have no abyssal mixing. *'Aha Huliko'a Hawaiian Winter Workshop*, Honolulu, SOEST special publications, 85-93.
- Kunze, E. and T. B. Sanford, 1996: Abyssal mixing: Where it is not. *Journal of Physical Oceanography*, **26**, 2286-2296.
- Kunze, E. and J. M. Toole, 1997: Tidally driven vorticity, diurnal shear, and turbulence atop Fieberling Seamount. *Journal of Physical Oceanography*, **27**, 2663-2693.
- Kunze, E., E. Firing, J. M. Hummon, T. K. Chereskin, and A. M. Thurnherr, 2006a: Global abyssal mixing inferred from lowered ADCP shear and CTD strain profiles. *Journal of Physical Oceanography*, **36**, 1553-1576.
- Kunze, E., J. F. Dower, I. Beveridge, R. Dewey, and K. P. Bartlett, 2006b: Observations of biologically generated turbulence in a coastal inlet. *Science*, **313**, 1768-1770.
- Large, W. G., J. C. McWilliams, and S. C. Doney, 1994: Oceanic Vertical Mixing - a Review and a Model with a Nonlocal Boundary-Layer Parameterization. *Reviews of Geophysics*, **32**, 363-403.
- Ledwell, J. R., A. J. Watson, and C. S. Law, 1993: Evidence for Slow Mixing across the Pycnocline from an Open-Ocean Tracer-Release Experiment. *Nature*, **364**, 701-703.
- , 1998: Mixing of a tracer in the pycnocline. *Journal of Geophysical Research-Oceans*, **103**, 21499-21529.
- Ledwell, J. R., E. T. Montgomery, K. L. Polzin, L. C. St Laurent, R. W. Schmitt, and J. M. Toole, 2000: Evidence for enhanced mixing over rough topography in the abyssal ocean. *Nature*, **403**, 179-182.
- Lee, C., E. Kunze, T. B. Sanford, J. D. Nash, M. A. Merrifield, and P. E. Holloway, 2006: Internal Tides and Turbulence along the 3000-m Isobath of the Hawaiian Ridge. *Journal of Physical Oceanography*, **36**, 1166-1183.
- Legg, S., 2003: Internal wave breaking at variable topographic slopes. *Aha Huliko'a Hawaiian Winter Workshop*, Honolulu, SOEST.
- Levine, M. D. and T. J. Boyd, 2006a: Tidally forced internal waves and overturns observed on a slope: Results from HOME. *Journal of Physical Oceanography*, **36**, 1184-1201.
- , 2006b: Tidally forced internal waves and overturns observed on a slope: results from HOME. *Journal of Physical Oceanography*, **36**, 1184-1201.
- Lueck, R. and R. Reid, 1984: On the Production and Dissipation of Mechanical Energy in the Ocean. *Journal of Geophysical Research-Oceans*, **89**, 3439-3445.

- Lueck, R. G., 2005: Horizontal and vertical turbulence profilers. *Marine Turbulence: Theories, Observations and Models*, H. Baumert, J. Simpson, and J. Suendermann, Eds., Cambridge University Press, 89-100.
- Lueck, R. G. and T. D. Mudge, 1997: Topographically induced mixing around a shallow seamount. *Science*, **276**, 1831-1833.
- Lueck, R. G., F. Wolk, and H. Yamazki, 2002: Oceanic velocity microstructure measurements in the 20th century. *Journal of Physical Oceanography*, **58**, 153-174.
- Lukas, R., F. Santiago-Mandujano, F. Bingham, and A. Mantyla, 2001: Cold bottom water events observed in the Hawaii Ocean Time-series: implications for vertical mixing. *Deep-Sea Research Part I-Oceanographic Research Papers*, **48**, 995-1021.
- Lumpkin, R. and K. Speer, 2003: Large-scale vertical and horizontal circulation in the North Atlantic Ocean. *Journal of Physical Oceanography*, **33**, 1902-1920.
- , 2007: Global Ocean Meridional Overturning. *Journal of Physical Oceanography*, **37**, 2550-2562.
- Macdonald, A. M. and C. Wunsch, 1996: An estimate of global ocean circulation and heat fluxes. *Nature*, **382**, 436-439.
- MacKinnon, J. A., T. M. S. Johnston, and R. Pinkel, 2008: Strong transport and mixing of deep water through the Southwest Indian Ridge. *Nature Geoscience*, **1**, 755-758.
- Marshall, P. and A. C. Naveira Garabato, 2007: A conjecture on the role of bottom-enhanced diapycnal mixing in the parameterization of geostrophic eddies. *Journal of Physical Oceanography*, **38**, 1607-1613.
- Martin, J. P. and D. L. Rudnick, 2007: Inferences and observations of turbulent dissipation and mixing in the upper ocean at the Hawaiian Ridge. *Journal of Physical Oceanography*, **37**, 476-494.
- Martin, J. P., D. L. Rudnick, and R. Pinkel, 2006: Spatially broad observations of internal waves in the upper ocean at the Hawaiian Ridge. *Journal of Physical Oceanography*, **36**, 1085-1103.
- Mauritzen, C., K. L. Polzin, M. S. McCartney, R. C. Millard, and D. E. West-Mack, 2002: Evidence in hydrography and density fine structure for enhanced vertical mixing over the Mid-Atlantic Ridge in the western Atlantic. *Journal of Geophysical Research-Oceans*, **107**.
- Mecking, S. M., M. McCartney, C. Mauritzen, and K. Polzin, in preparation: Mixing in the Vema Fracture Zone.
- Merrifield, M. A. and P. E. Holloway, 2002: Model estimates of M-2 internal tide energetics at the Hawaiian Ridge. *Journal of Geophysical Research-Oceans*, **107**.
- Montgomery, E. T., 1998: High resolution profiler use in the Brazil basin tracer release experiment. *Woods Hole Institution Technical Report*, **98-08**.
- Montgomery, E. T. and J. M. Toole, 1993: Fine-and microstructure observations at Fieberling Guyot. R/V New Horizon cruise report. *Woods Hole Institution Technical Report*, **93-52**.
- Morris, M. Y., M. M. Hall, L. C. St Laurent, and N. G. Hogg, 2001: Abyssal mixing in the Brazil Basin. *Journal of Physical Oceanography*, **31**, 3331-3348.
- Muller, P. and N. Xu, 1992: Scattering of Oceanic Internal Gravity-Waves Off Random Bottom Topography. *Journal of Physical Oceanography*, **22**, 474-488.
- Munk, W., 1966: Abyssal Recipes. *Deep-Sea Research Part I-Oceanographic Research Papers*, **13**, 207-230

- Munk, W. and C. Wunsch, 1998: Abyssal recipes II: energetics of tidal and wind mixing. *Deep-Sea Research Part I-Oceanographic Research Papers*, **45**, 1977-2010.
- Nash, J. D. and J. M. Moum, 1999: Estimating salinity variance dissipation rates from conductivity microstructure measurements. *Journal of Physical Oceanography*, **16**, 263-274.
- Nash, J. D., E. Kunze, J. M. Toole, and R. W. Schmitt, 2004: Internal tide reflection and turbulent mixing on the continental slope. *Journal of Physical Oceanography*, **34**, 1117-1134.
- Oakey, N. S., 1982: Determination of the Rate of Dissipation of Turbulent Energy from Simultaneous Temperature and Velocity Shear Microstructure Measurements. *Journal of Physical Oceanography*, **12**, 256-271.
- Osborn, T. R., 1980: Estimates of the Local-Rate of Vertical Diffusion from Dissipation Measurements. *Journal of Physical Oceanography*, **10**, 83-89.
- Polzin, K., 1992: observations of turbulence, internal waves and background flows: An inquiry into relationships between scales of motion. Ph. D. dissertation. *MIT-WHOI Joint Program in Oceanography*.
- , 1999: A rough recipe for the energy balance of quasi-steady internal lee waves. *Aha Huliko'a Hawaiian Winter Workshop*, Honolulu, SOEST.
- , 2004a: A heuristic description of internal wave dynamics. *Journal of Physical Oceanography*, **34**, 214-230.
- , 2004b: Idealized solutions for the energy balance of the finescale internal wave field. *Journal of Physical Oceanography*, **34**, 231-246.
- , 2009: An abyssal recipe. *Ocean Modelling*, **30**, 289-309.
- Polzin, K. and E. T. Montgomery, 1996: Microstructure profiling with the HRP. *ONR workshop on microstructure sensors*, Mt. Hood, OR.
- Polzin, K. and E. Firing, 1997: Estimates of diapycnal mixing using LADCP and CTD data from I8S. *International WOCE Newsletter*, **29**, 39-42.
- Polzin, K. L., J. M. Toole, and R. W. Schmitt, 1995: Finescale Parameterizations of Turbulent Dissipation. *Journal of Physical Oceanography*, **25**, 306-328.
- Polzin, K. L., K. G. Speer, J. M. Toole, and R. W. Schmitt, 1996: Intense mixing of Antarctic Bottom Water in the equatorial Atlantic Ocean. *Nature*, **380**, 54-57.
- Polzin, K. L., J. M. Toole, J. R. Ledwell, and R. W. Schmitt, 1997: Spatial variability of turbulent mixing in the abyssal ocean. *Science*, **276**, 93-96.
- Rainville, L. and R. Pinkel, 2006a: Baroclinic energy flux at the Hawaiian Ridge: Observations from the R/P FLIP. *Journal of Physical Oceanography*, **36**, 1104-1122.
- , 2006b: Propagation of low-mode internal waves through the ocean. *Journal of Physical Oceanography*, **36**, 1220-1236.
- Robinson, A. R. and H. Stommel, 1959: The oceanic thermocline and the associated thermohaline circulation. *Tellus*, **11**, 295-385.
- Roemmich, D., S. Hautala, and D. Rudnick, 1996: Northward abyssal transport through the Samoan passage and adjacent regions. *Journal of Geophysical Research-Oceans*, **101**, 14039-14055.
- Rudnick, D. L., T. J. Boyd, R. E. Brainard, G. S. Carter, G. D. Egbert, M. C. Gregg, P. E. Holloway, J. M. Klymak, E. Kunze, C. M. Lee, M. D. Levine, D. S. Luther, J. P. Martin, M. A. Merrifield, J. N. Moum, J. D. Nash, R. Pinkel, L. Rainville, and T. B.

- Sanford, 2003: From tides to mixing along the Hawaiian ridge. *Science*, **301**, 355-357.
- Saenko, O. A., 2006: The effect of localized mixing on the ocean circulation and time-dependent climate change. *Journal of Physical Oceanography*, **36**, 140-160.
- , 2008: On the strong seasonal currents in the deep ocean. *Journal of Climate*, **21**, 5642-5656.
- Saenko, O. A. and W. J. Merryfield, 2005: On the effect of topographically enhanced mixing on the global ocean circulation. *Journal of Physical Oceanography*, **35**, 826-834.
- Samelson, R. M., 1998: Large-scale circulation with locally enhanced vertical mixing. *Journal of Physical Oceanography*, **28**, 712-726.
- Sandstrom, J. W., 1908: Dynamische versuche mit Meerwasser. *Annalen der hydrographie und der maritimen meteorologie*, **36**, 26-32.
- , 1916: Meteorologische studien im Schwedische Hochgebirge. *Goteborgs K. Ventenskaps-och Vitterhetssamhallets Handl.*, **22**, 48.
- Saunders, P. M., 1987: Flow through Discovery Gap. *Journal of Physical Oceanography*, **17**, 631-643.
- Seber, G. A. F. and C. J. Wild, 1989: *Nonlinear regression*. John Wiley & Sons Inc.
- Simmons, H. L., R. W. Hallberg, and B. K. Arbic, 2004a: Internal wave generation in a global baroclinic tide model. *Deep-Sea Research Part Ii-Topical Studies in Oceanography*, **51**, 3043-3068.
- Simmons, H. L., S. R. Jayne, L. C. St Laurent, and A. J. Weaver, 2004b: Tidally driven mixing in a numerical model of the ocean general circulation. *Ocean Modelling*, **6**, 245-263.
- Sloyan, B. M., 2005: Spatial variability of mixing in the Southern Ocean. *Geophysical Research Letters*, **32**.
- Smith, W. H. F. and D. T. Sandwell, 1997: Global Sea Floor Topography from Satellite Altimetry and and Ship Depth Soundings. *Science*, **277**, 1956-1962.
- St Laurent, L. and H. Simmons, 2006: Estimates of power consumed by mixing in the ocean interior. *Journal of Climate*, **19**, 4877-4890.
- St Laurent, L. C., 1999: Diapycnal advection by double diffusion and turbulence in the ocean. Ph. D dissertation. *MIT-WHOI Joint Program in Oceanography*.
- St Laurent, L. C. and J. D. Nash, 2003: Internal tide energy dissipated near topography. *'Aha Huliko'a Hawaiian Winter Workshop*, Honolulu, SOEST
- St Laurent, L. C. and A. M. Thurnherr, 2007: Intense mixing of lower thermocline water on the crest of the Mid-Atlantic Ridge. *Nature*, **448**, 680-683.
- St Laurent, L. C., J. M. Toole, and R. W. Schmitt, 2001: Buoyancy forcing by turbulence above rough topography in the abyssal Brazil Basin. *Journal of Physical Oceanography*, **31**, 3476-3495.
- St Laurent, L. C., H. L. Simmons, and S. R. Jayne, 2002: Estimating tidally driven mixing in the deep ocean. *Geophysical Research Letters*, **29**.
- Stewart, R. H., 2008: *Introduction to physical oceanography* Texas A&M University.
- Stewart, R. H. and H. L. Grant, 1999: Early measurements of turbulence in the ocean: Motives and techniques. *Journal of Atmospheric and Oceanic Technology*, **16**, 1467-1473.
- Stommel, H., A. Arons, and A. Faller, 1958: Some examples of stationary planetary flow patterns in bounded basins. *Tellus*, **10**, 179-187.

- Talley, L. D., 2003: Shallow, intermediate and deep overturning components of the global heat budget. *Journal of Physical Oceanography*, **33**, 530-560.
- Talley, L. D., J. L. Reid, and P. E. Robbins, 2003: Data-based meridional overturning streamfunctions for the global ocean. *Journal of Climate*, **16**, 3213-3226.
- Taylor, G. I., 1915: Eddy motion in the atmosphere. *Philosophical Transactions of the Royal Society of London*, **215**, 1-16.
- Thurnherr, A. M., 2006: Diapycnal mixing associated with an overflow in a deep submarine canyon. *Deep-Sea Research Part II-Topical Studies in Oceanography*, **53**, 194-206.
- Thurnherr, A. M., L. C. St Laurent, K. G. Speer, J. M. Toole, and J. R. Ledwell, 2005: Mixing associated with sills in a canyon on the midocean ridge flank. *Journal of Physical Oceanography*, **35**, 1370-1381.
- Toggweiler, J. R. and B. Samuels, 1995: Effect of the Drake Passage on the global thermohaline circulation. *Deep-Sea Research*, **42**, 477-500.
- , 1998: On the ocean's large-scale circulation near the limit of no vertical mixing. *Journal of Physical Oceanography*, **28**, 1832-1852.
- Toggweiler, J. R. and R. M. Key, 2001: Thermohaline Circulation. *Encyclopedia of ocean sciences*, J. H. Steele, S. A. Thorpe, and K. K. Turekian, Eds., Academic Press, 2941-2947.
- Toole, J. M., 1998: Turbulent mixing in the ocean. *Ocean Modeling and Parameterization*, E. Chassignet and J. Verron, Eds., Kluwer, 171-190.
- , 2007: Temporal characteristics of abyssal finescale motions above rough bathymetry. *Journal of Physical Oceanography*, **37**, 409-427.
- Toole, J. M., R. W. Schmitt, K. L. Polzin, and E. Kunze, 1997: Near-boundary mixing above the flanks of a midlatitude seamount. *Journal of Geophysical Research-Oceans*, **102**, 947-959.
- Visser, A. W., 2007: Biomixing of the oceans? *Science*, **316**, 838-839.
- Warren, B. A., 1981: Deep Circulation of the World Ocean. *Evolution of Physical Oceanography*, The MIT Press, 6-41.
- Webb, D. J. and N. Sugimotohara, 2001: Oceanography - Vertical mixing in the ocean. *Nature*, **409**, 37-37.
- Wei, M. and D. T. Sandwell, 2006: Estimates of heat flow from Cenozoic seafloor using global depth and age data. *Tectonophysics*, **417**, 325-335.
- Whittaker, J. M., R. D. Mueller, W. R. Roest, P. Wessel, and W. H. F. Smith, 2008: How supercontinents and superoceans affect seafloor roughness. *Nature*, **456**, 938-942.
- Williams, P. D., T. W. Haine, and P. I. Read, 2008: Inertia-gravity waves emitted from balanced flow: observations, properties and consequences *Journal of the Atmospheric Sciences*, **65**, 3543-3556.
- Wunsch, C. and R. Ferrari, 2004: Vertical mixing, energy and the general circulation of the oceans. *Annual Review of Fluid Mechanics*, **36**, 281-314.
- Wyrtki, K., 1961: The Thermohaline Circulation in Relation to the General Circulation in the Oceans. *Deep-Sea Research*, 39-64.
- Zaron, E. D. and G. D. Egbert, 2006: Estimating open-ocean barotropic tidal dissipation: The Hawaiian Ridge. *Journal of Physical Oceanography*, **36**, 1019-1035.
- Zhang, J. B., R. W. Schmidt, and R. X. Huang, 1999: The relative influence of diapycnal mixing and hydrologic forcing on the stability of the thermohaline circulation. *Journal of Physical Oceanography*, **29**, 1096-1108.

